79

5 54355

Pgs 80

NASA TN D-1650

NASA TN D-1650

CN 63-13100
code 1

TECHNICAL NOTE

D-1650

AERODYNAMIC CHARACTERISTICS OF A LARGE-SCALE MODEL
WITH TWO HIGH DISK-LOADING FANS
MOUNTED IN THE WING

By David H. Hickey and Leo P. Hall

Ames Research Center
Moffett Field, Calif.

NATIONAL AERONAUTICS AND SPACE ADMINISTRATION

WASHINGTON February 1963

NATIONAL AERONAUTICS AND SPACE ADMINISTRATION

TECHNICAL NOTE D-1650

AERODYNAMIC CHARACTERISTICS OF A LARGE-SCALE MODEL WITH TWO HIGH DISK-LOADING FANS MOUNTED IN THE WING

By David H. Hickey and Leo P. Hall

SUMMARY

13100

The aerodynamic characteristics and performance of direct lifting fans mounted in both wing panels of a large scale VTOL airplane were investigated during low-speed flight. The model had a shoulder-mounted wing of aspect ratio 3.5. The effects on longitudinal characteristics of fan operation, of thrust control by means of deflecting the fan efflux, and of trailing-edge flap deflection were studied. Control power available from throttling the fans with differential exit louver deflection was also determined.

The lifting-fan performance, three-component longitudinal characteristics, wing-surface static-pressure distributions, and downwash at the horizontal tail are included herein.

INTRODUCTION

Full-scale studies of the fan performance and aerodynamic characteristics of a model with the General Electric X353-5 high disk-loading lifting fan mounted in the fuselage (refs. 1, 2, and 3) demonstrated the feasibility of the particular lifting-fan configuration. When two fans became available the present full-scale investigation was made with the fans mounted in the wings. Small-scale results of a similar investigation on a semispan wing are reported in reference 4.

A shoulder-mounted wing configuration was selected to provide favorable aerodynamic characteristics and to minimize ground effect. The fans were mounted in the wing as near to the fuselage as practicable, with the fan axis at 40 percent of the local chord. The effects on aerodynamic characteristics of exit-vane deflection, flap deflection, wing geometry (with and without the wing tips removed), and several fan inlets were obtained over the transition speed range.

Fan performance, general aerodynamic characteristics, wing-surface static-pressure distributions, and longitudinal stability and control results were obtained with the basic configuration. Power and control requirements for balanced flight through transition were calculated.

NOTATION

A	fan exit area, sq ft, or wing aspect ratio
b	wing span, ft
c	wing chord parallel to plane of symmetry, or vane chord, ft
$\bar{c}$	mean aerodynamic chord, $\frac{2}{S}\int_0^{b/2} c^2 dy$
C_l	rolling-moment coefficient, $\frac{R}{qSb}$
C_L	lift coefficient, $\frac{L}{qS}$
C_D	drag coefficient, $\frac{D}{qS}$
C_m	pitching-moment coefficient, $\frac{M}{qS\bar{c}}$
C_n	yawing-moment coefficient, $\frac{N}{qSb}$
C_y	side-force coefficient, $\frac{Y}{qS}$
D	drag, lb, or rotor diameter, ft
i_t	horizontal-tail incidence angle, deg
L	total lift on model, lb
M	pitching moment, ft-lb
M_r	reaction moment required at low speed, ft-lb
N	yawing moment, ft-lb
p_l	local static pressure, lb/sq ft
p_s	test section static pressure, lb/sq ft
P	pressure coefficient, $\frac{p_l - p_s}{q}$
P_o	standard atmospheric pressure, 2116 lb/sq ft
q	free-stream dynamic pressure, lb/sq ft
R	Reynolds number, or rolling moment, ft-lb

RPM	corrected fan rotational speed
S	wing area, sq ft
T	complete ducted fan thrust in the lift direction with $\alpha = 0^{\circ}$ and $\beta = 0^{\circ}$ $\rho A v_j^2$, lb
v	air velocity, ft/sec
V	free-stream air velocity, knots
W	gross weight, lb
x	distance from the leading edge of the wing, ft
y	spanwise distance perpendicular to the plane of symmetry, ft
Y	side force, lb
z	perpendicular distance from the chord line to the airfoil, ft
α	angle of attack of the wing chord plane, deg
β	fan exit-vane deflection angle from the fan axis, deg
$\Delta\beta$	difference in exit-vane angle of alternate vanes, or difference between exit-vane angles of the left and right fans, $\beta_L - \beta_R$, deg
δ	relative static pressure, $\frac{p_s}{p_o}$
δ_f	trailing-edge flap deflection measured normal to the hinge line, deg
θ	articulated inlet vane angle with respect to the fan axis, deg
ϵ	average downwash angle at the horizontal tail, deg
η	fraction of wing semispan, $\frac{2y}{b}$
λ	wing taper ratio
μ	tip-speed ratio, $\frac{V_\infty}{\omega R}$
ρ	density, lb-sec^2/ft^4
φ	angle between the fan axis and the fixed portion of the articulated inlet vanes, deg
ω	fan rotational speed, radians/sec

Subscripts

a	average
f	fan
j	fan exit
r	in a direction to produce roll
L	left
T	reaction control
R	right
s	static conditions
t	in a direction to reduce thrust
u	uncorrected
v	forward speed condition
y	in a direction to produce yaw
α	variable angle of attack
β	variable exit-vane angle
1, 2 . . .	a particular inlet vane when used with θ (fig. 4), or moment center (fig. 2)

MODEL AND APPARATUS

Photographs of the model as mounted in the Ames 40- by 80-Foot Wind Tunnel are presented in figure 1. A sketch of the model giving pertinent dimensions is shown in figure 2.

Model Details

Wing geometry.- Wing configuration 1 had an aspect ratio of 3.5, taper ratio of 0.5, and sweepback of 16° at the quarter-chord line. The wing upper surface was tangent to the fuselage top at the maximum thickness point. An NACA 65A-210 airfoil section (coordinates are in table I) was basic for the wing. The fan inlet was designed for an untapered wing; the resultant bulge and fairing increase wing thickness to 10.9 percent at the outboard edge of the fan (η = 0.51). Normal airfoil contour was regained at η = 0.57. Unless otherwise stated, the results are for wing configuration 1.

Wing configuration 2 was the same as 1 except that the wing tip, the outboard 36 percent semispan of configuration 1, was removed. The resultant geometry had an aspect ratio of 2.05 and taper ratio of 0.68.

Details of the plain trailing-edge flap are shown in figure 3. The flap extended from 16.8 to 64 percent semispan. Flap deflections of 0°, 30°, and 60° were tested. The figure also shows the location of pressure instrumentation on the wing and in the fans. Although not shown on the figure, the right wing had chordwise static-pressure stations from 0 to 5 percent chord.

Fuselage.- The fuselage had a maximum diameter of 6.5 feet. Forward of the maximum thickness point the cross sections were circular; aft of this point the fuselage gradually became elliptical with the major axis in the horizontal direction. The YJ-85-5 gas generators for driving the fans were partially contained in the fuselage.

Tail.- Geometry and location of the tail are shown in figure 2. The all-movable horizontal tail was pivoted at the quarter chord and had a range from -10° to $+30^\circ$ incidence. For the tests indicated "tail off," both the vertical and horizontal tails were removed.

Propulsion System

The General Electric X353-5 lifting-fan engine passes the exhaust gases from a gas generator through the fan tip-mounted turbine to drive the fan. The fans were designed to be operated in conjunction with J85-5 gas generators. Both fans rotated in a counterclockwise direction when viewed from above the model.

Fan installation.- The wing completely enclosed the fan except for the hub, which protruded from the wing upper surface. A diverter valve installed in the tail pipe of the gas generator allowed the exhaust from the gas generator to be used either to drive the fan or to provide direct thrust. As can be seen in figures 1 and 2, the gas generators and diverter valves were partially submerged in the fuselage.

Fan details.- The 62.5-inch-diameter fan has a single rotor with 36 blades. A single stage of stators was employed behind the rotor, and a cascade of exit vanes was mounted downstream of the stators. These vanes extended across the tip turbine exhaust and were used both to vector the fan flow and as a lower surface wing closure ($\beta = 90^\circ$). Alternate vanes were linked together to provide two independent gangs of exit louvers per fan. The louvers had independent drive systems so that thrust could be controlled by throttling the fan with the two exit louver gangs. The vane airfoil sections had a maximum thickness of 10-percent chord at 20-percent chord and had a maximum of 2.3-percent-chord camber of the mean line at 35-percent chord.

Fan inlets.- Photographs and details of the three inlets tested are shown in figure 4. Inlet 1 consisted only of the fixed circular vane portion shown in figure 4(b). This vane had a 12-percent thickness to chord ratio located at 25-percent chord and a camber of 10 percent of the mean line located at 45-percent chord. Inlet 2 consisted of the circular vane of inlet 1 with five additional fixed spanwise vanes. A sketch of the inlet is shown in figure 4(b), and details of the inlet vanes are listed in table II. Unless otherwise stipulated, the presented data are with inlet 2. The inlets mentioned thus far have been small and uncomplicated. All these vanes fit within the wing contour; covers are required in cruising flight to close the fan aperture. Inlet 3, with variable inlet vane angle capability, combines the inlet with the fan aperture closure (fig. 4(c)). The vanes (five in all) consisted of a fixed trailing-edge portion and the large, movable forward portion which also served as a wing closure. The movable portions were linked together so that movement of each vane was preprogrammed. The interrelationship between these vanes is shown in figure 4(d).

TESTING AND PROCEDURE

Longitudinal force and moment data were obtained through an angle-of-attack range from -4° to $+20^{\circ}$. Fan performance and wing surface pressure distributions were also measured. Airspeed of the tests varied from 0 to 100 knots, corresponding to maximum Reynolds numbers of 12.4 million. Fan RPM was varied from 1100 to 2400.

Tests With Constant Angle of Attack

At 0° angle of attack, fan speed and wind-tunnel velocity were varied independently. Results were obtained for several exit-vane angles and combinations of differential exit-vane angles, three inlets, and three flap deflections, and with the tail on and off.

Tests With Varying Angle of Attack

Fan RPM was maintained essentially constant when angle of attack was varied. These data were obtained at several values of fan RPM and tunnel airspeed. The model variables tested in this manner are the same as those mentioned above.

CORRECTIONS

Force data obtained without the fan operating were corrected for the effect of the wind-tunnel wall interference, as follows:

$$\alpha = \alpha_u + 0.92C_{L_u}$$

$$C_D = C_{D_u} + 0.016C_{L_u}$$

$$C_m = C_{m_u} + 0.0105C_{L_u} \text{ (tail on only)}$$

No wind-tunnel wall corrections were made to the force data obtained with the fan operating since the effect of the fan air flow on wind-tunnel corrections is unknown. The drag of the model support structure is also unknown; hence no drag tare corrections were applied.

RESULTS

Tip-speed ratio, μ, will be used as the independent parameter in the following data presentation. The relationship between tip-speed ratio and the more general parameter, free-stream to fan-velocity ratio, is shown in figure 5.

Unless otherwise noted the following results are for wing configuration 1 and fan inlet 2.

Fan Characteristics

The effect of test and configuration variables on fan performance when installed in a wing is shown by the following results.

Figures 6 through 9 present the fan performance as installed in the wing. Figure 6 shows zero airspeed total lift on the model with both fans operating. Comparable results from reference 1 are included in the figure. Figure 7 presents the variation of fan thrust with airspeed (tip-speed ratio) at 0° angle of attack for several flap deflections, all three inlets, and both the right and the left fan. Figures 8 and 9 show the effect of exit-vane angle and angle of attack, respectively, on thrust of the right fan with the trailing-edge flap deflected 30°.

Aerodynamic Characteristics

The following results show the effect of fan operating variables and configuration variables on longitudinal characteristics of the model.

Angle of attack of zero.- Data in figures 10 through 14 show the effect of airspeed and fan RPM (tip-speed ratio) on longitudinal characteristics. The variation with tip-speed ratio of the ratio of lift at forward speed to static lift with 0° exit-vane angle is shown in figure 10. Similar results from reference 1 and fan thrust from the present investigation and reference 1 are included. Figure 11 shows the variation of longitudinal characteristics with tip-speed ratio for several exit-vane angles, with two trailing-edge flap deflections, and with the tail off. Moments are presented for two moment centers (see fig. 2). Similar results with the horizontal tail on are presented in figure 12, and for wing configuration 2 (short-span wing) in figure 13. The effect of the articulated inlet (inlet 3) on the variation of longitudinal characteristics with tip-speed ratio is shown in figure 14. For comparison, similar results with the fixed vane inlet are included on the figure.

Figures 15 through 21 show wing surface-pressure distributions. Chordwise distributions through the fan axis are presented in figures 15 through 19 for 0° and 30° flap deflections, several exit-vane angles, and at different tip-speed ratios. Chordwise pressure distributions at several spanwise stations are presented in figure 20 for several exit-vane angles and tip-speed ratios. Minimum leading-edge pressures for the left and right wing panels are shown in figure 21 for several tip-speed ratios and 0° exit-vane angle.

The variation of average downwash at the tail with tip-speed ratio is shown in figure 22 for several exit-vane angles.

Variable angle of attack.- Data in figures 23 through 34 show the variation of longitudinal characteristics with angle of attack. Figures 23 through 26 present power-off longitudinal characteristics. Data with the fan inlets and exits closed show, in figure 23, the effect of flap deflection with the tail on and off and, in figure 24, the effect of Reynolds number; figure 25 presents the power-off longitudinal characteristics of wing configuration 2 (short-span wing). The effect of various open or partly open fan inlets and exits on longitudinal characteristics is shown in figure 26.

Figures 27 through 34 show longitudinal characteristics with the fans operating. Low-speed forces and moments with and without the tail and for two exit-vane angle settings are shown in figure 27. Figures 28 and 29 present results at higher speed in coefficient form; data for three exit-vane angles are presented in figure 28, for the tail off, and in figure 29, for the tail on. Higher speed longitudinal characteristics, which would be encountered beyond the normal speed for conversion from fan-supported to wing-supported flight, are shown in figure 30. The effect of inlets 1 and 3 on longitudinal characteristics is shown in figures 31 and 32, respectively. Longitudinal charactersitics with symmetrical differential exit-vane settings to reduce thrust are shown in figure 33. Longitudinal characteristics with wing configuration 2 are shown in figure 34.

Pitching-moment curve slope with the tail off for both moment centers is shown as a function of tip-speed ratio in figure 35 for three exit-vane angles. Horizontal-tail effectiveness is presented in figure 36.

Control Power of Differentially Deflected Exit Vanes

Operation of alternate rows of exit vanes to reduce fan exit area and thrust offers a means of controlling thrust and roll with rapid response rates. Thrust was controlled by symmetrically throttling each fan with two exit louver gangs. Yaw was controlled by the asymmetric operation of the complete exit-louver cascade, and roll was controlled by throttling only one of the fans.

Data in figures 37 and 38 show the effects of differential louver operation to reduce fan thrust. Static thrust reduction is shown in figure 37, and its effect on longitudinal characteristics is shown in figure 38. The effectiveness of differentially operating the louvers to produce yaw and roll moments at several tip-speed ratios is shown in figure 39; these results are for longitudinal and lateral characteristics.

Balanced Flight

Power and control requirements for balanced flight (L = W, D = 0), as computed from the test results, are presented in figure 40 to illustrate possible techniques for performing transitions. These requirements can be considered as an average between accelerating and decelerating transitions for the particular transition techniques chosen. Many other transition techniques are possible. Results presented in figure 40 are for two center of gravity positions for wing configuration 1, and for one center of gravity position for wing configuration 2. It was assumed that the conversion from fan-supported to wing-supported flight would occur at 130 percent of the power-off stall speed. Figure 40(a) presents the angle-of-attack variation with airspeed, and the required fan RPM and exit-vane angle for balanced flight. Figure 40(b) presents the moment to be trimmed for the flight plans in figure 40(a), the tail incidence angle for trim or for a maximum tail angle of attack of 12°, and the reaction moment required to balance at low speed.

DISCUSSION

Fan Performance

Fan static thrust in this investigation was essentially the same as that reported in reference 1 (see fig. 6).

Effect of airspeed.- One of the most significant differences between the fan-in-fuselage installation and the fan-in-wing installation was the effect of airspeed on fan thrust. The results in figures 7 and 10 show that in contrast to data in reference 1, for the fan-in-fuselage model, fan thrust decreased with increasing airspeed. This reduction in thrust of both left and right wing rotors occurred for all wing configurations and for all inlets tested. Observation of exit survey rakes indicated that inlets 1 and 2 were ineffective in turning the air, and fan internal performance suffered as a result. Inlet 3 was effective in turning the air and improved the fan internal performance; however, fan thrust was the same as with the other inlets. Performance of the right fan was characterized by premature inlet separation (as compared with the left fan) as tip-speed ratio or angle of attack were increased; a more rapid reduction of lift with airspeed also occurred. One possible explanation for the differing performance is that the retreating blade on the right side of the model was in a flow field that can be influenced by leakage from the fan turbine, thus the right fan could be more sensitive to adverse flow conditions. Results in figure 8 show that increasing exit-vane angles increased thrust rather than decreased it at higher tip-speed ratios. Apparently the inclined flow environment provided by the ineffective inlets resulte in reduced thrust for the fan with the exit-vane angle at 0°.

Available thrust for propulsion.- Available thrust is defined as the increment between the power-off and power-on drag of the model, so that the term included ram drag from the fan air flows and pressure drag caused by the interaction of the fan efflux and the model flow field. Figure 41 presents these results with and without flaps. Similar results from reference 1 are included in the figure. In spite of the reduction in fan performance noted with the wing installation at high speed, more horizontal thrust was available than in the fuselage installation. Thi result is probably due to the different exit-van throttling characteristics and reduction in interaction drag in the wing installation. The increase in thrust available with the flap deflected indicates a further reduction of interference dra

Aerodynamic Characteristics

Longitudinal characteristics.- Results of small-scale tests (ref. 5) and theoretical studies (ref. 6) have indicated that jets or air flow from fans mounted in wings will cause a loss of lift as forward speed is increased from hover; this lift reduction has been called "suck down" or "lift droop" and has been shown to exist with or without the effect of the ground. The magnitude of the ratio of fan area to wing area of the model configurations reported herein is such that results would be subject to the lift loss effect based on the small-scale tests. No evidence of lift loss was found for any of the flap or exit-vane conditions studied. In fact for all configurations, even though forward speed reduced fan thrust, the induced effects of the fan on the wing were sufficiently large to give an increase in total lift with increasing forward speed.

The exit vanes acted essentially as a device for varying horizontal force at any given speed for small louver angles on either side of the angle required for unaccelerated level flight. Maximum lift coefficient was virtually unaffected by louver angle; however, the angle of attack for maximum lift was increased at low tip-speed ratios and slightly decreased at high tip-speed ratios. At low angles of attack very little lift change occurred when the exit vanes were deflected from 0° to 20°; but a significant reduction did occur over the entire speed range when the vanes were deflected from 20° to 40°.

Angle-of-attack stability, shown in figure 35, was only slightly affected by power, airspeed, and exit-vane angle as long as the horizontal tail was unstalled. The downwash from fan operation stalled the lower surface of the horizontal tail below tip-speed ratios of 0.15 and 0° tail incidence.

With these aerodynamic characteristics, it should be possible for fan-in-wing aircraft to have good flying characteristics throughout the fan-powered flight range of airspeeds. The small effect of exit-vane deflection on the model lift indicates that, with the independent drag control available with the exit vanes, rapid and large flight-path changes can be made without adversely affecting wing aerodynamics; hence, large angles of descent should be possible at low airspeeds.

Moments required for trimmed flight.- Figure 42 presents the ratio of moment to be trimmed for unaccelerated flight to aircraft gross weight as a function of airspeed for the fan-in-fuselage model of reference 2 and the present fan-in-wing model. The moment center of the model of reference 2 has been adjusted to give the same ratio of unbalance at hover as moment center 2 in the present investigation. Data in figure 42 show that with the flaps up, the moment variation with airspeed for the fan-in-fuselage model was about twice the value for the fan-in-wing model. This difference is caused primarily by the different moment arms of the horizontal force couple. The deep fuselage of the fan-in-fuselage model causes a large couple moment arm which produces a large moment due to the horizontal force required for trim. The pitch-down contribution of the trailing-edge flaps and reduced power requirement with flaps down produced a further reduction in pitching moment for trim. The rounding of curves at higher transition speeds is at least partially caused by the low turning efficiency of the inlet.

It should be noted that, with the center-of-gravity position under consideration, moments to be trimmed are of the same order of magnitude or less than the moment contributed by deflection of trailing-edge flaps. Therefore, a lifting-fan aircraft can be designed to have a trim moment no larger than that for a flapped wing, and the moment change during conversion from fan-supported to wing-supported flight may be no larger than that arising from extending the flap on a normal aircraft.

Ames Research Center
National Aeronautics and Space Administration
Moffett Field, Calif., Nov. 7, 1962

REFERENCES

1. Aoyagi, Kiyoshi, Hickey, David H., and deSavigny, Richard A.: Aerodynamic Characteristics of a Large-Scale Model With a High Disk-Loading Lifting Fan Mounted in the Fuselage. NASA TN D-775, 1961.

2. Maki, Ralph L., and Hickey, David H.: Aerodynamics of a Fan-in-Fuselage Model. NASA TN D-789, 1961.

3. deSavigny, Richard A., and Hickey, David H.: Aerodynamic Characteristics in Ground Effect of a Large-Scale Model With a High Disk-Loading Lifting Fan Mounted in the Fuselage. NASA TN D-1557, 1962.

4. Hickey, David H., and Ellis, David R.: Wind-Tunnel Tests of a Semispan Wing With a Fan Rotating in the Plane of the Wing. NASA TN D-88, 1959.

5. Spreemann, Kenneth P.: Induced Interference Effects on Jet and Buried-Fan VTOL Configurations in Transition. NASA TN D-731, 1961.

6. Norland, Sven-Anders: An Investigation of the Lift Produced by a Fan in a Two-Dimensional Wing. Massachusetts Institute of Technology, 1962.

TABLE I.- COORDINATES OF WING AIRFOIL SECTION (NACA 65-210 MODIFIED) PARALLEL TO MODEL PLANE OF SYMMETRY

Upper surface		Lower surface	
x/c	z/c	x/c	z/c
0	0	0	0
.00435	.00819	.00569	-.00776
.00678	.00999	.00827	-.00925
.01169	.01273	.01337	-.01141
.02408	.01757	.02598	-.01498
.04898	.02491	.05110	-.02014
.07394	.03069	.07614	-.02431
.09894	.03555	.10417	-.02812
.14899	.04338	.13889	-.03194
.19909	.04938	.17361	-.03486
.24921	.05397	.20833	-.03708
.29936	.05732	.27778	-.03868
.34951	.05954	.34722	-.03910
.39968	.06067	.41667	-.03924
.44984	.06058	.48611	-.03861
.50000	.05915	.55556	-.03618
.55014	.05625	.62500	-.03146
.60027	.05217	.65972	-.02806
.65036	.04712	.69954	-.02404
.70043	.04128	.74952	-.01867
.75045	.03479	.79953	-.01325
.80044	.02783	.84959	-.00803
.85038	.02057	.89970	-.00344
.90028	.01327	.94985	.00009
.95014	.00622	1.00000	0
1.00000	0		

Leading-edge radius: 0.00687
Slope of radius through leading-edge: 0.084

TABLE II.- DETAILS OF FIXED INLET VANE CHARACTERISTICS

	Circular vane	Fixed vane 1	Fixed vane 2	Fixed vane 3	Fixed vane 4	Fixed vane 5
Maximum thickness, percent c	12.0	9.0	9.7	9.0	9.9	9.1
Location of maximum thickness, percent c	25.5	20.0	20.0	20.0	20.0	20.0
Camber of mean line, percent c	9.7	3.0	3.0	3.0	1.5	0
Location of camber of mean line, percent c	46.8	40.0	50.0	45.0	40.0	0
Chord	5.12	6.0	6.0	6.0	6.0	5.85

A-28399

(a) Overhead view.

Figure 1.- Model mounted in Ames 40- by 80-Foot Wind Tunnel.

A-28400

(b) Three-quarter front view.

Figure 1.- Concluded.

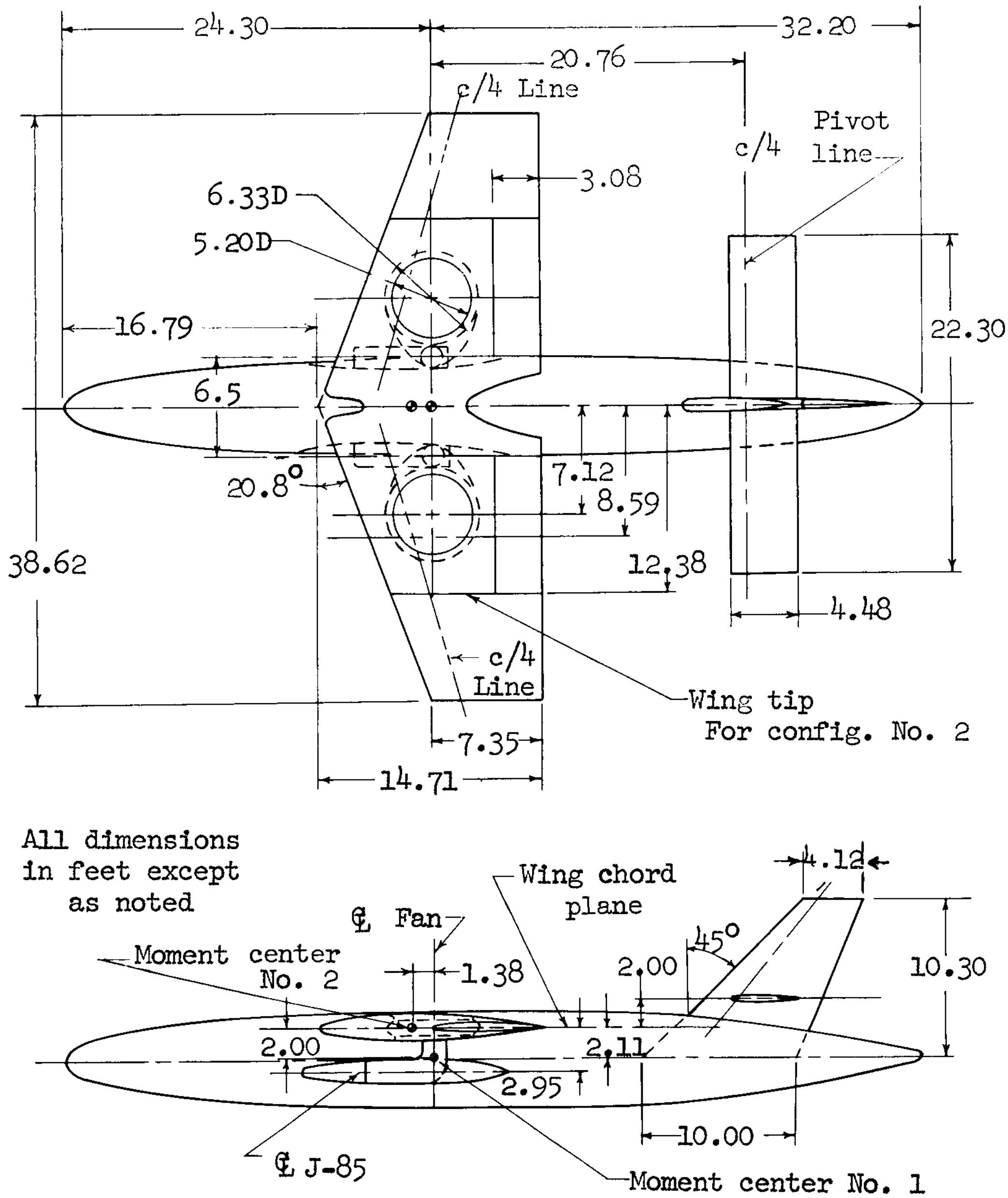

	Wing Config 1	Wing Config 2	Horizontal Tail
Area, sq ft	426.0	305.9	100.0
Aspect ratio	3.5	2.05	4.97
Taper ratio	0.5	.68	1.0
Airfoil section	65A-210	65A-210	63-009
$\bar{c}$	11.44	12.50	4.48

Figure 2.- Geometric details of the model.

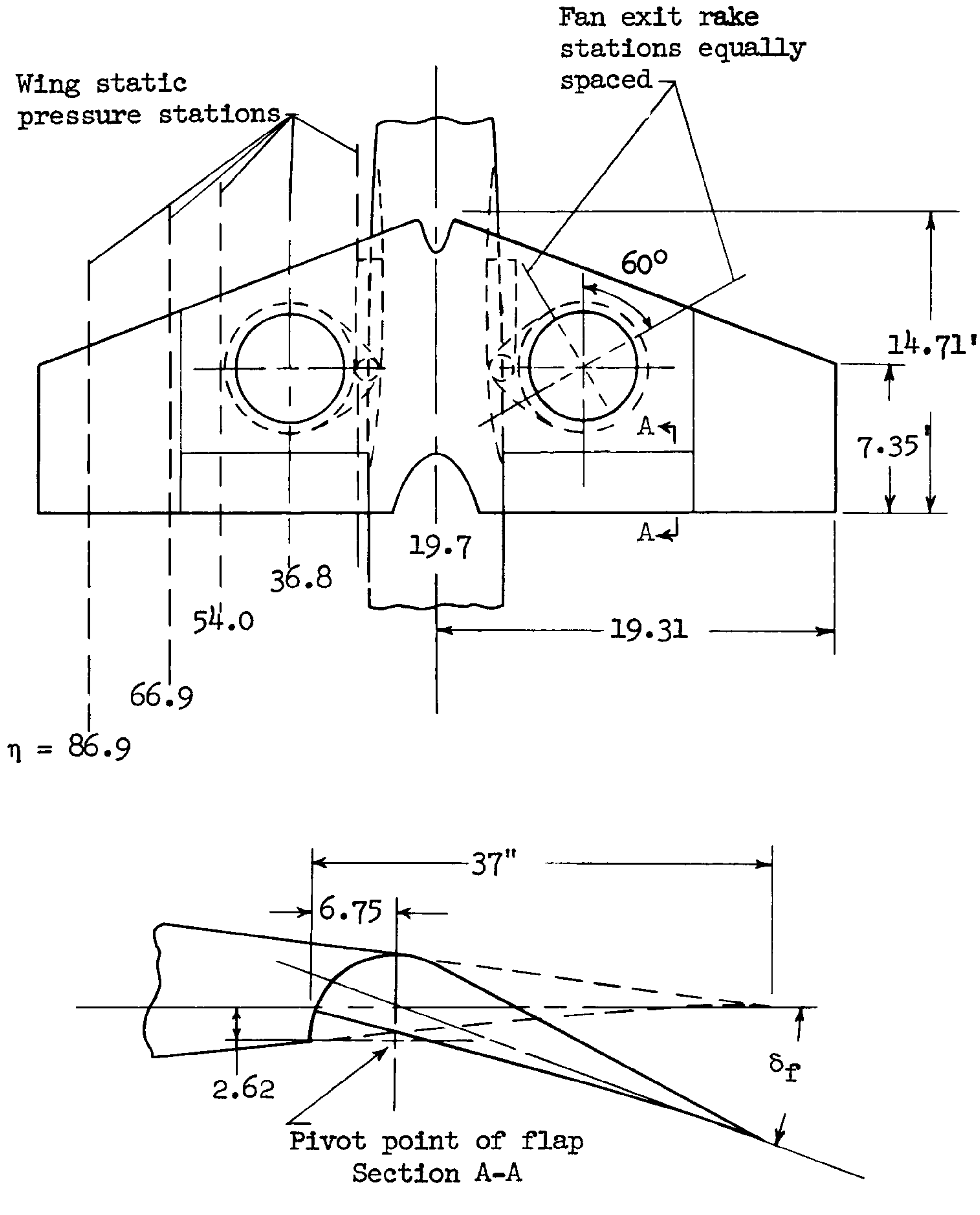

Figure 3.- Details of the trailing-edge flap and pressure instrumentation.

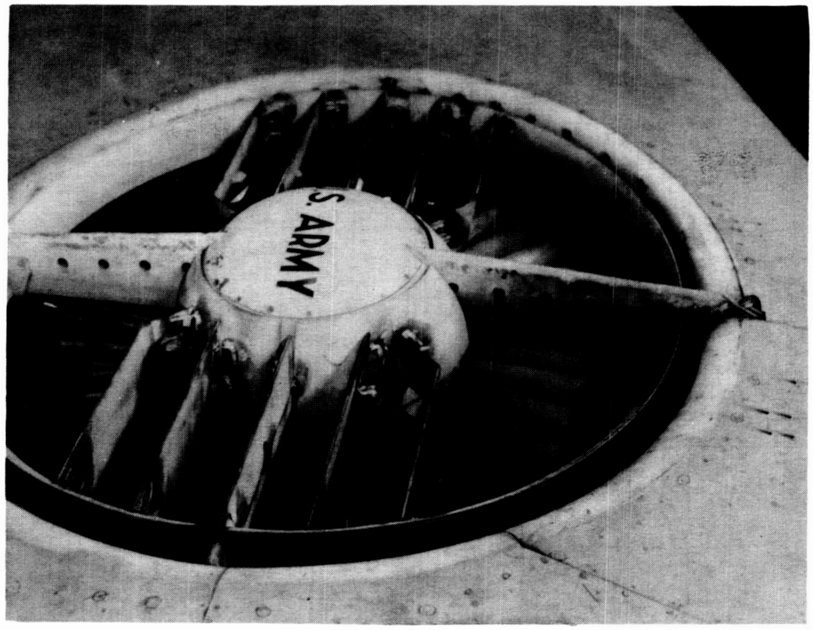

A-30114-1

Inlet number 2
Fixed inlet vanes

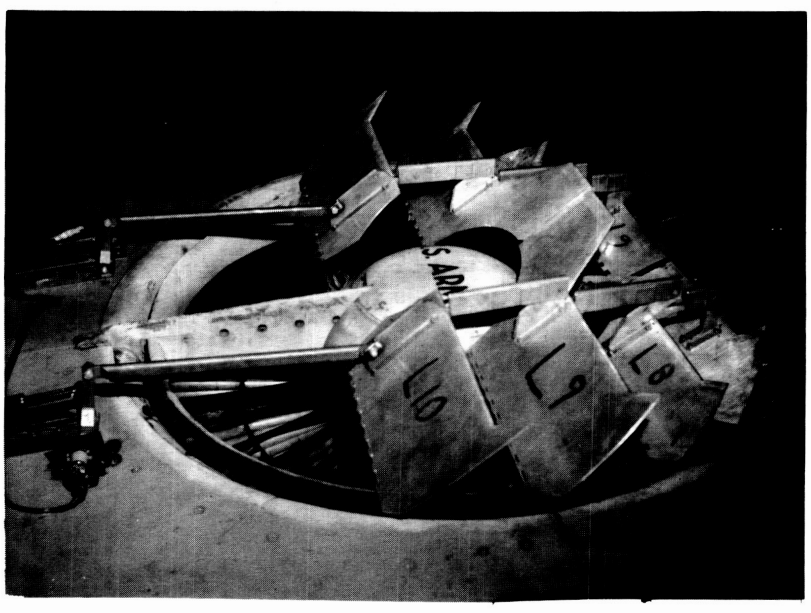

A-30114-2

Inlet number 3
Articulated inlet vanes

(a) Photographs of inlets tested.

Figure 4.- Details of the fan inlets.

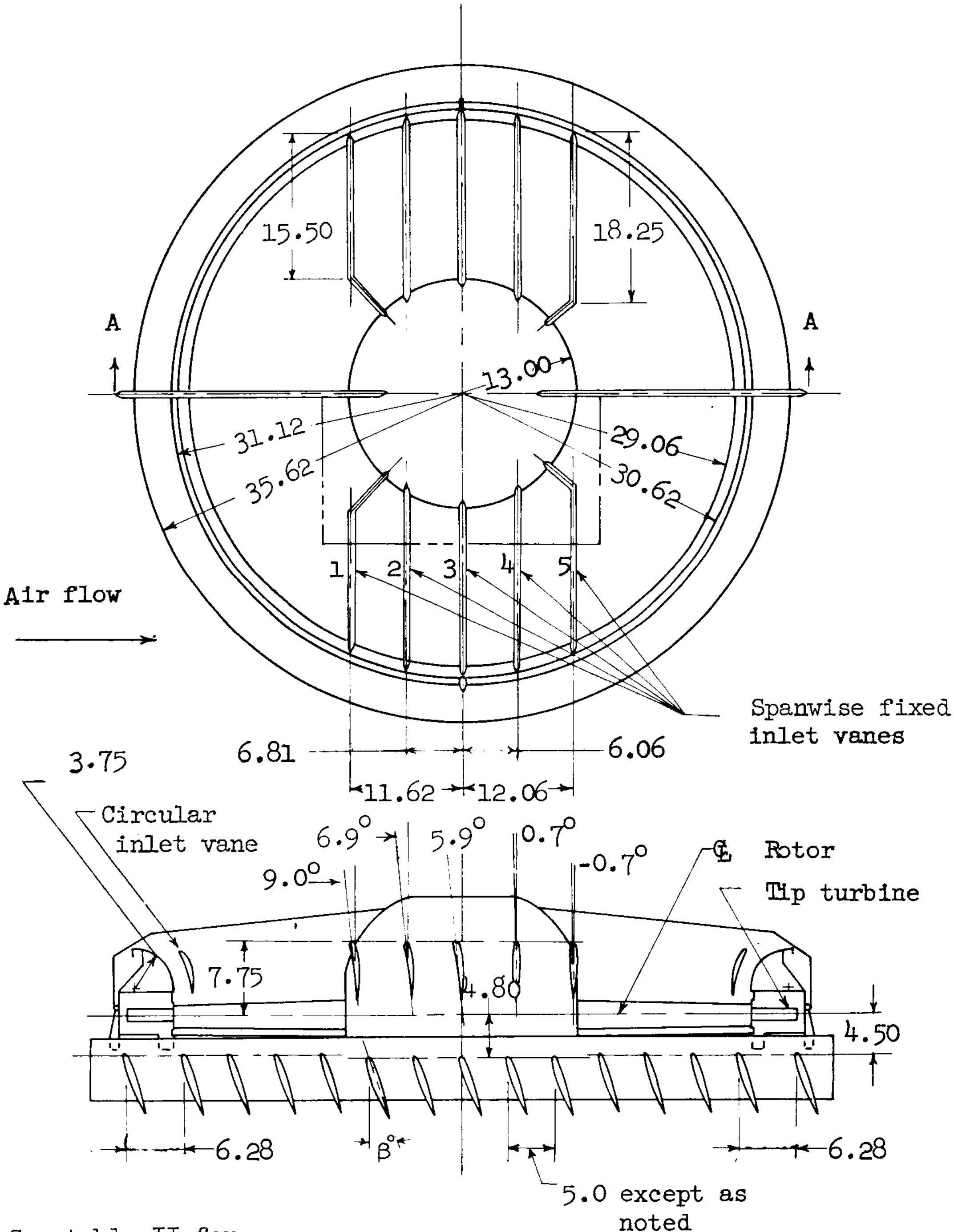

See table II for
inlet vane details

Section A-A

(All dimensions in inches
except as noted)

(b) Details of inlet 2.

Figure 4.- Continued.

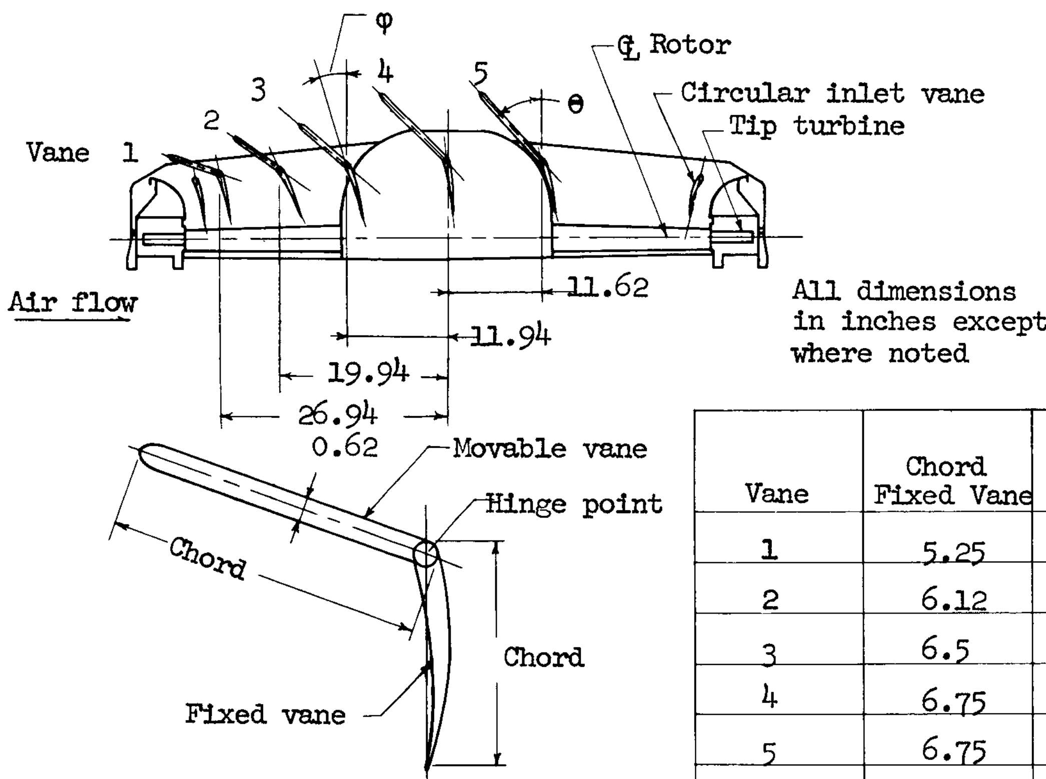

Vane	Chord Fixed Vane	Chord Movable Vane	φ, deg
1	5.25	7.5	11
2	6.12	7.06	22
3	6.5	7.87	16
4	6.75	11.75	6
5	6.75	11.87	13.5
Circular	5.06		16

(c) Details of inlet 3.

Figure 4.- Continued.

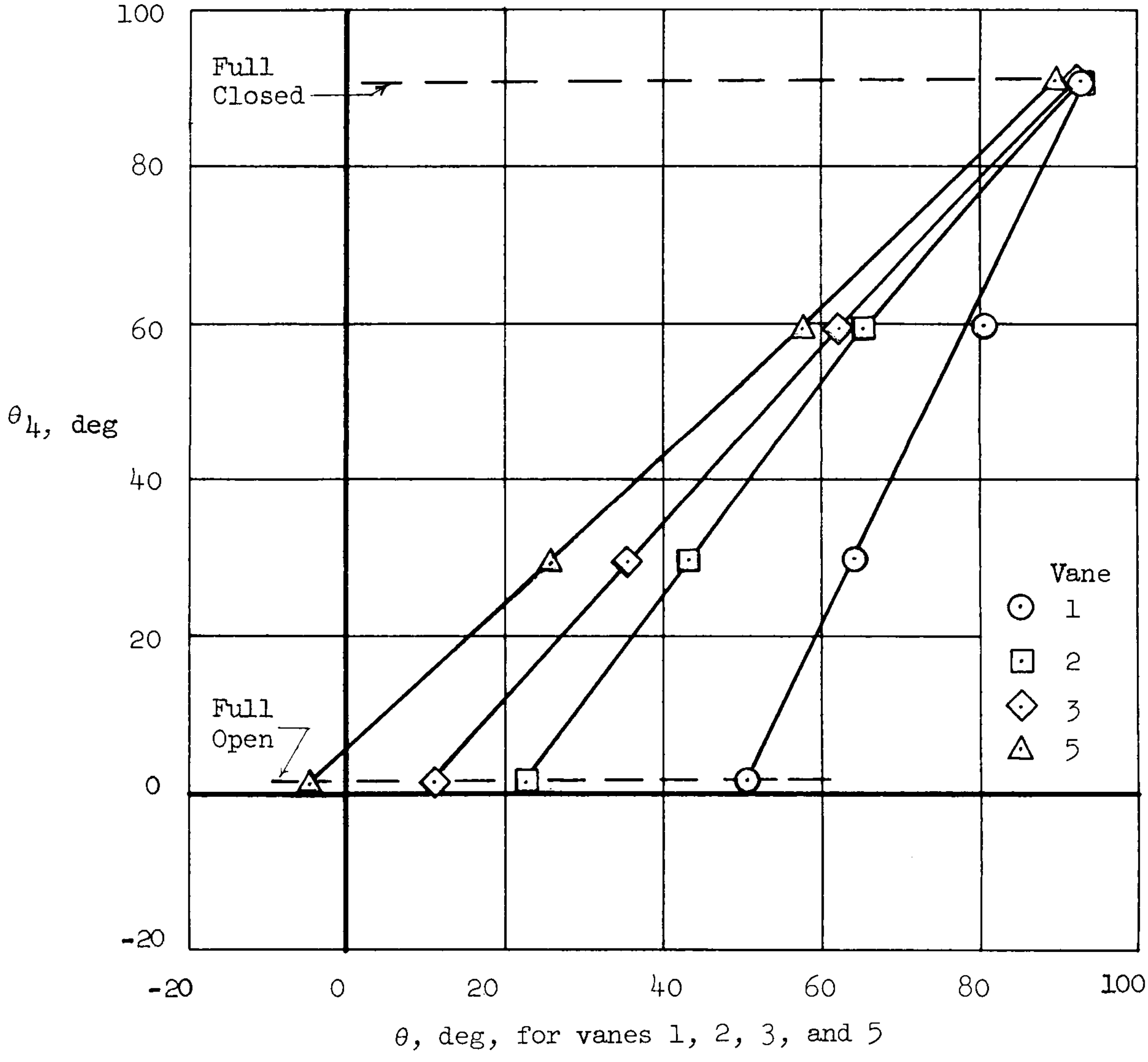

(d) Interrelationship of the articulated inlet vanes.

Figure 4.- Concluded.

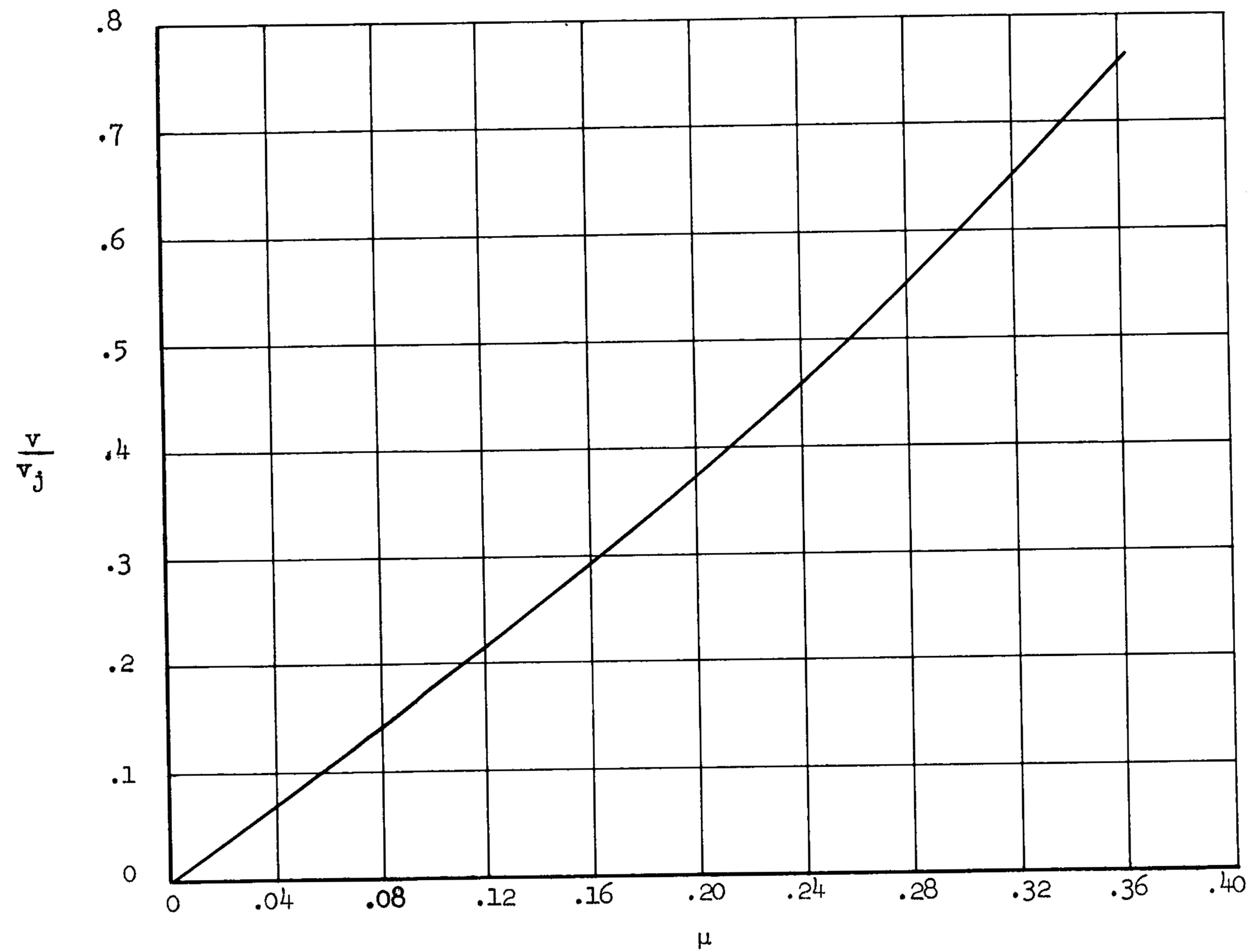

Figure 5.- The average variation of velocity ratio with tip-speed ratio; $\beta = 0^{\circ}$.

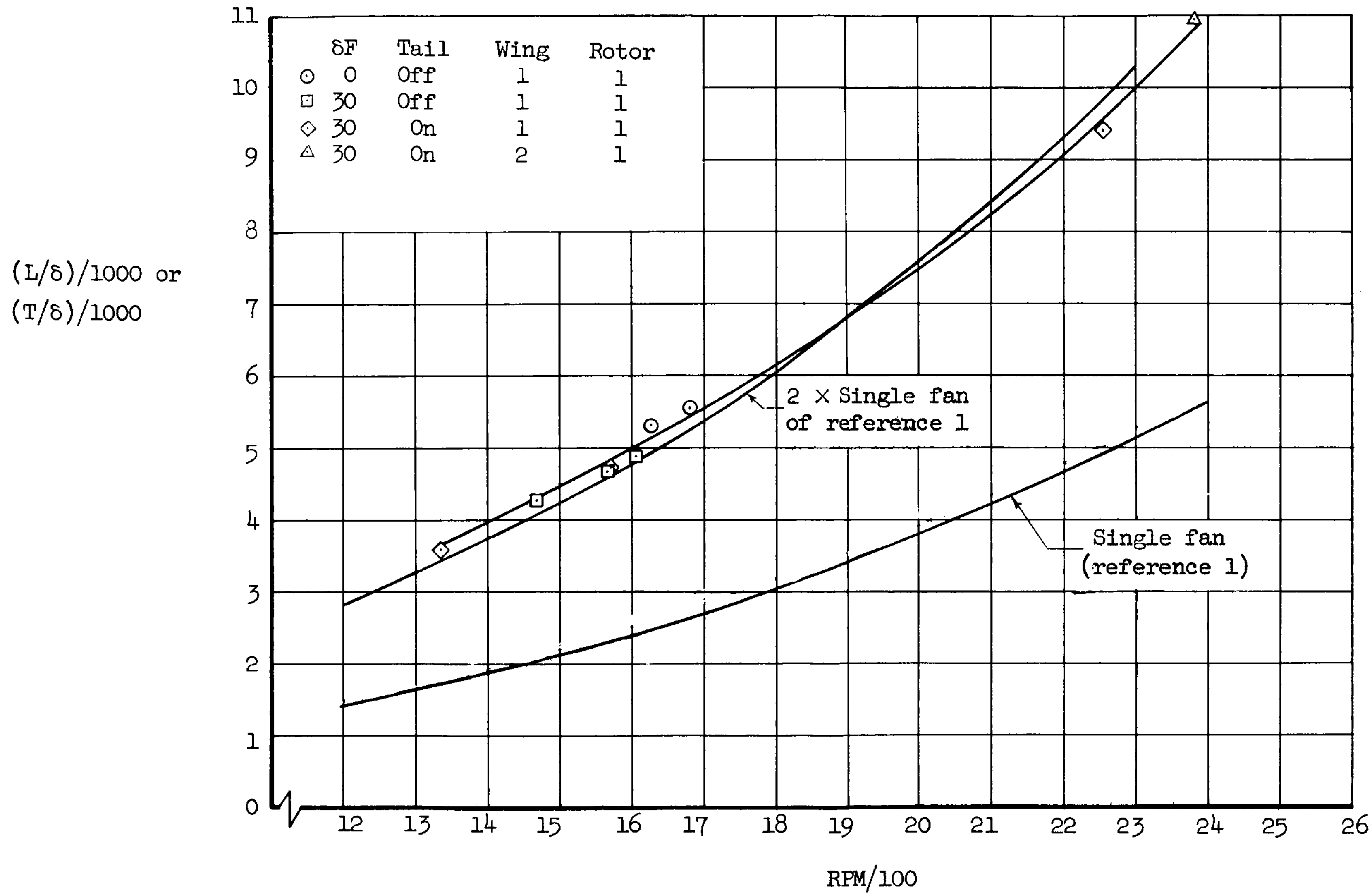

Figure 6.- Zero airspeed performance of the fan as installed in the wing; $\alpha = 0^{\circ}$, $\beta = 0^{\circ}$.

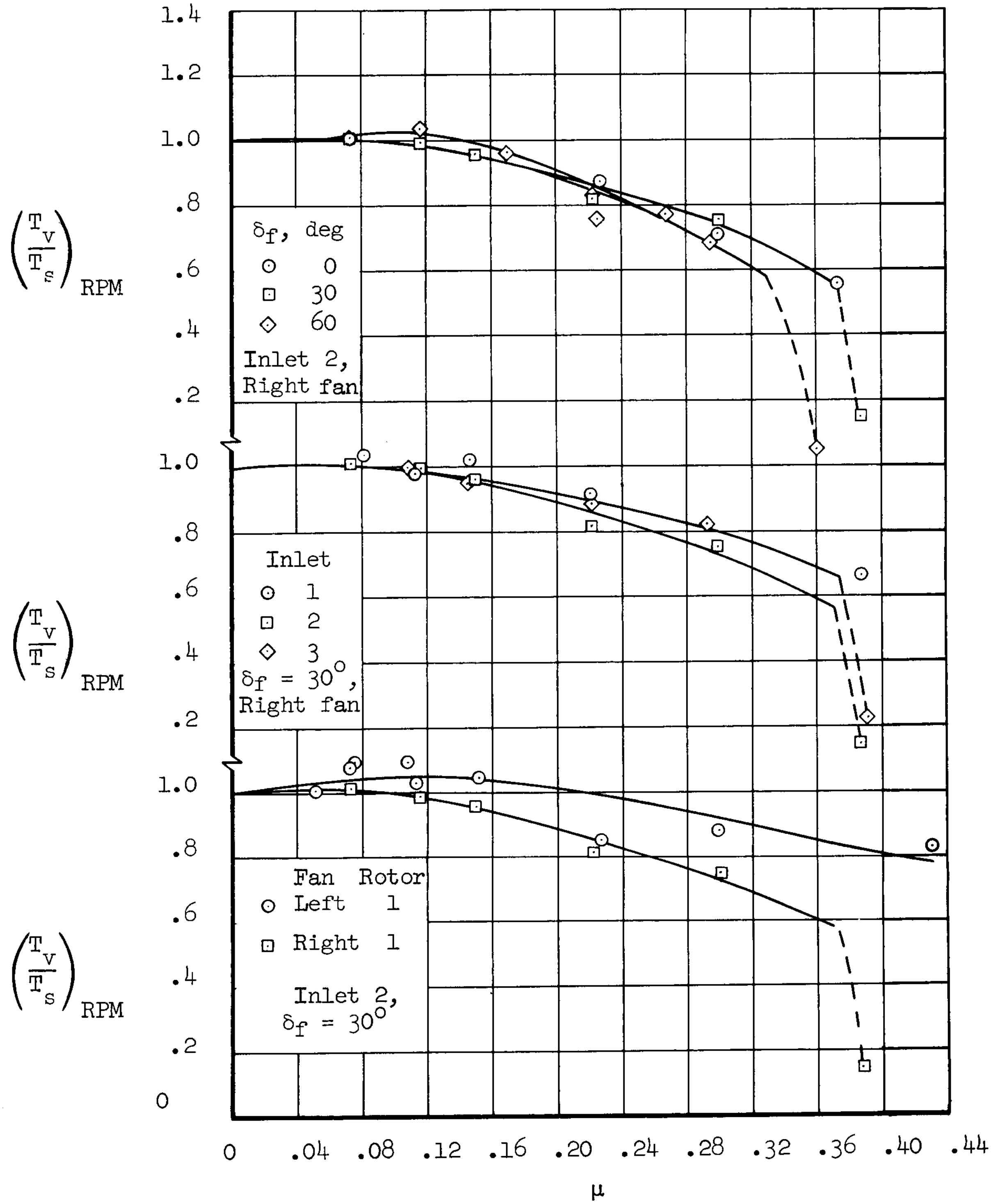

Figure 7.- The effect of airspeed (tip-speed ratio) on fan thrust; $\alpha = 0^\circ$, $\beta = 0^\circ$, 1100 to 2400 RPM.

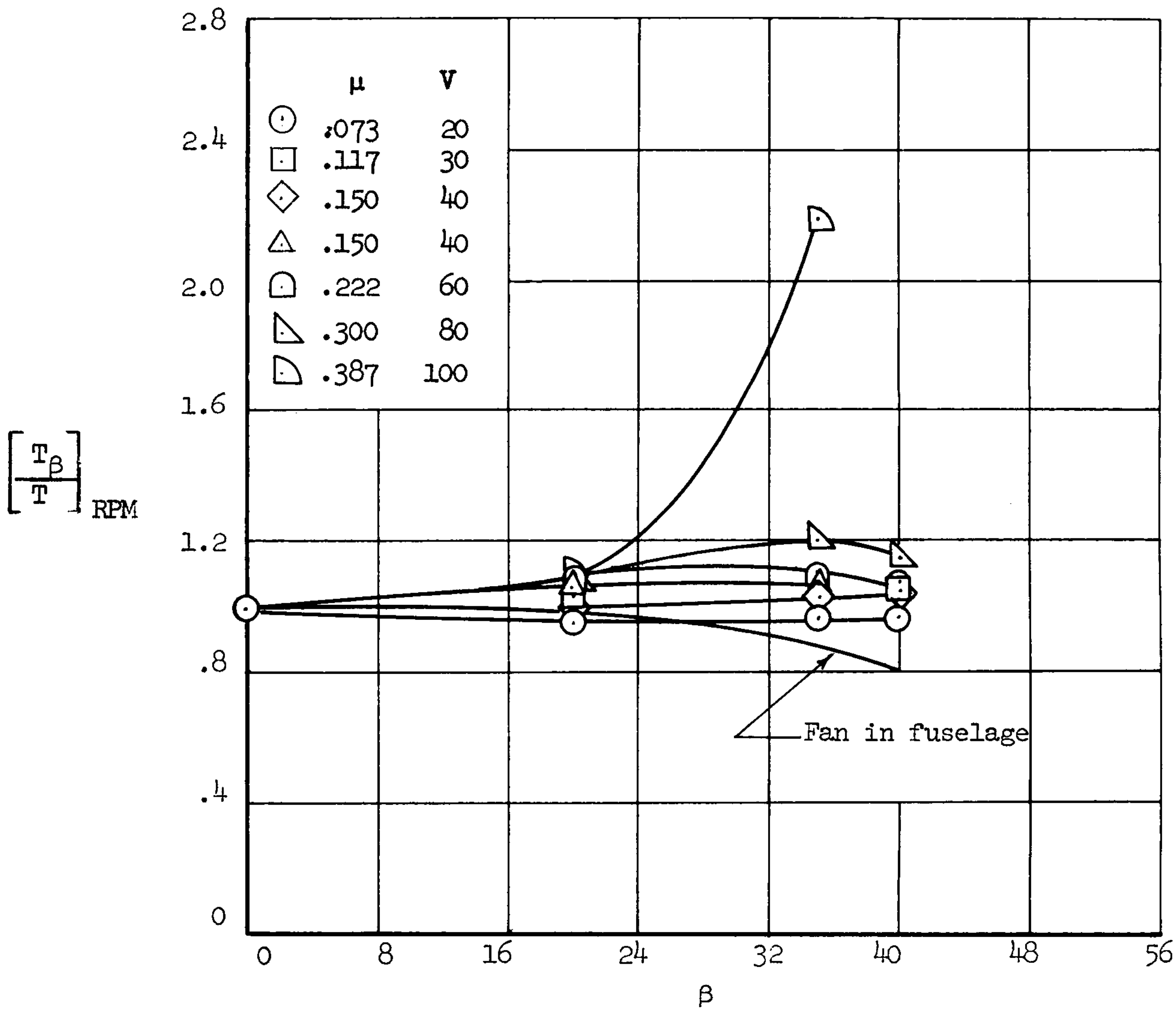

Figure 8.- The effect of exit-vane angle deflection on right fan thrust at several forward speeds; $\alpha = 0^{\circ}$, $\delta_f = 30^{\circ}$, 1700 RPM.

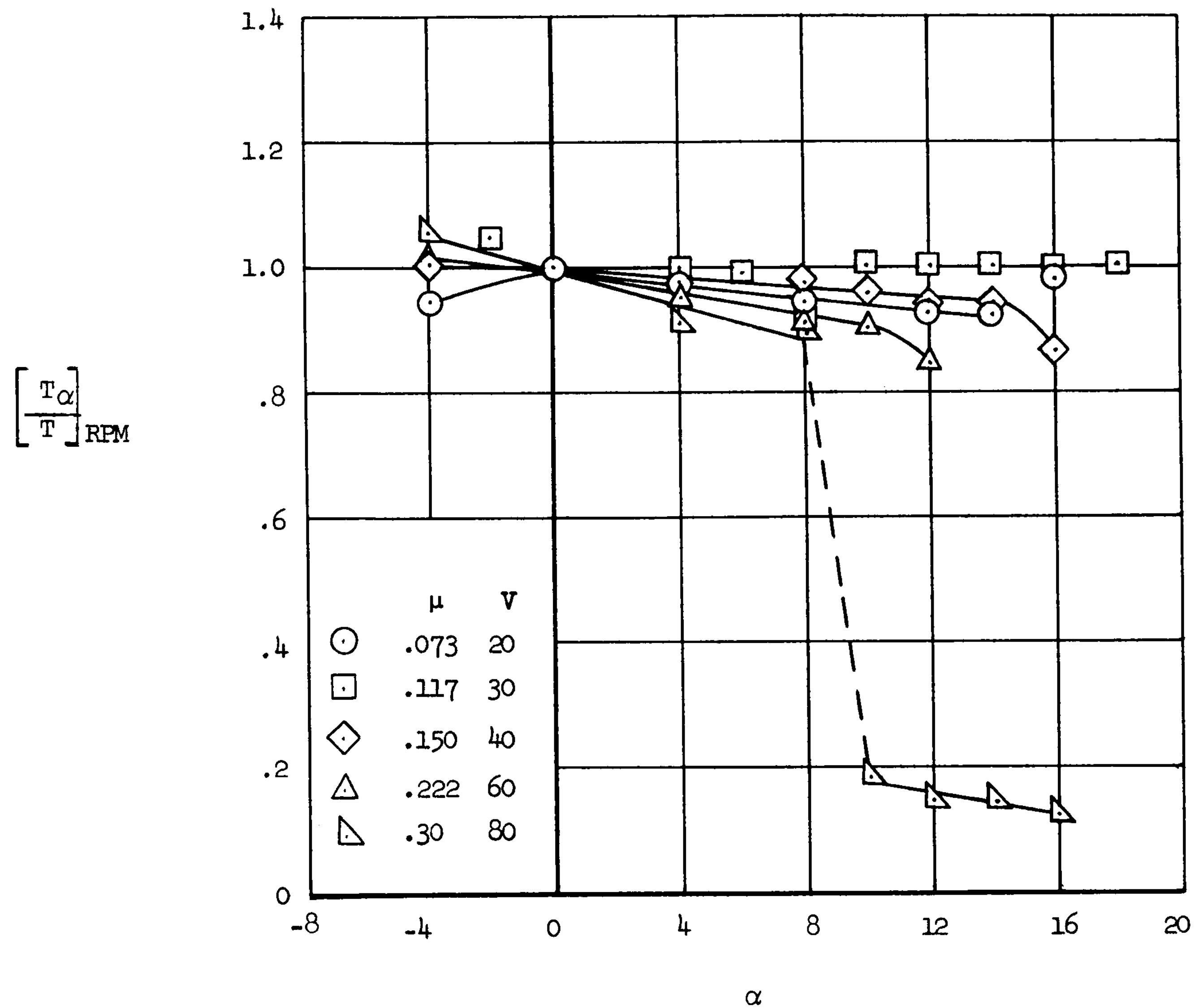

Figure 9.- The effect of angle of attack on thrust of right fan at several forward speeds; $\beta = 0^\circ$, $\delta_f = 30^\circ$, 1700 RPM.

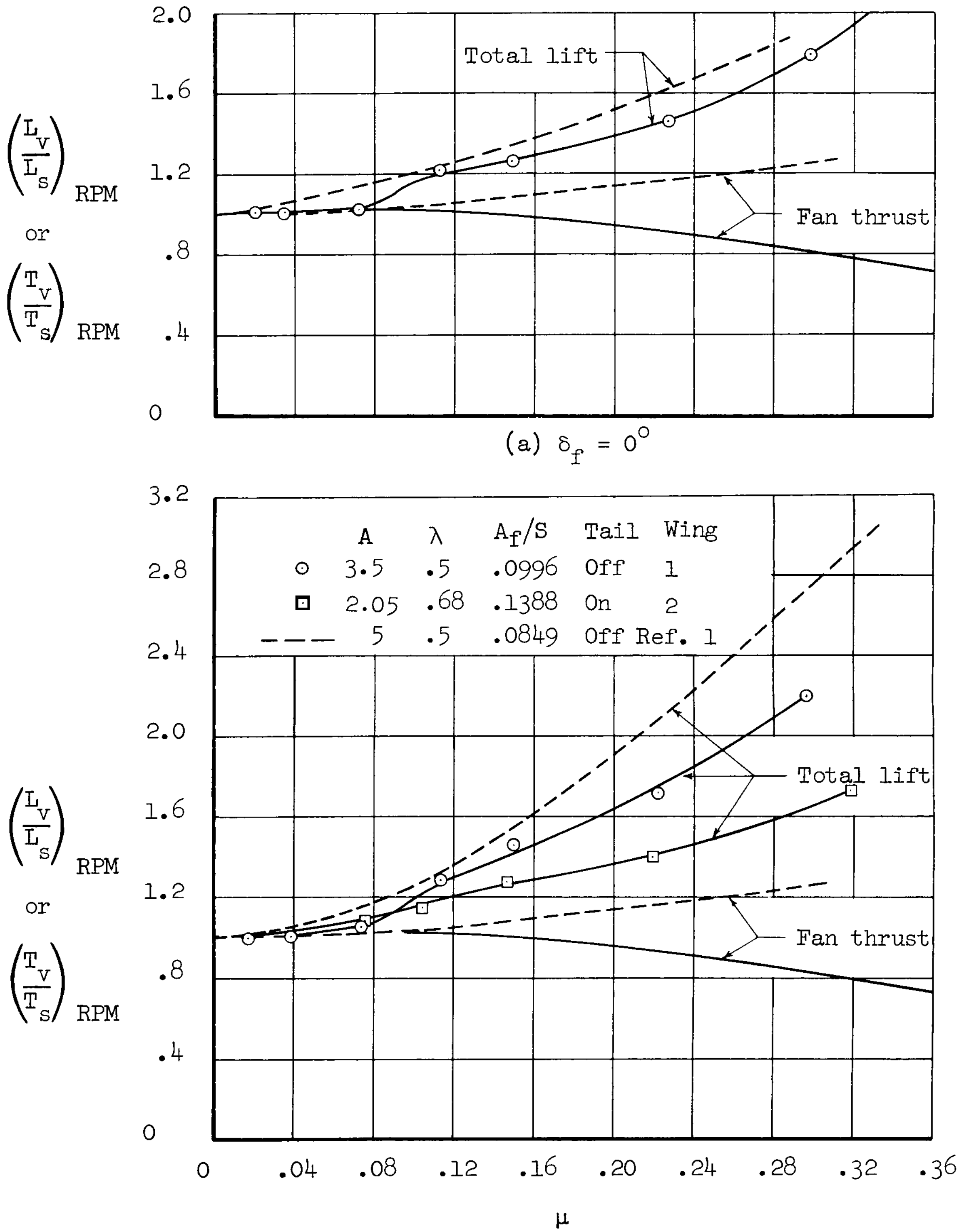

Figure 10.- The effect of forward speed and fan RPM (tip-speed ratio) on lift and thrust, tail off; $\alpha = 0^{\circ}$, $\beta = 0^{\circ}$.

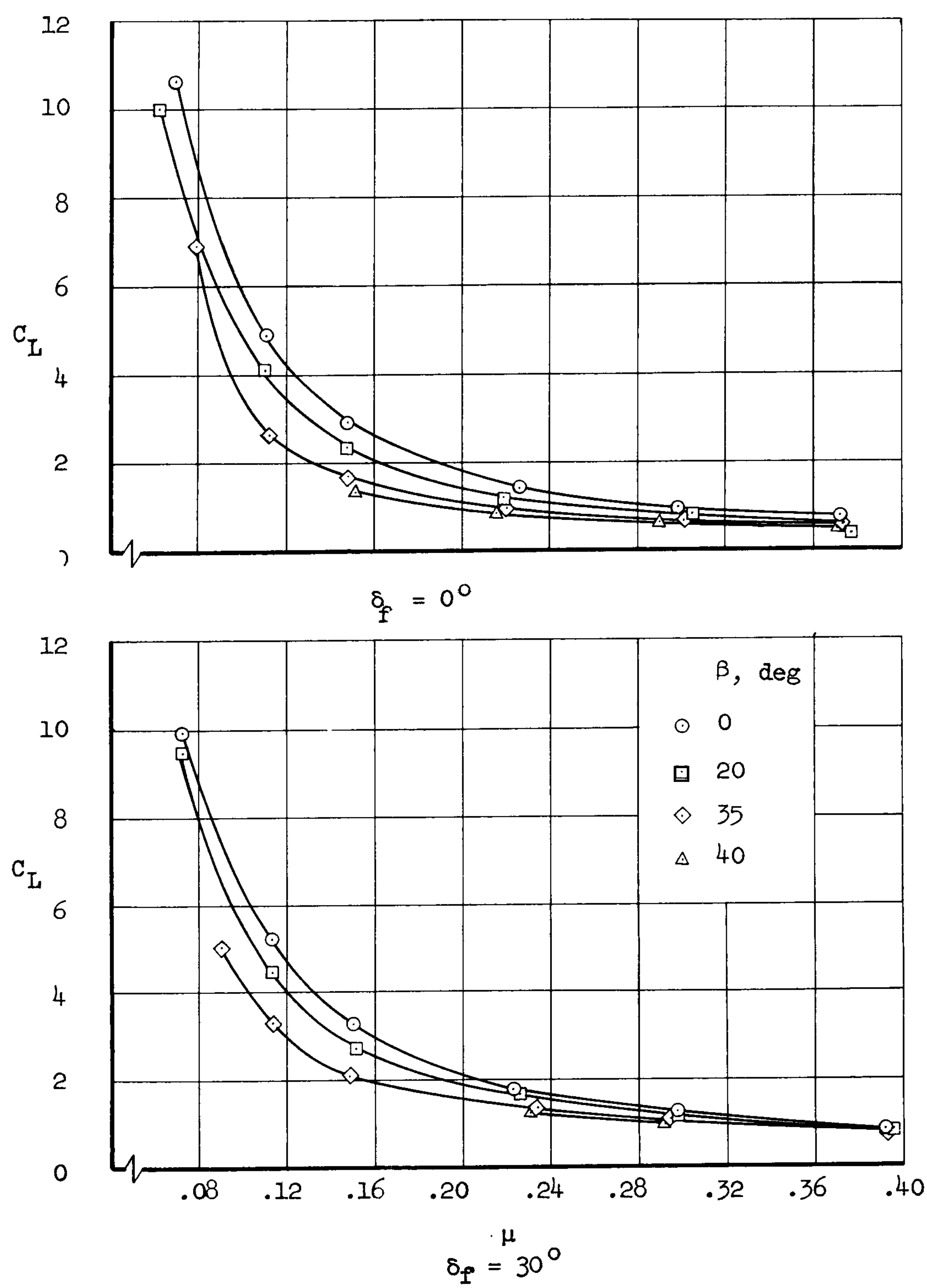

(a) Variation of lift coefficient.

Figure 11.- Variation of longitudinal characteristics with tip-speed ratio; tail off; $\alpha = 0^\circ$, 1700 RPM.

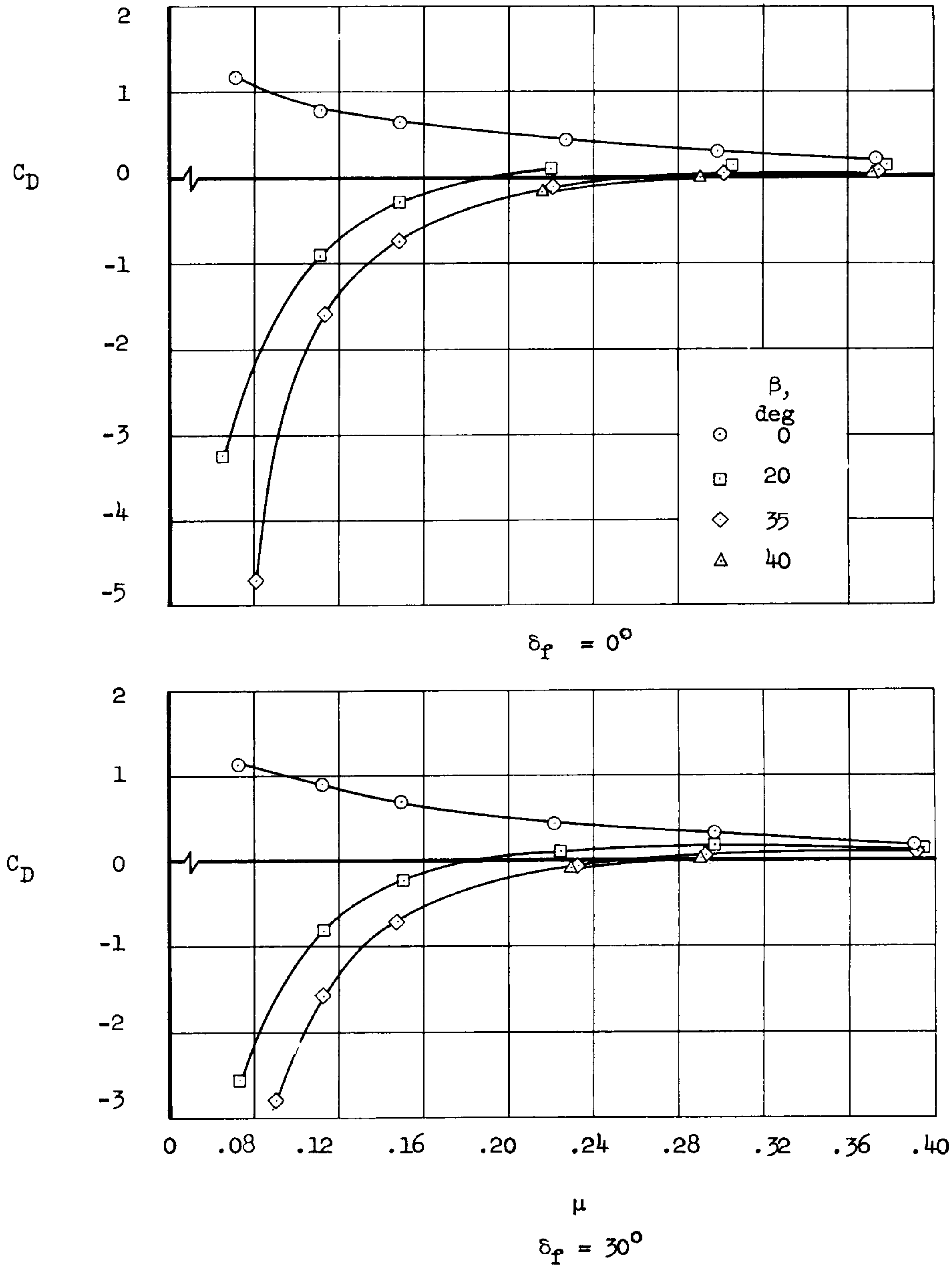

(b) Variation of drag coefficient

Figure 11.- Continued.

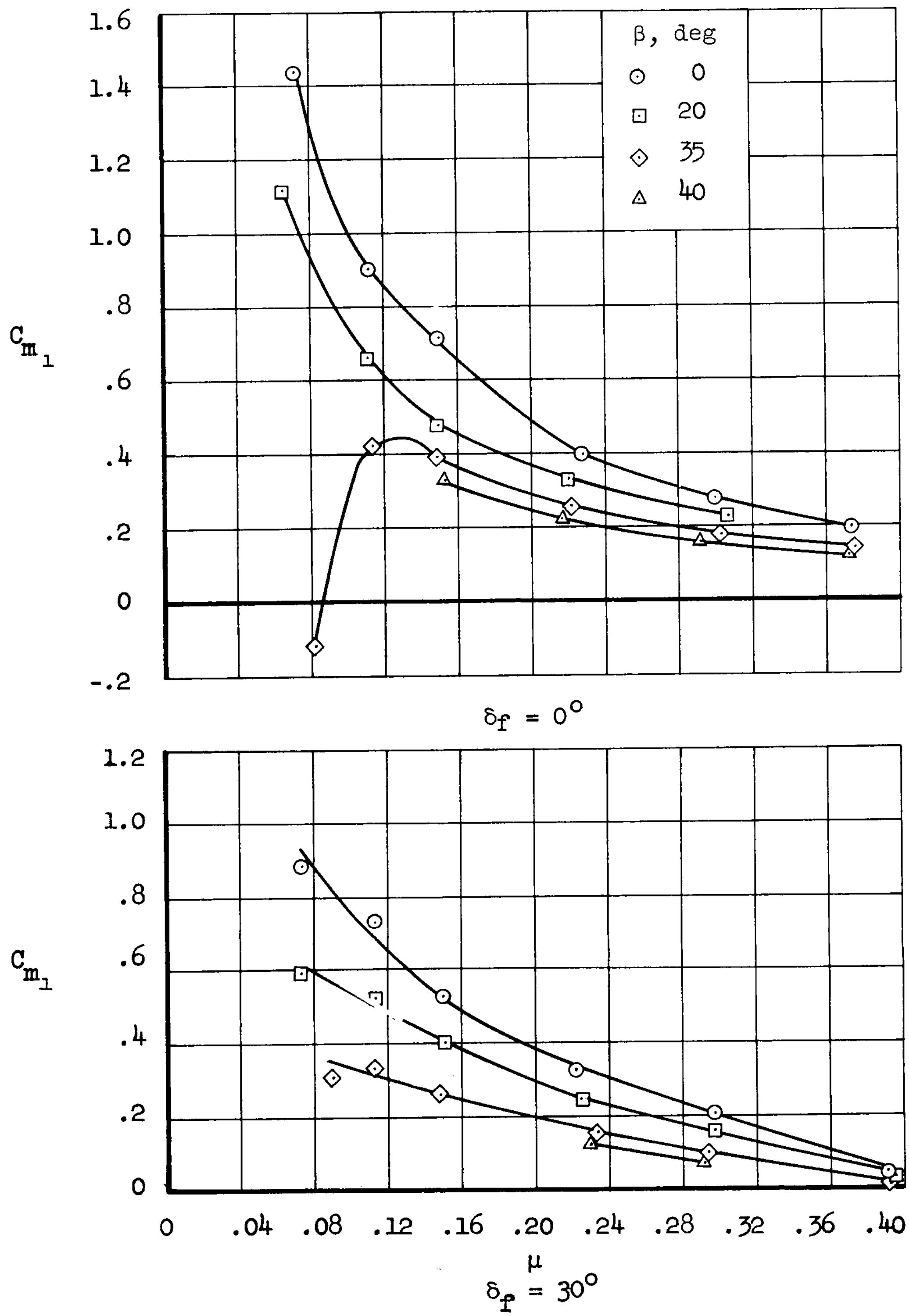

(c) Variation of moment coefficient, moment center 1.

Figure 11.- Continued.

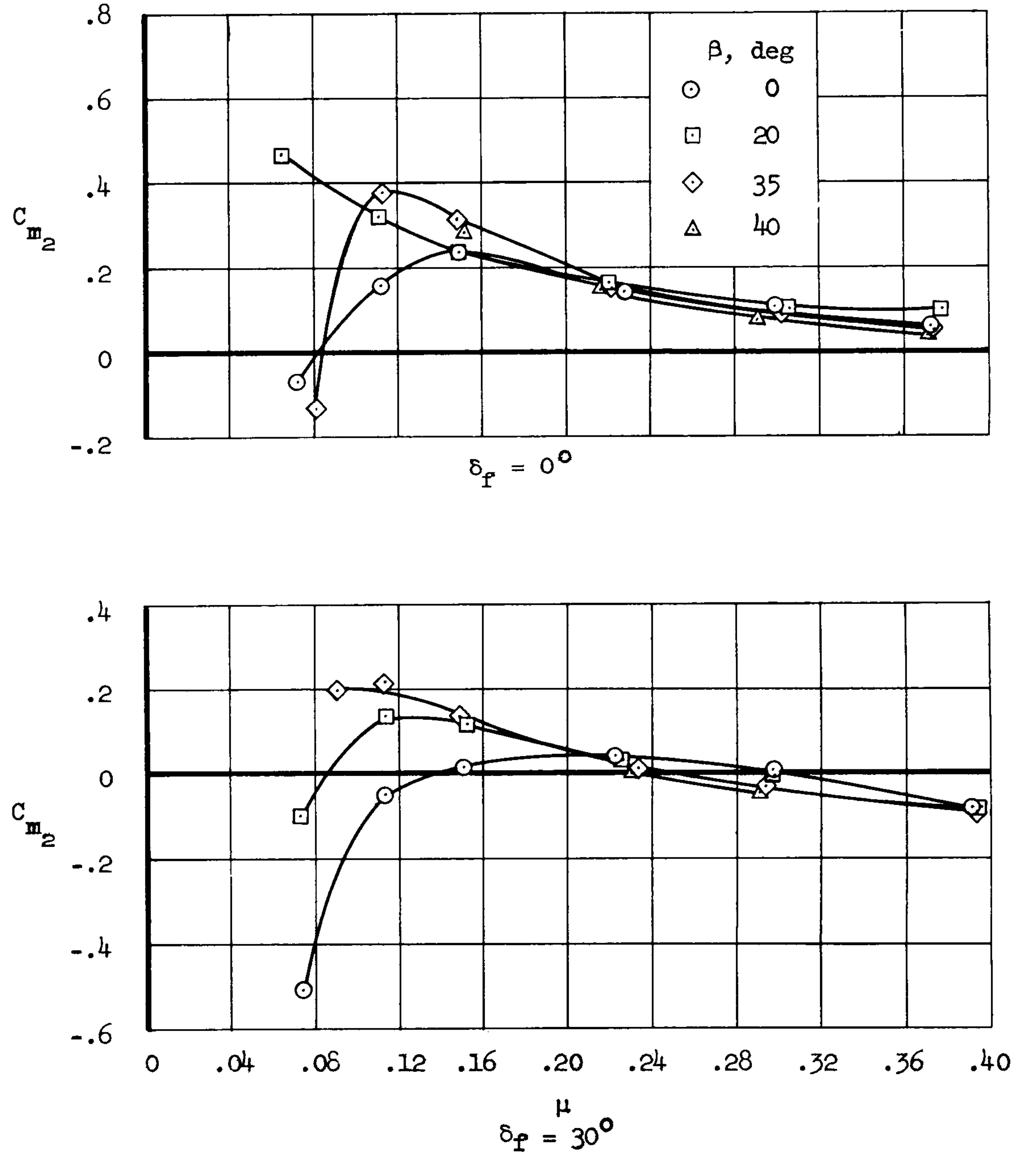

(d) Variation of moment coefficient, moment center 2.

Figure 11.- Concluded.

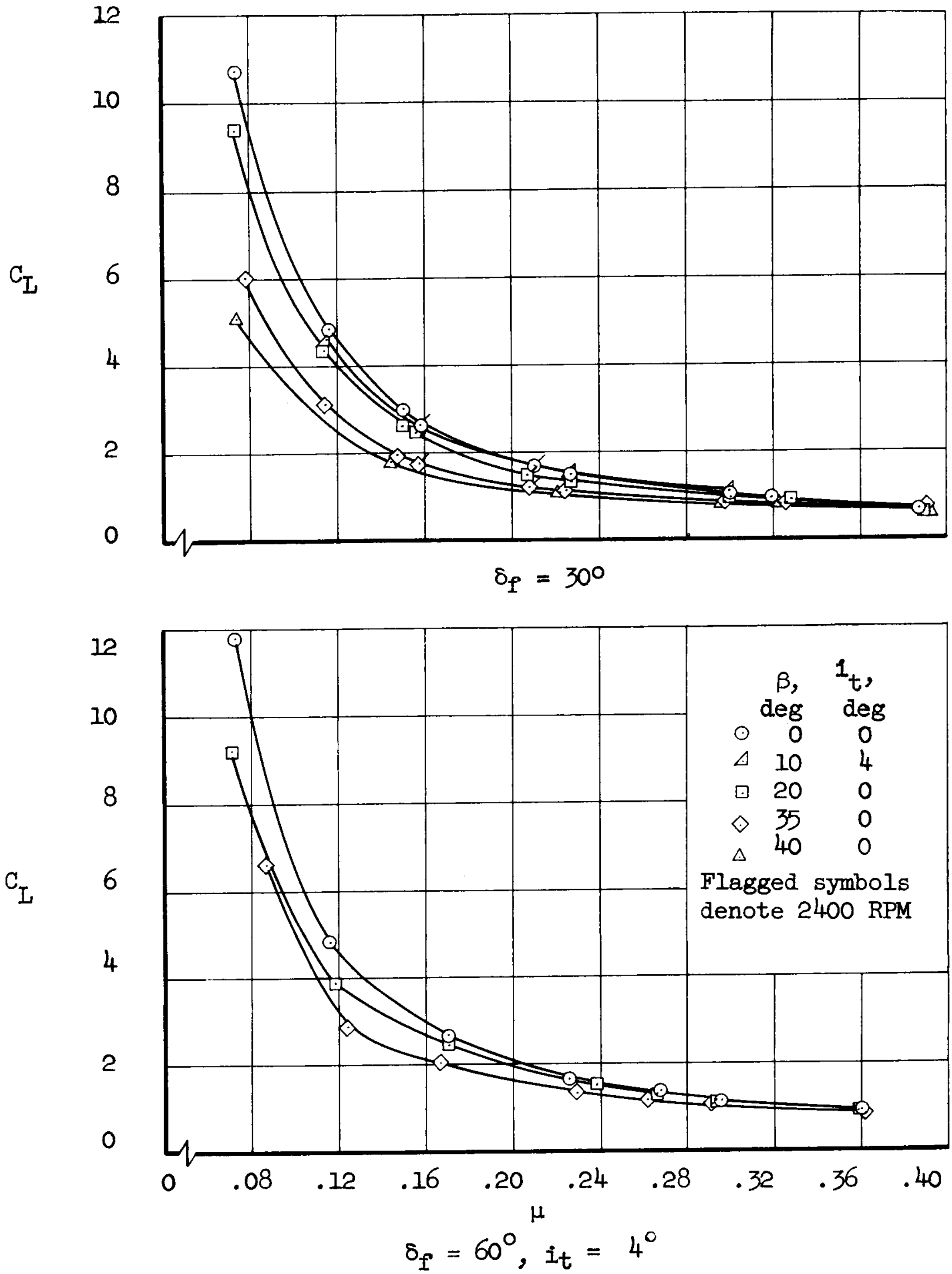

(a) Variation of lift coefficient.

Figure 12.- Variation of longitudinal characteristics with tip-speed ratio; tail on, $\alpha = 0^\circ$, 1700 RPM.

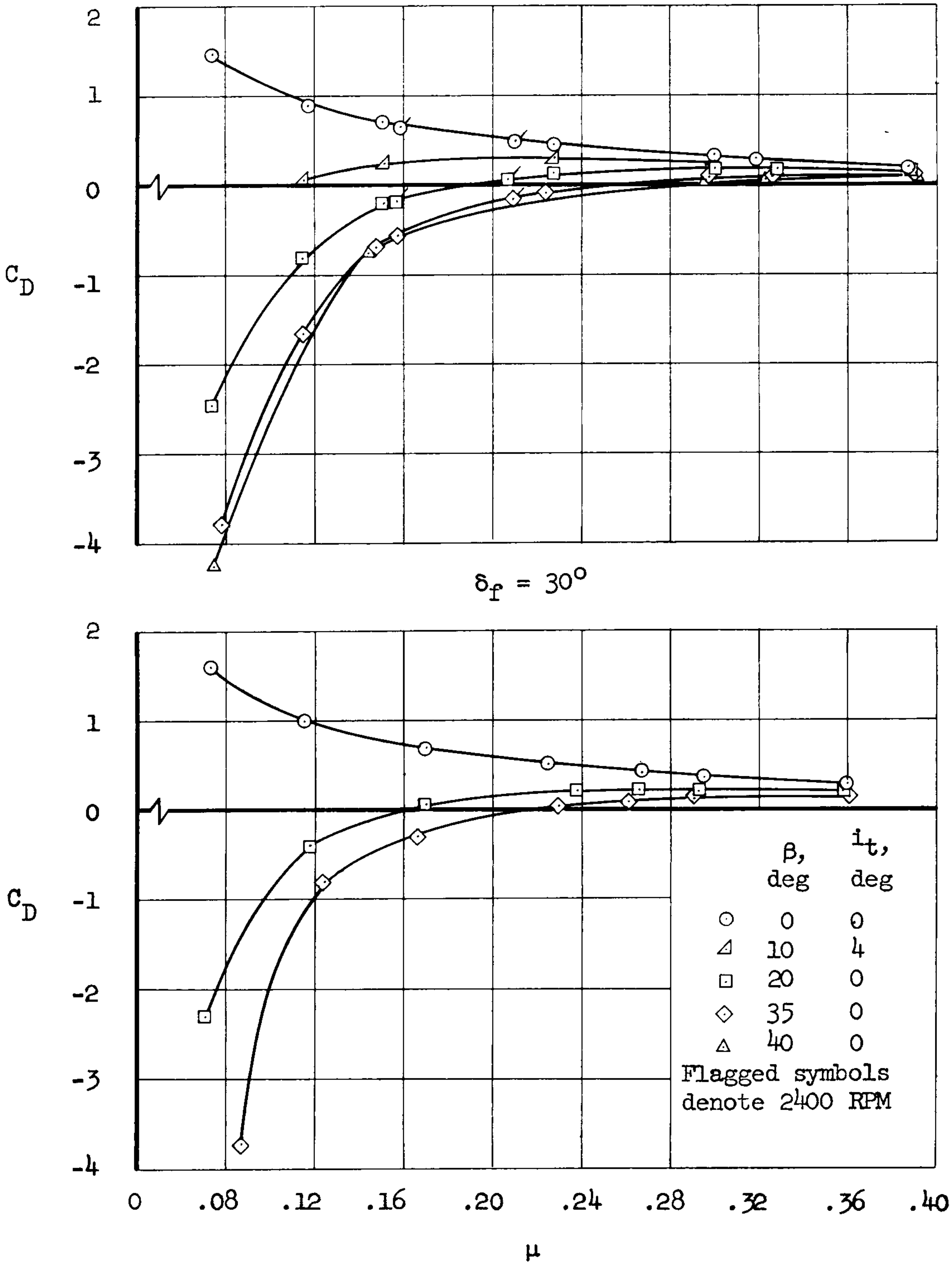

$\delta_f = 60^\circ \quad i_t = 4^\circ$

(b) Variation of drag coefficient.

Figure 12.- Continued.

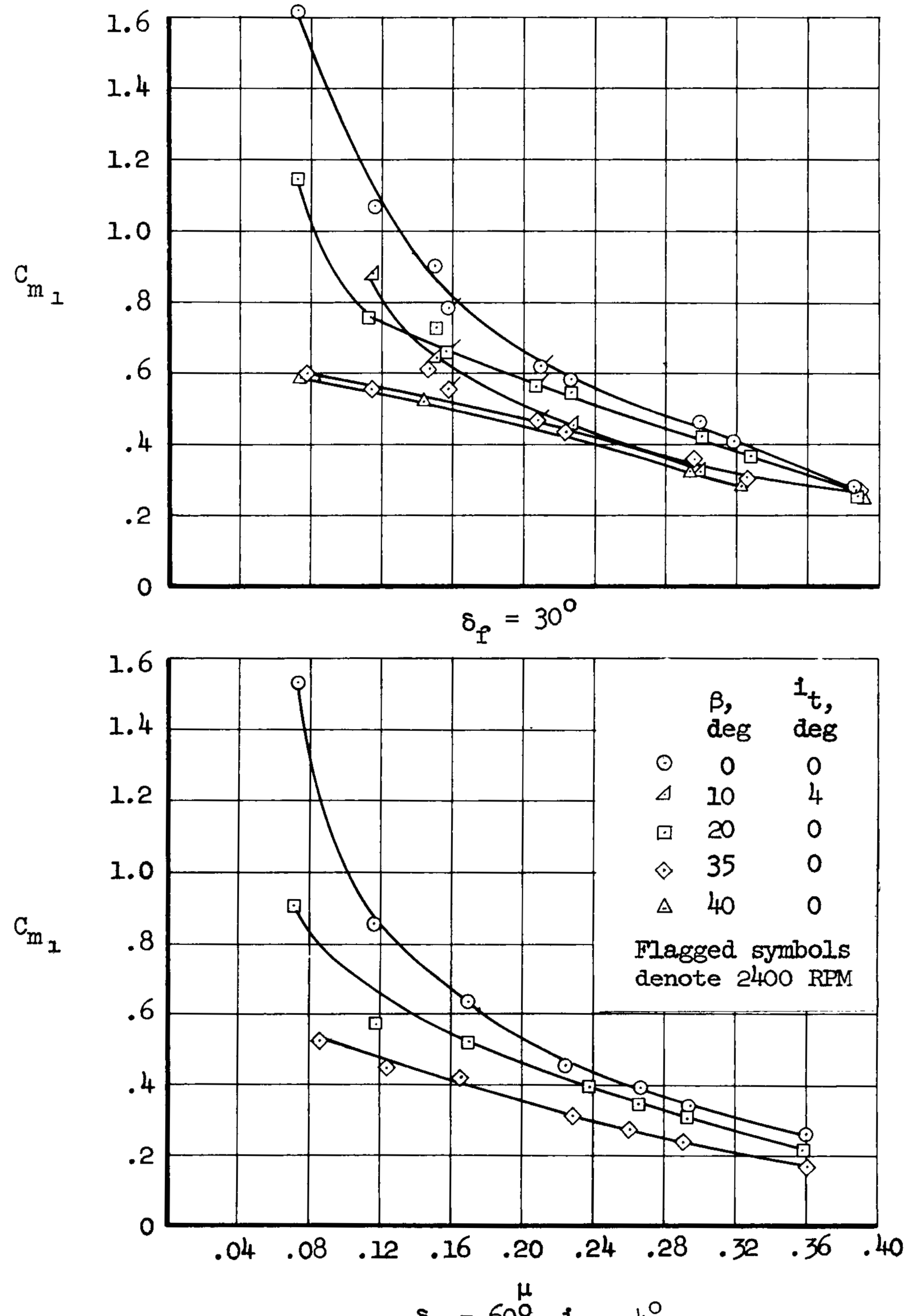

(c) Variation of moment coefficient, moment center 1.

Figure 12.- Continued.

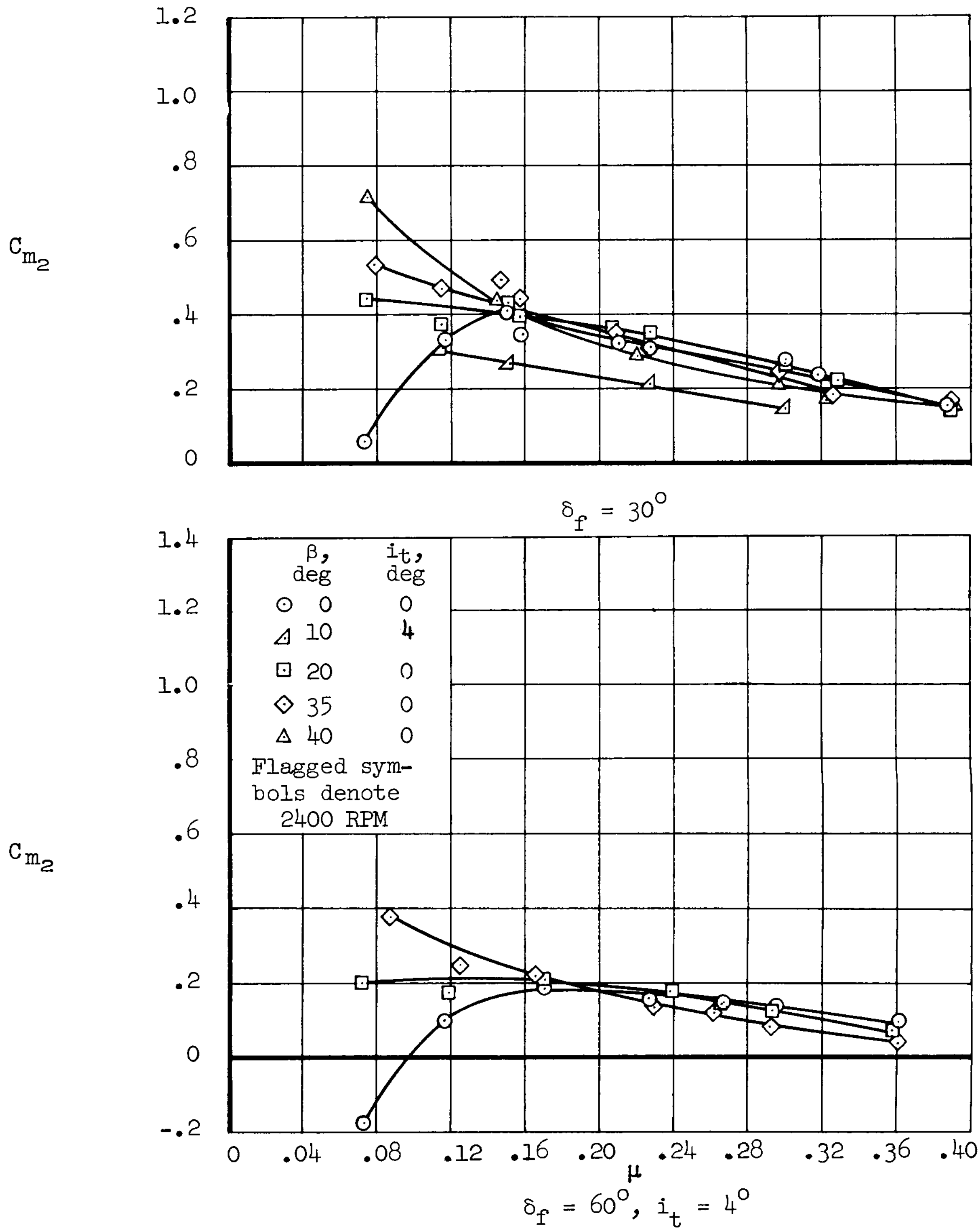

(d) Variation of moment coefficient, moment center 2.

Figure 12.- Concluded.

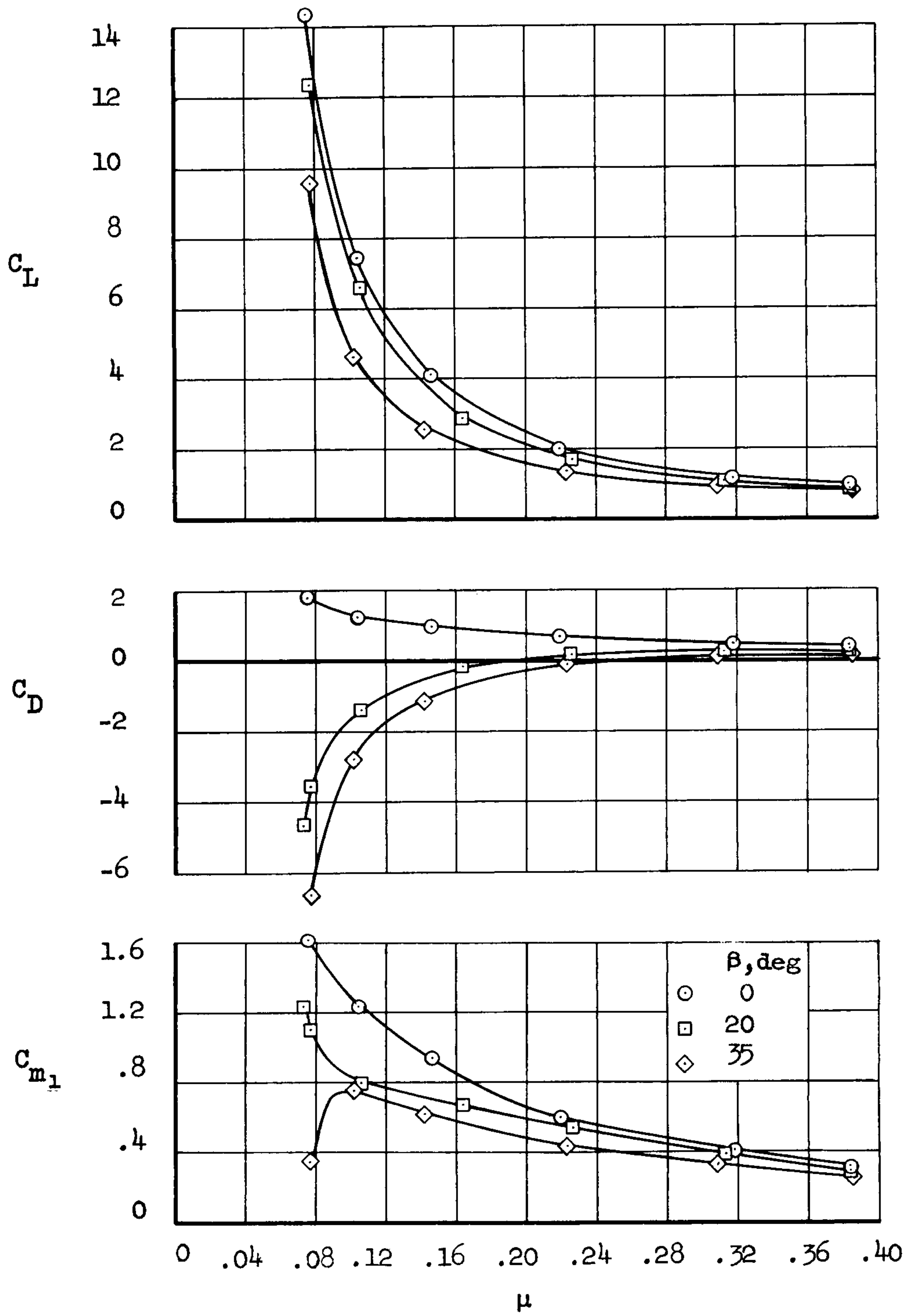

Figure 13.- Variation of longitudinal characteristics with tip-speed ratio; wing 2, tail on, $i_t = 4^\circ$, $\alpha = 0^\circ$, $\delta_f = 30^\circ$.

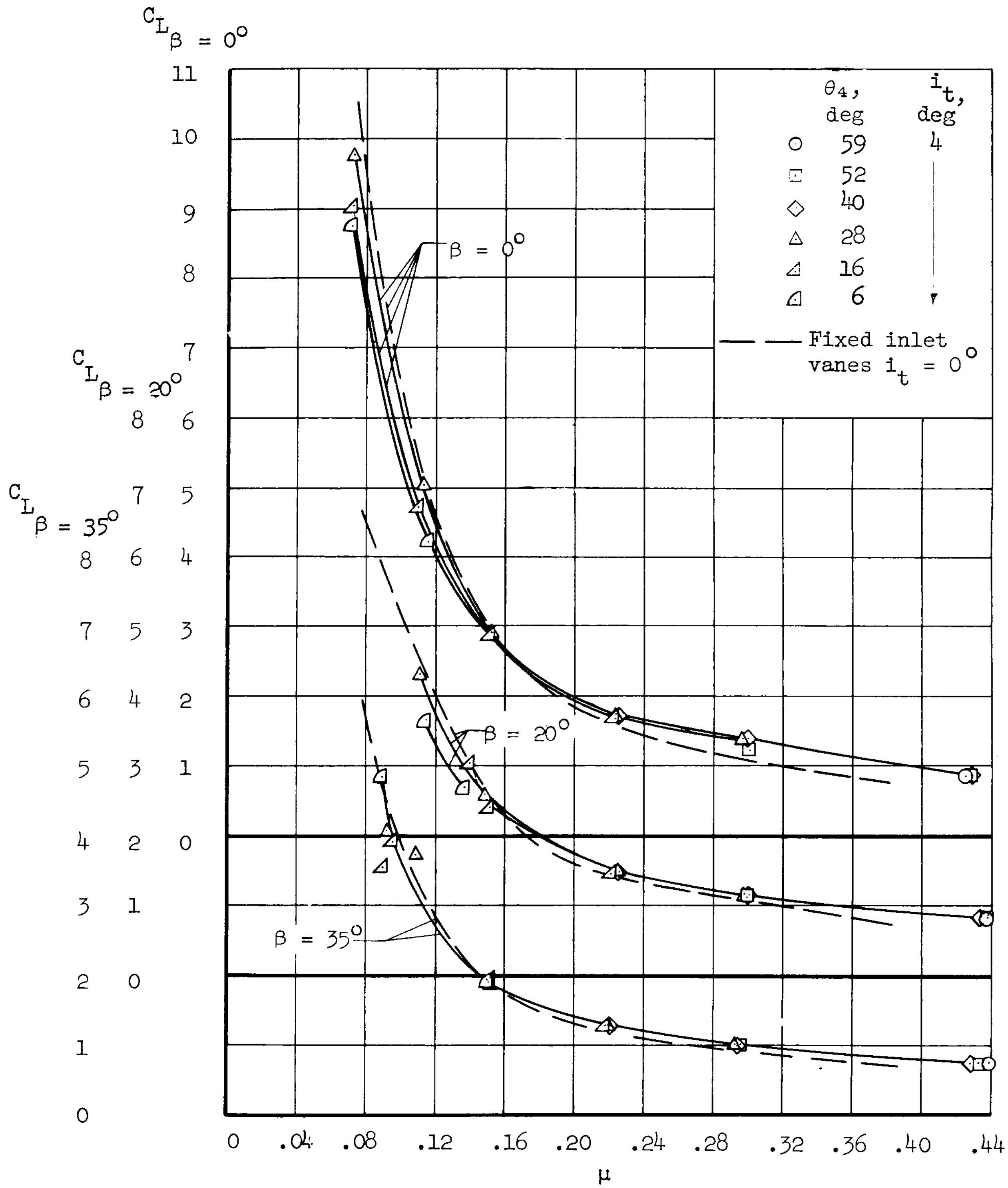

(a) Variation of lift coefficient.

Figure 14.- Variation of longitudinal characteristics with tip-speed ratio; inlet number 3, tail on, $\alpha = 0^{\circ}$, $\delta_f = 30^{\circ}$.

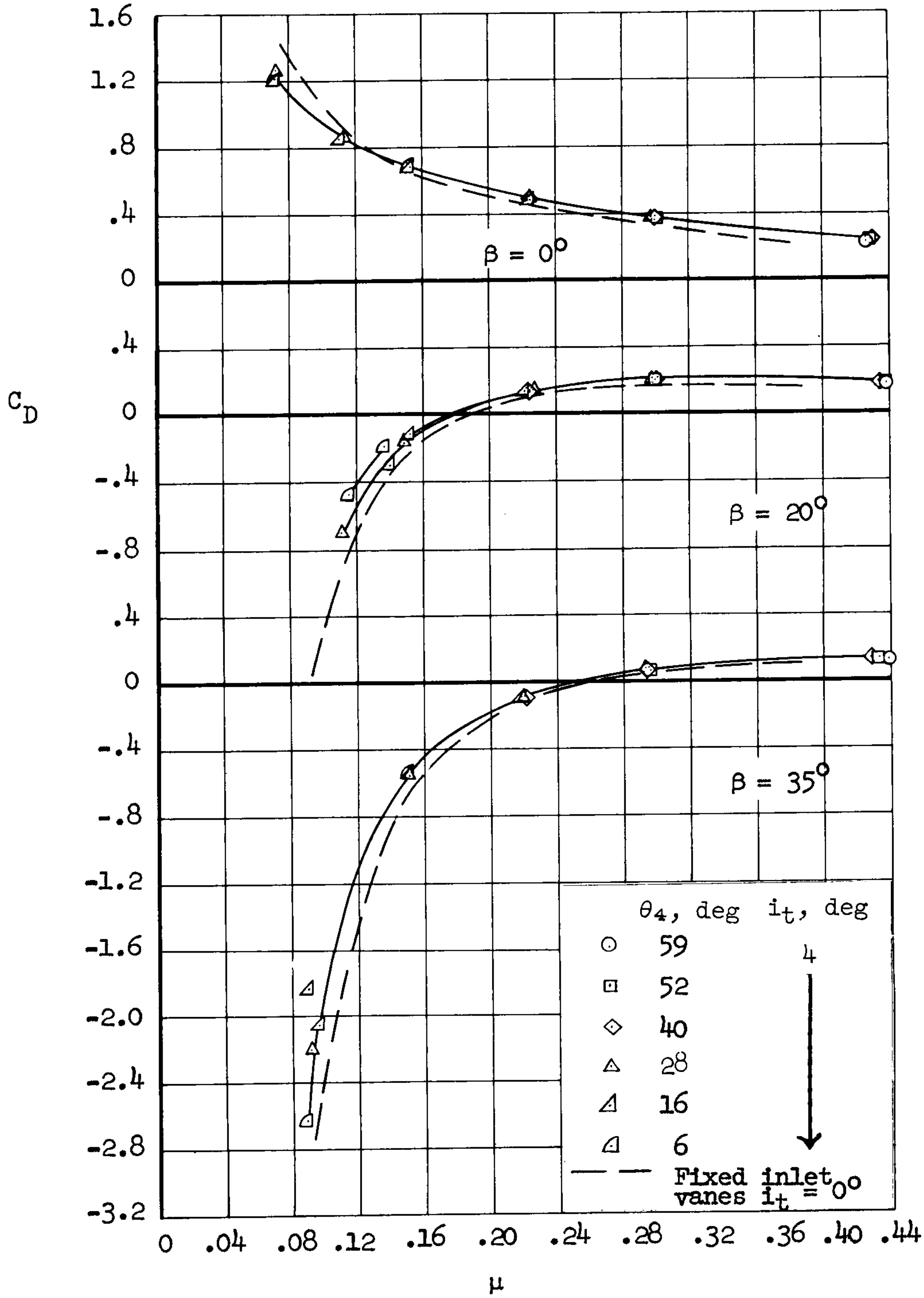

(b) Variation of drag coefficient.

Figure 14.- Continued.

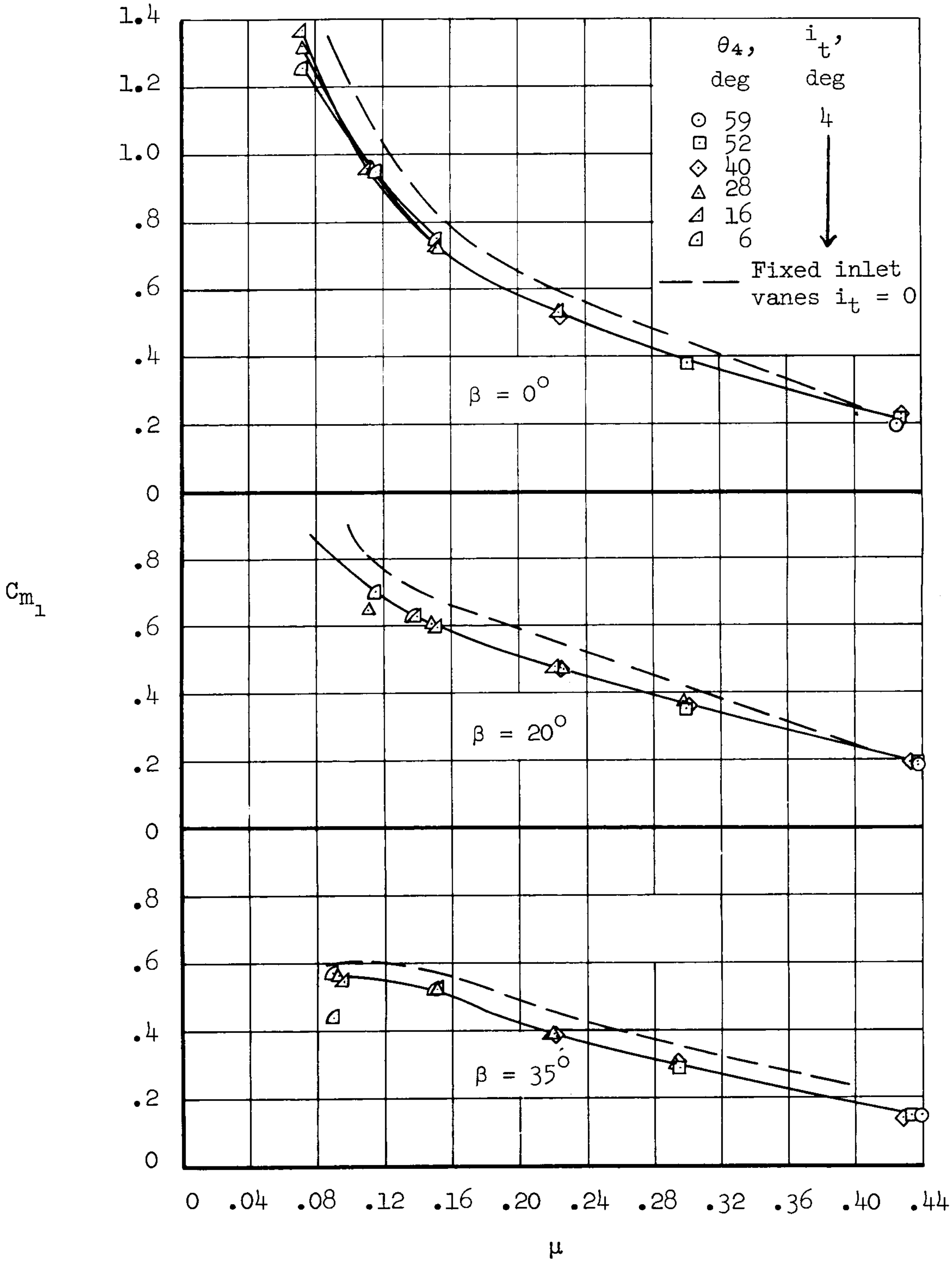

(c) Variation of moment coefficient.

Figure 14.- Concluded.

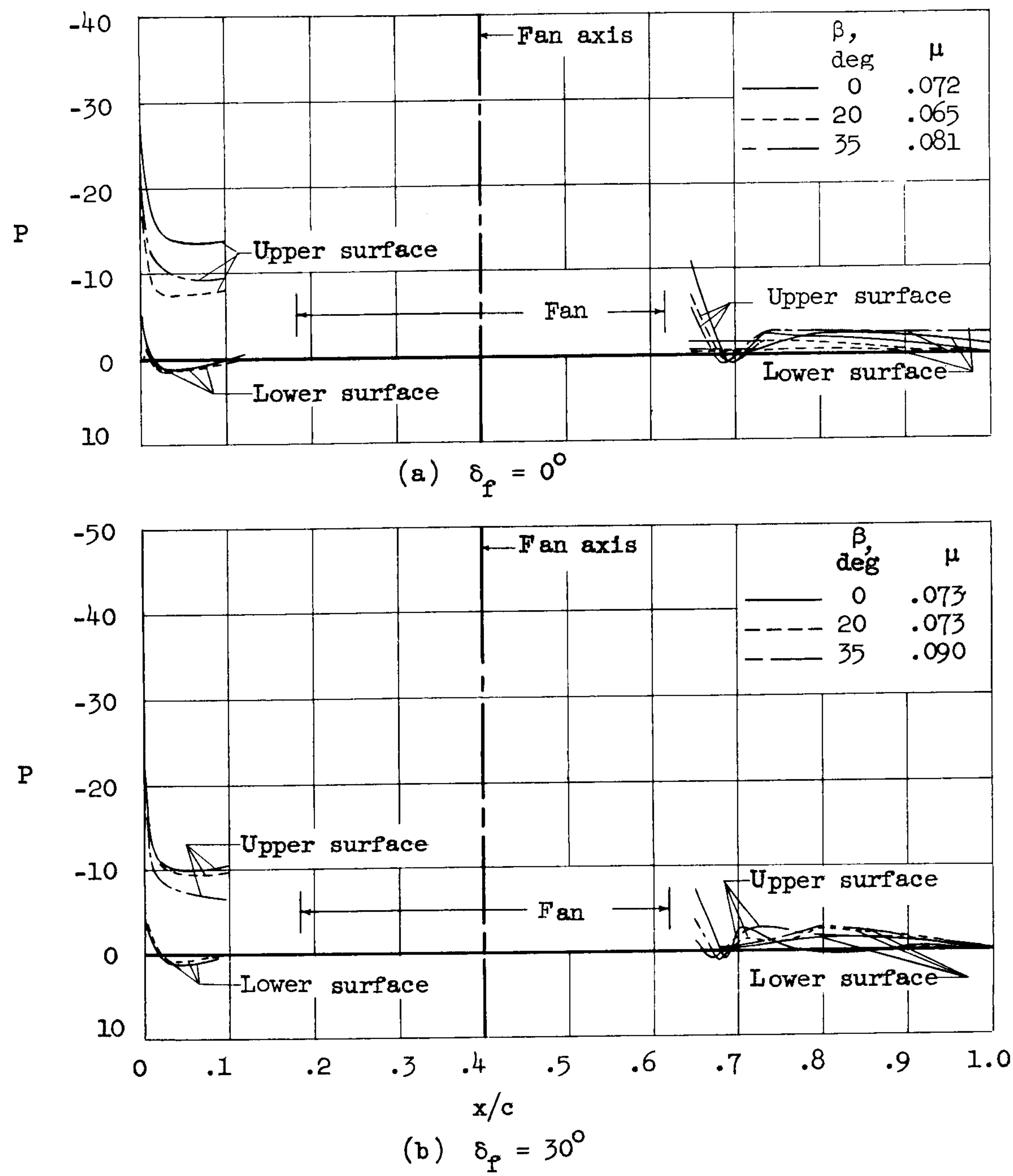

Figure 15.- Streamwise wing surface pressure distribution through the fan axis; $\mu = 0.07$, $V = 20$, $\alpha = 0^o$, 1700 RPM.

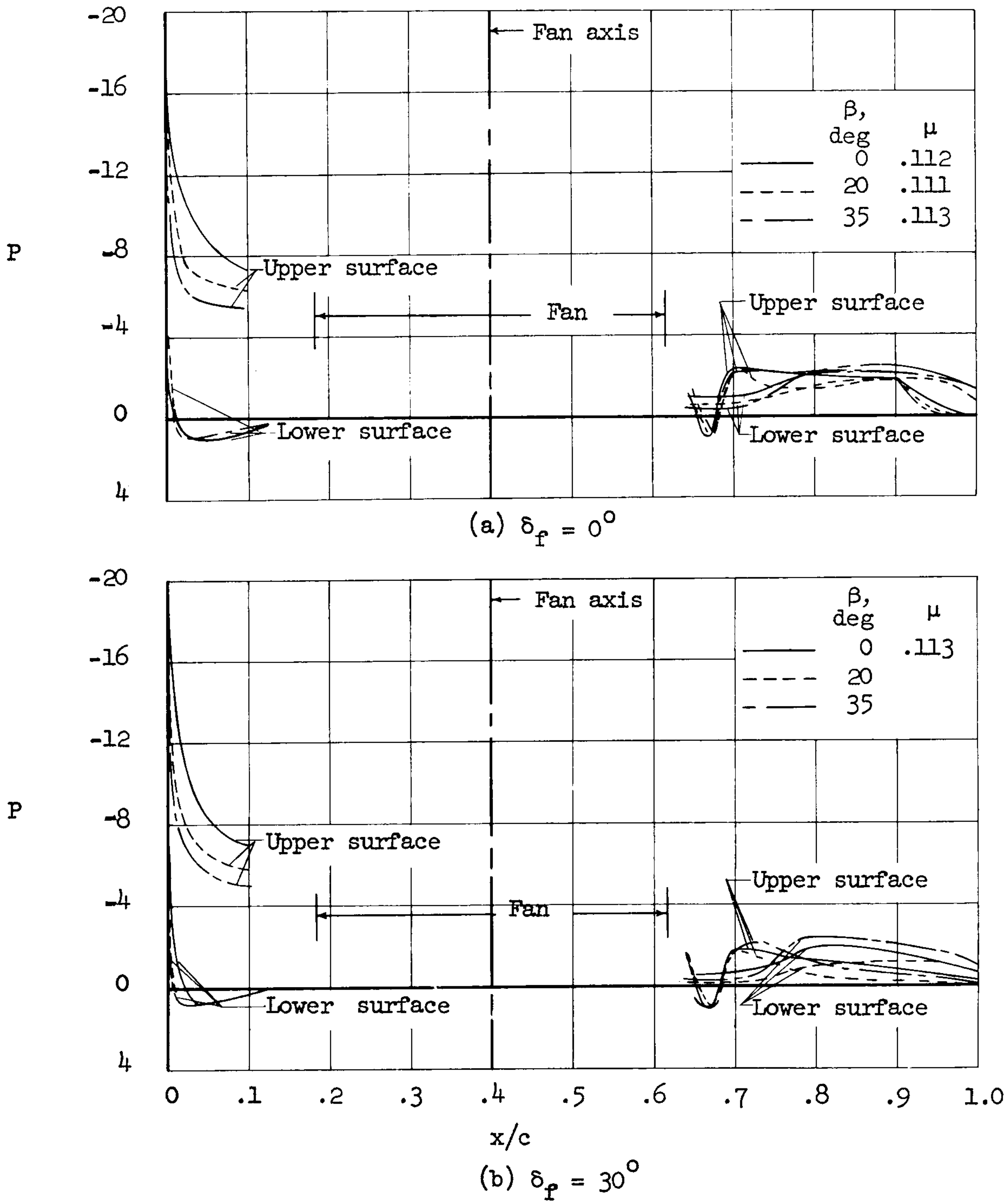

Figure 16.- Streamwise wing surface pressure distributions through fan axis; $\mu = 0.11$, $V = 30$, $\alpha = 0^\circ$, 1700 RPM.

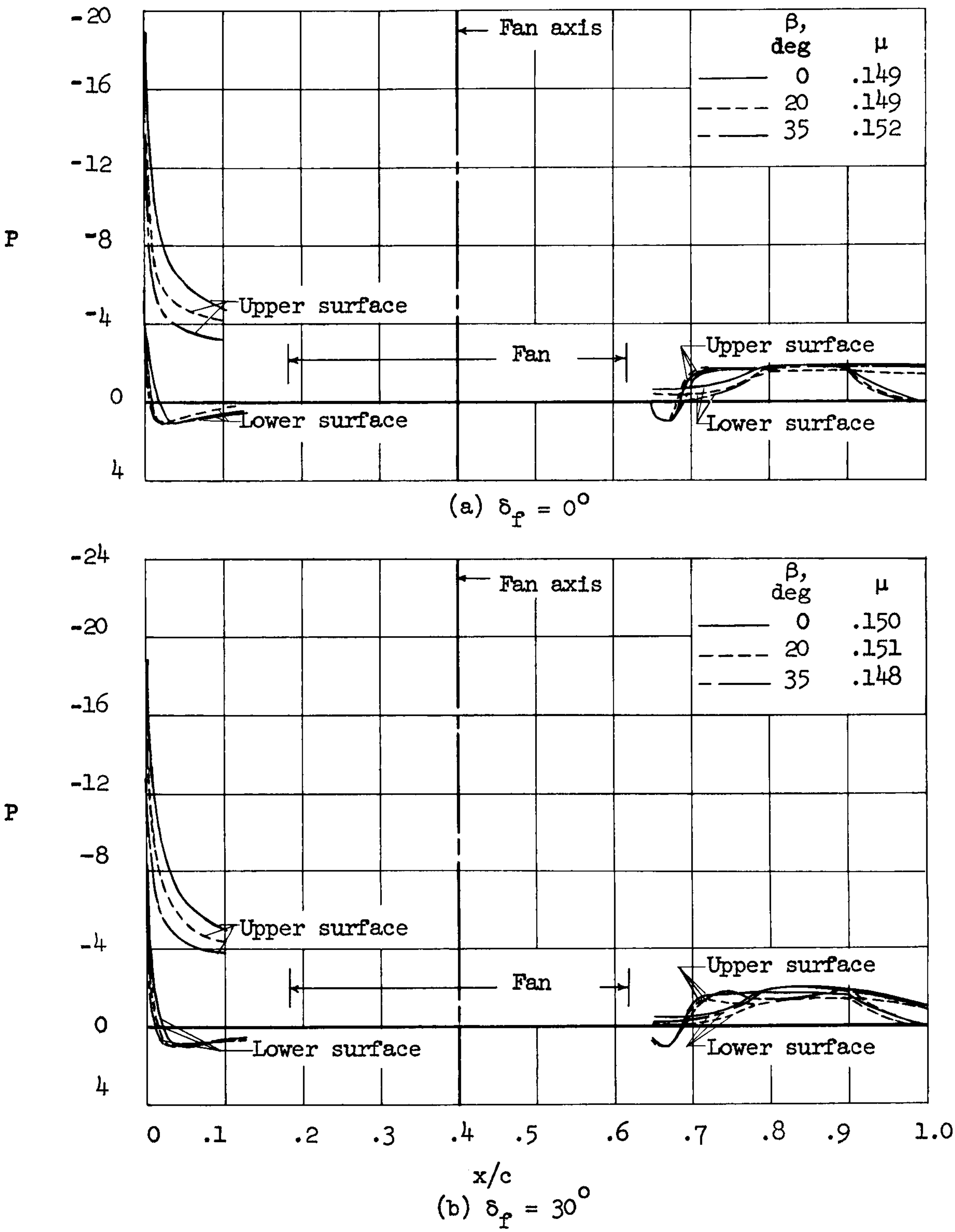

Figure 17.- Streamwise wing surface pressure distribution through the fan axis; $\mu = 0.15$, $V = 40$, $\alpha = 0^\circ$, 1700 RPM.

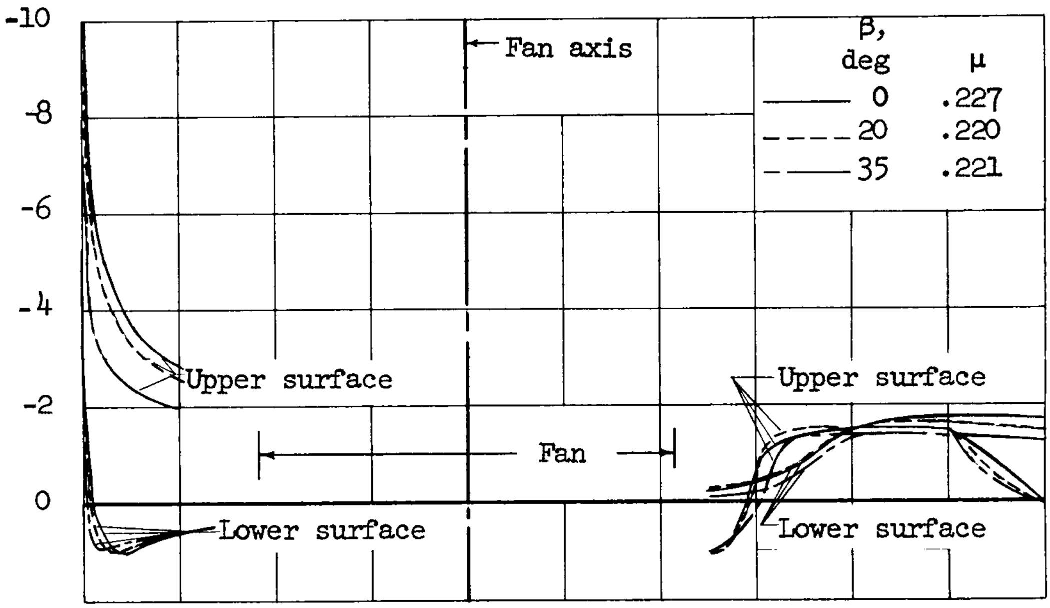

(a) $\delta_f = 0^\circ$

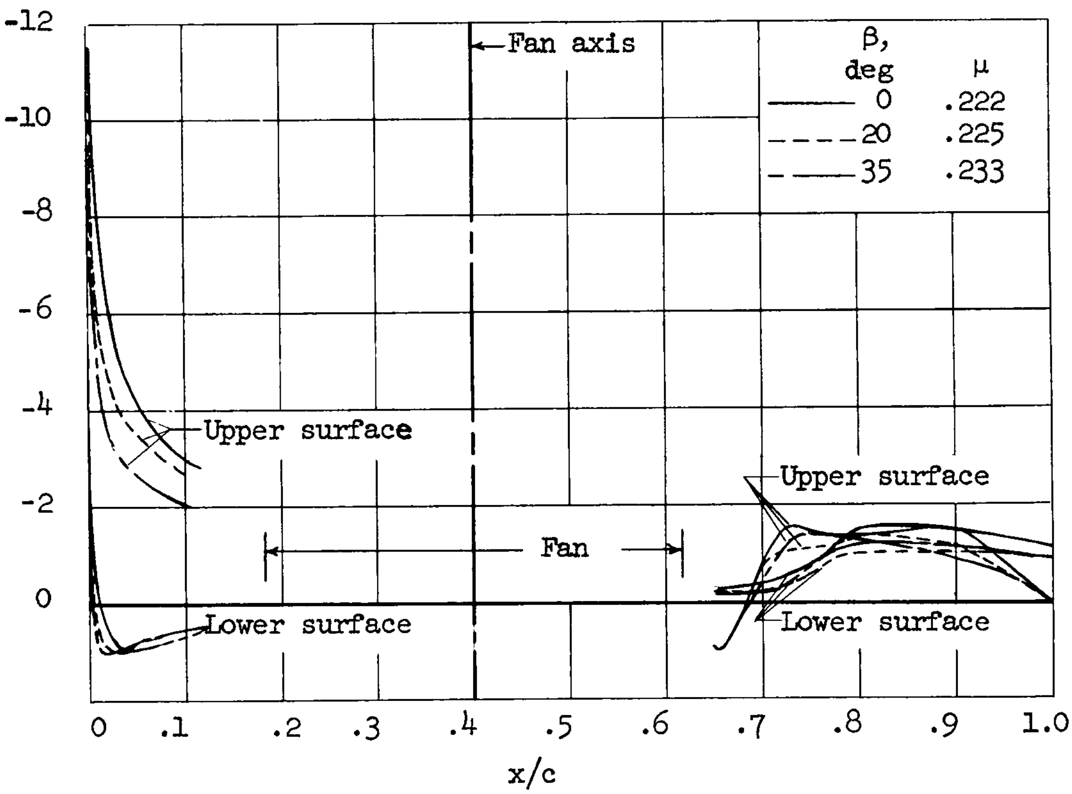

(b) $\delta_f = 30^\circ$

Figure 18.- Streamwise wing surface pressure distributions through the fan axis; $\mu = 0.22$, $V = 60$, $\alpha = 0^\circ$, 1700 RPM.

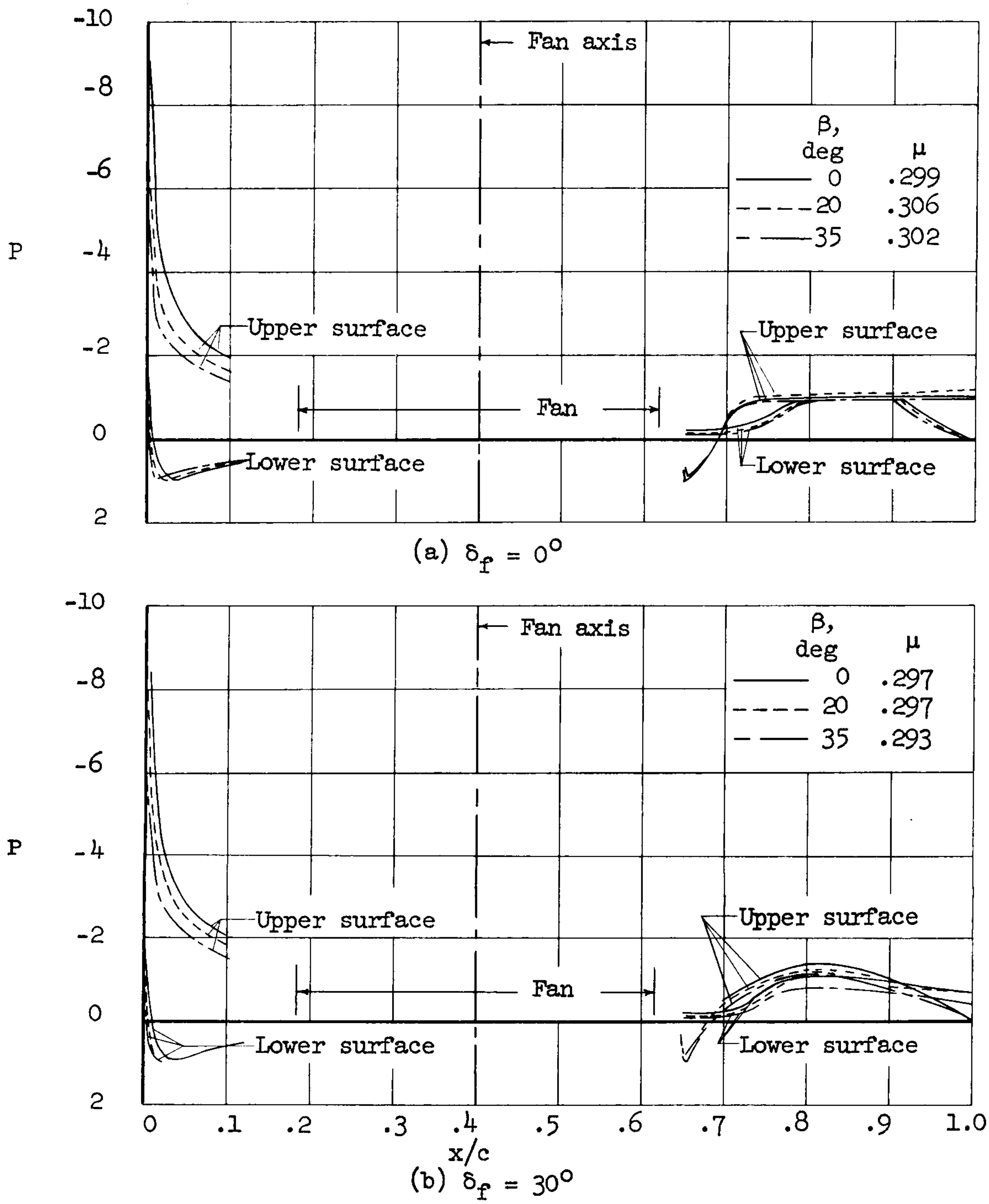

Figure 19.- Streamwise wing surface pressure distributions through the fan axis; $\mu = 0.30$, $V = 80$, $\alpha = 0^\circ$, 1700 RPM.

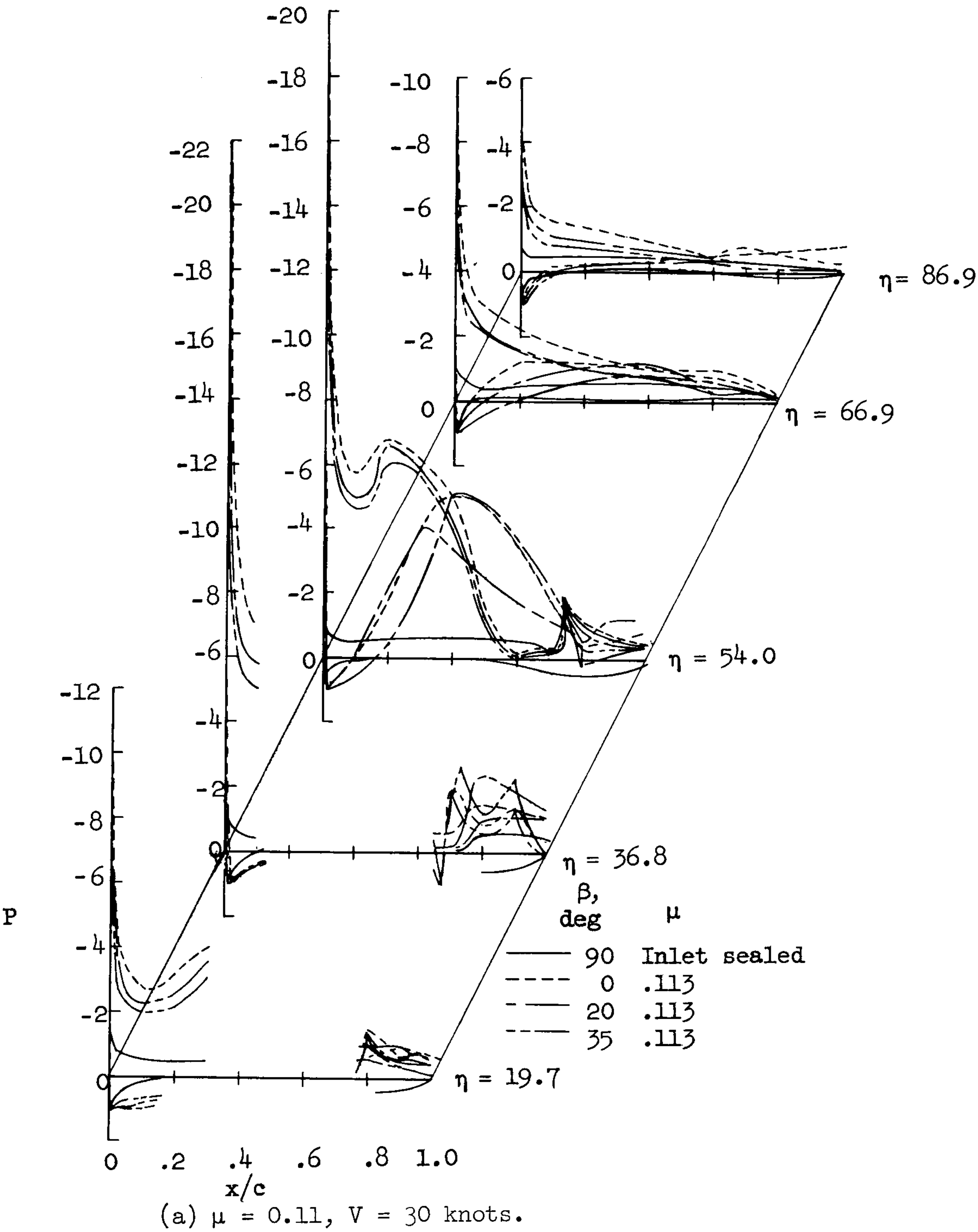

(a) μ = 0.11, V = 30 knots.

Figure 20.- Chordwise pressure distributions on the wing; $\delta_f = 30^\circ$, $\alpha = 0^\circ$, 1700 RPM.

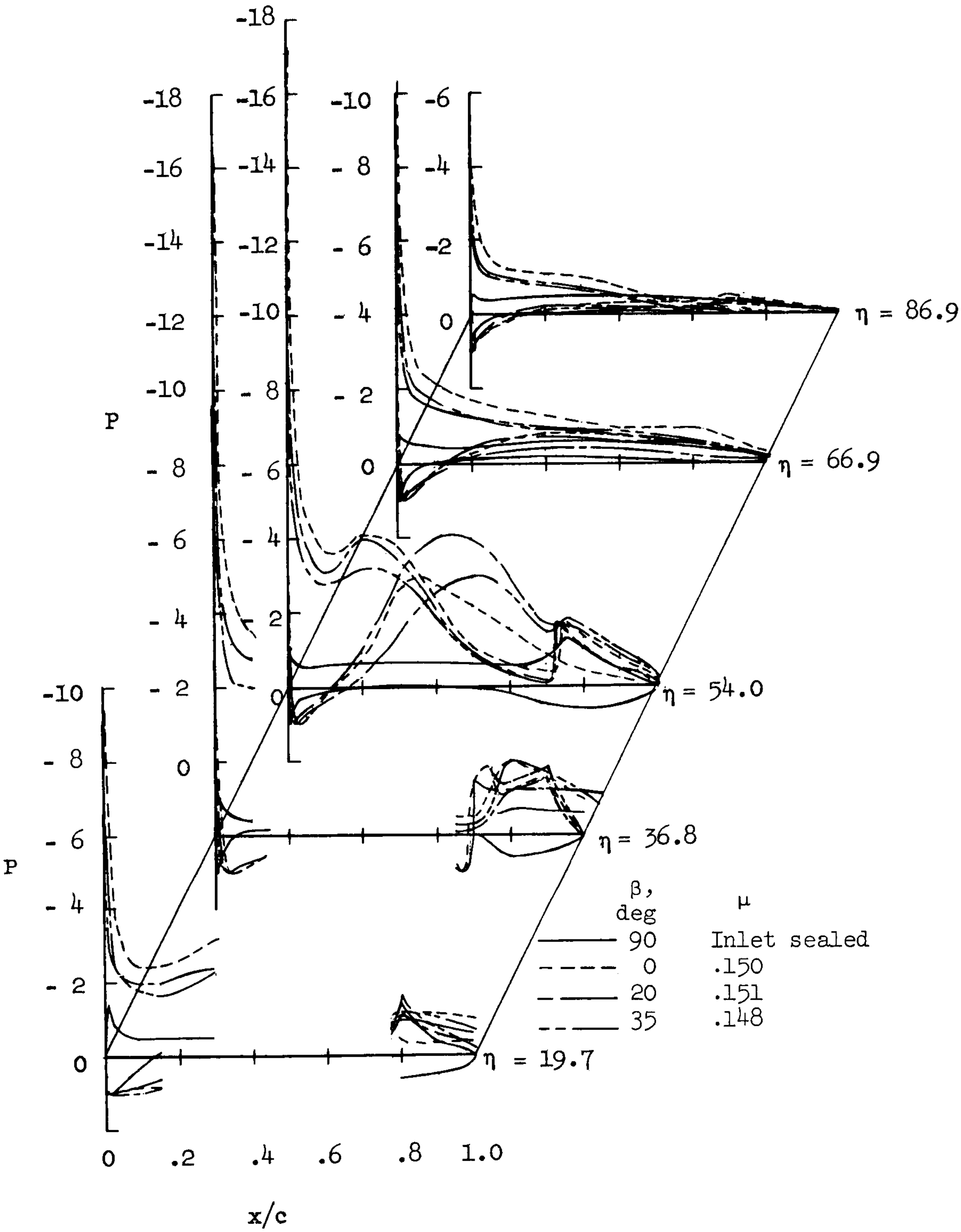

(b) μ = 0.15, V = 40 knots.

Figure 20.- Continued.

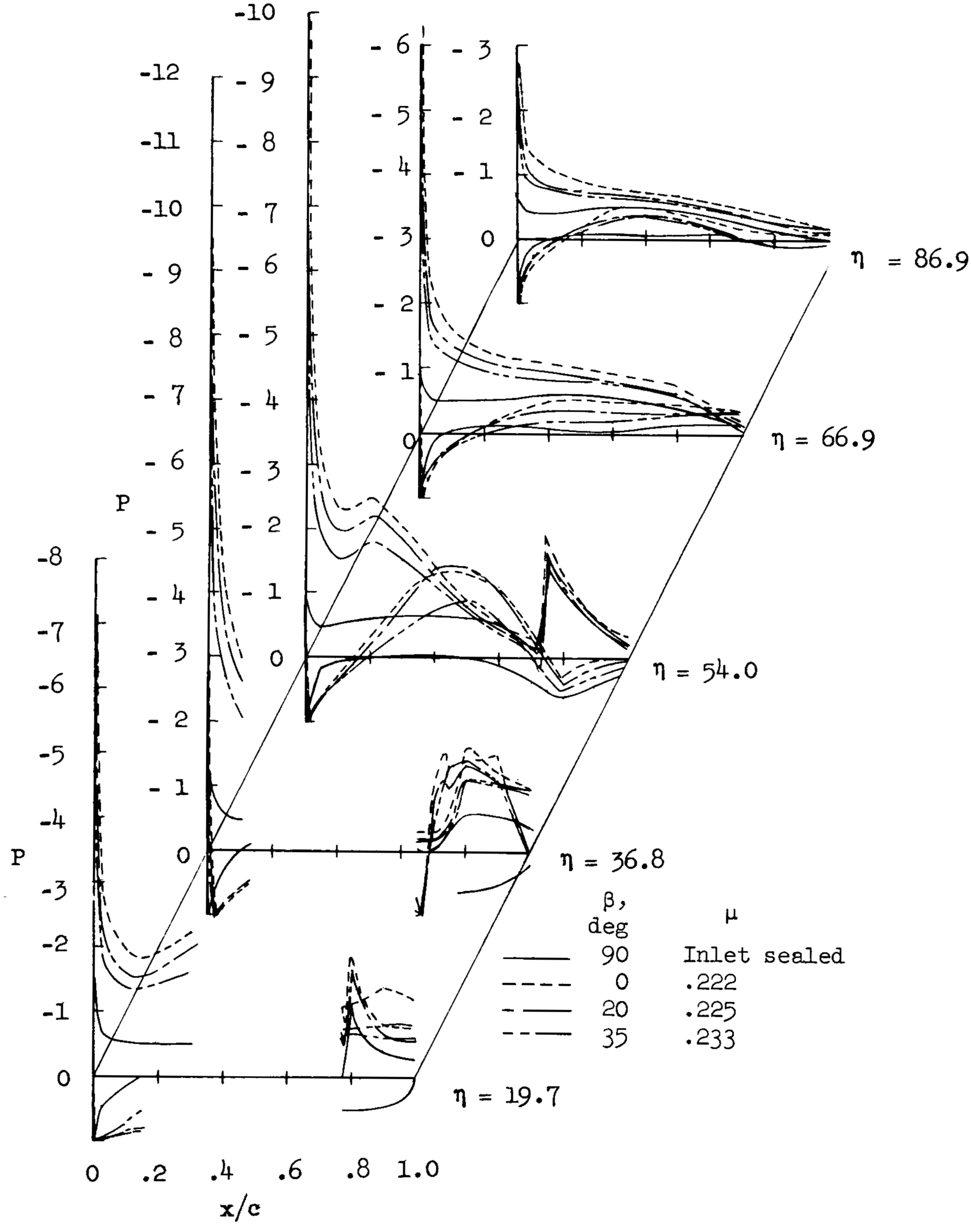

(c) μ = 0.22, V = 60 knots.

Figure 20.- Continued.

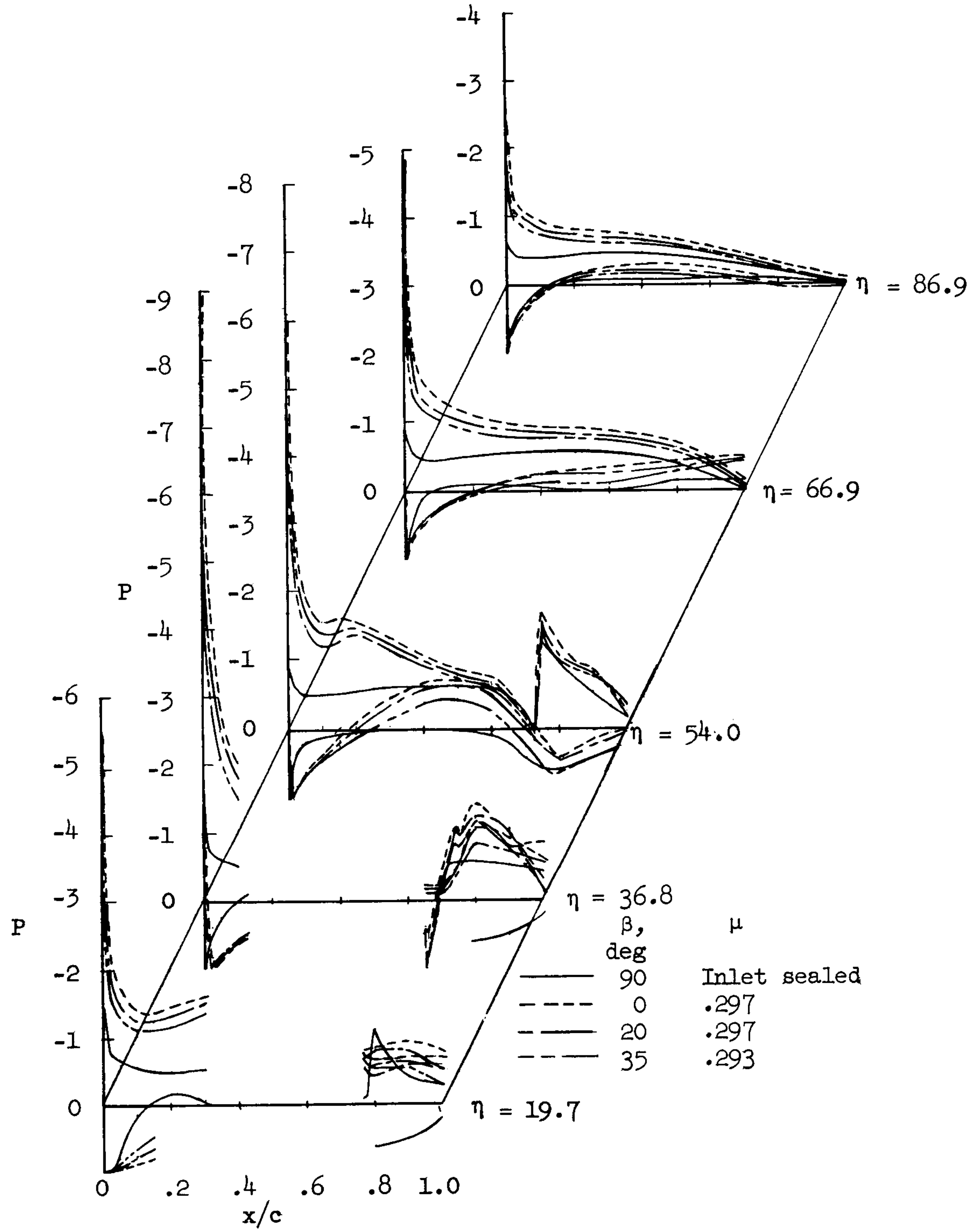

(d) μ = 0.30, V = 80 knots.

Figure 20.- Concluded.

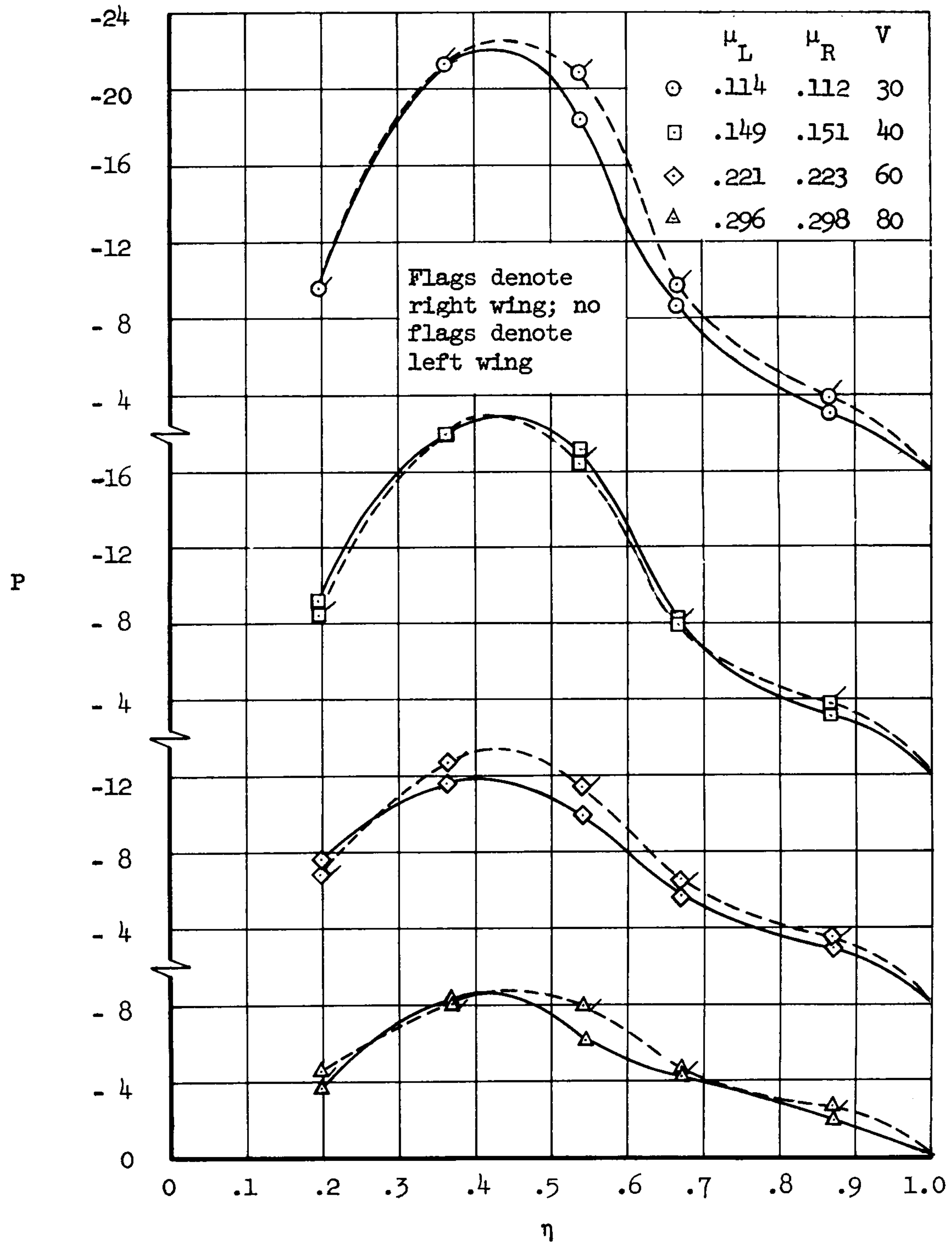

Figure 21.- Minimum pressure coefficients on the wing leading edge; $\delta_f = 30^\circ$, $\beta = 0^\circ$, $\alpha = 0^\circ$, 1700 RPM.

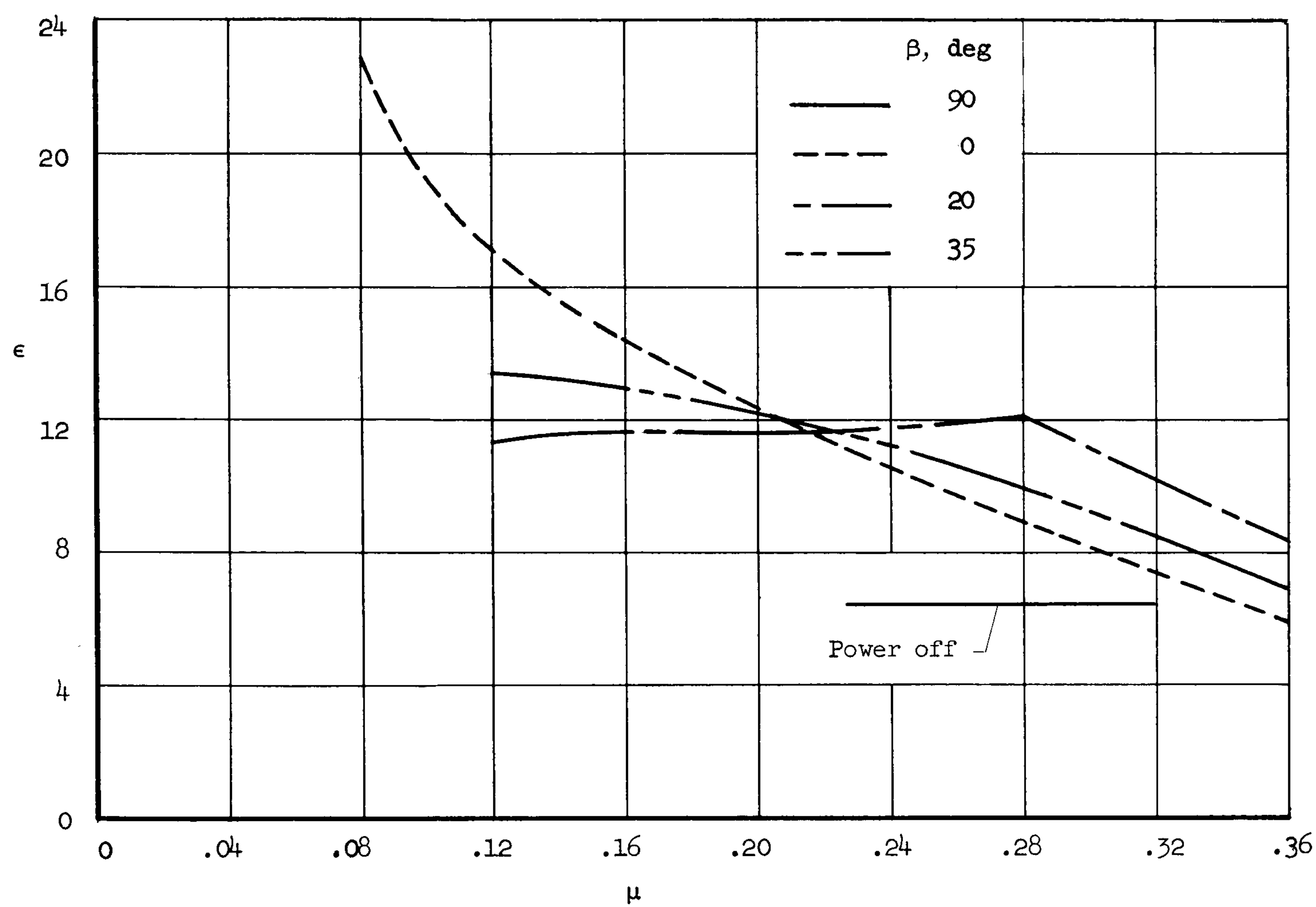

Figure 22.- Variation of average downwash at the horizontal tail with tip-speed ratio; $\delta_f = 30^\circ$, $\alpha = 0^\circ$.

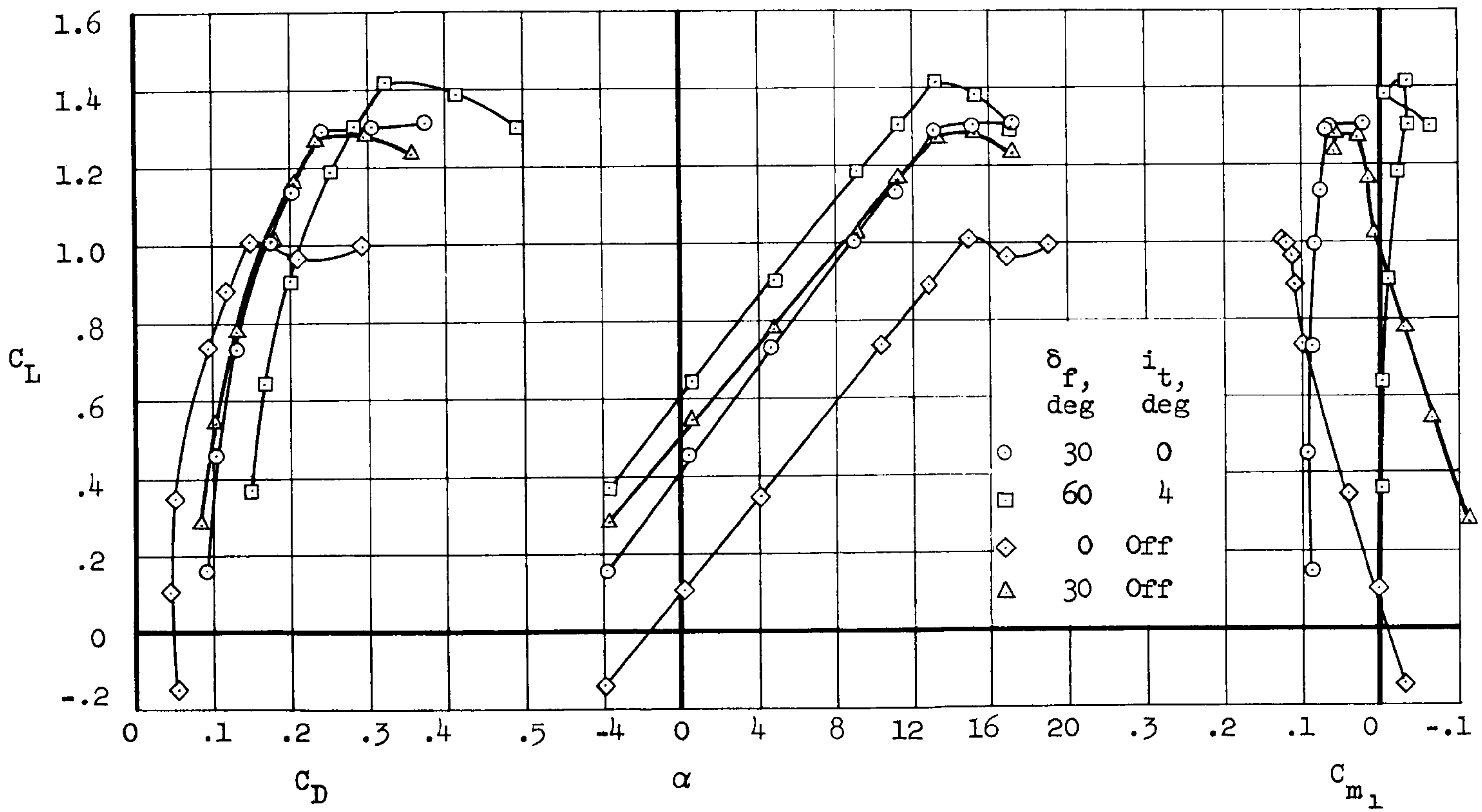

Figure 23.- Longitudinal characteristics with power off; inlets sealed, tail on, $\beta = 90^{\circ}$, V = 60 knots.

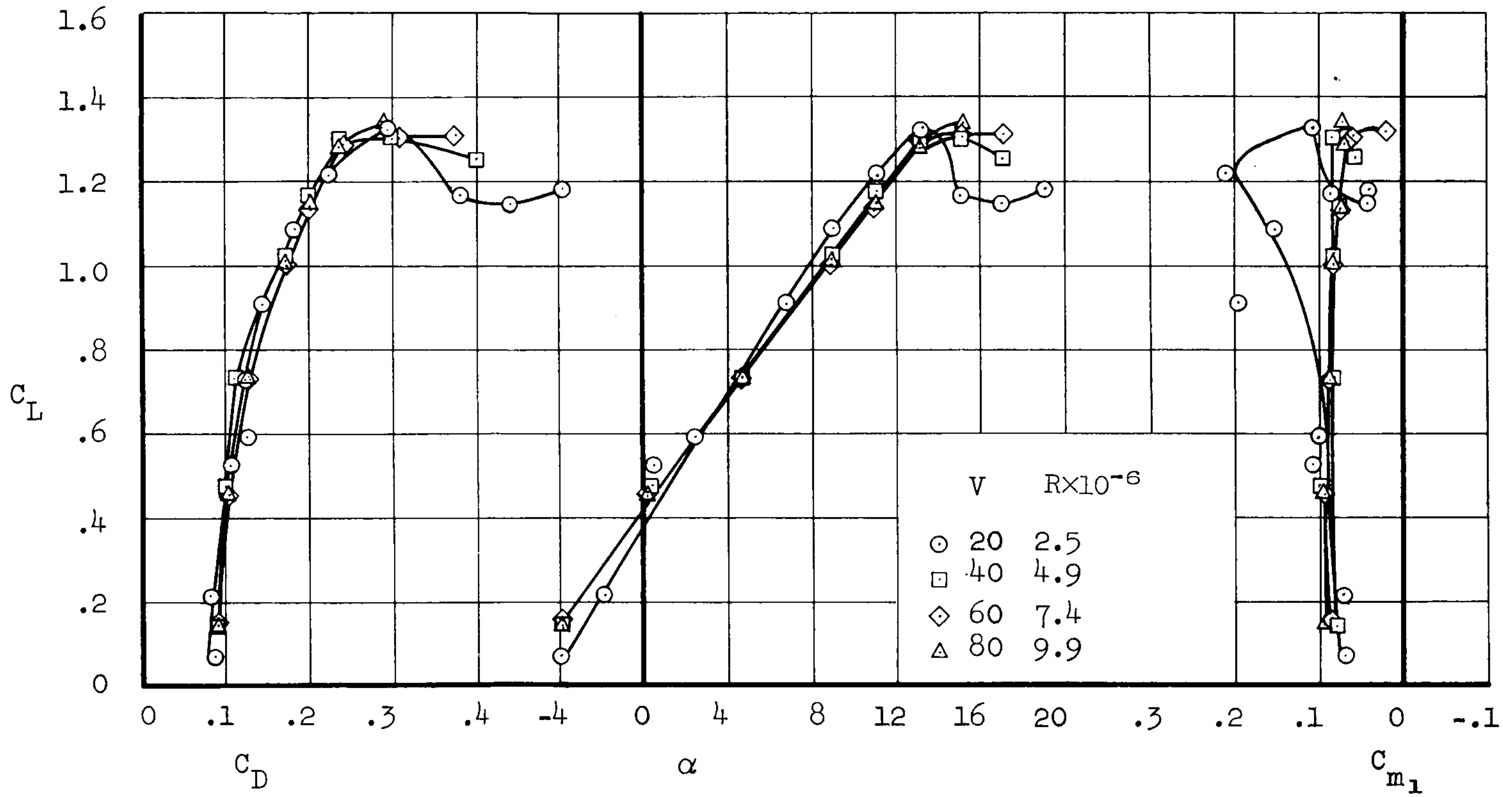

Figure 24.- Effect of Reynolds number on power-off longitudinal characteristics; tail on, $i_t = 0^\circ$, $\delta_f = 30^\circ$, inlets sealed, $\beta = 90^\circ$.

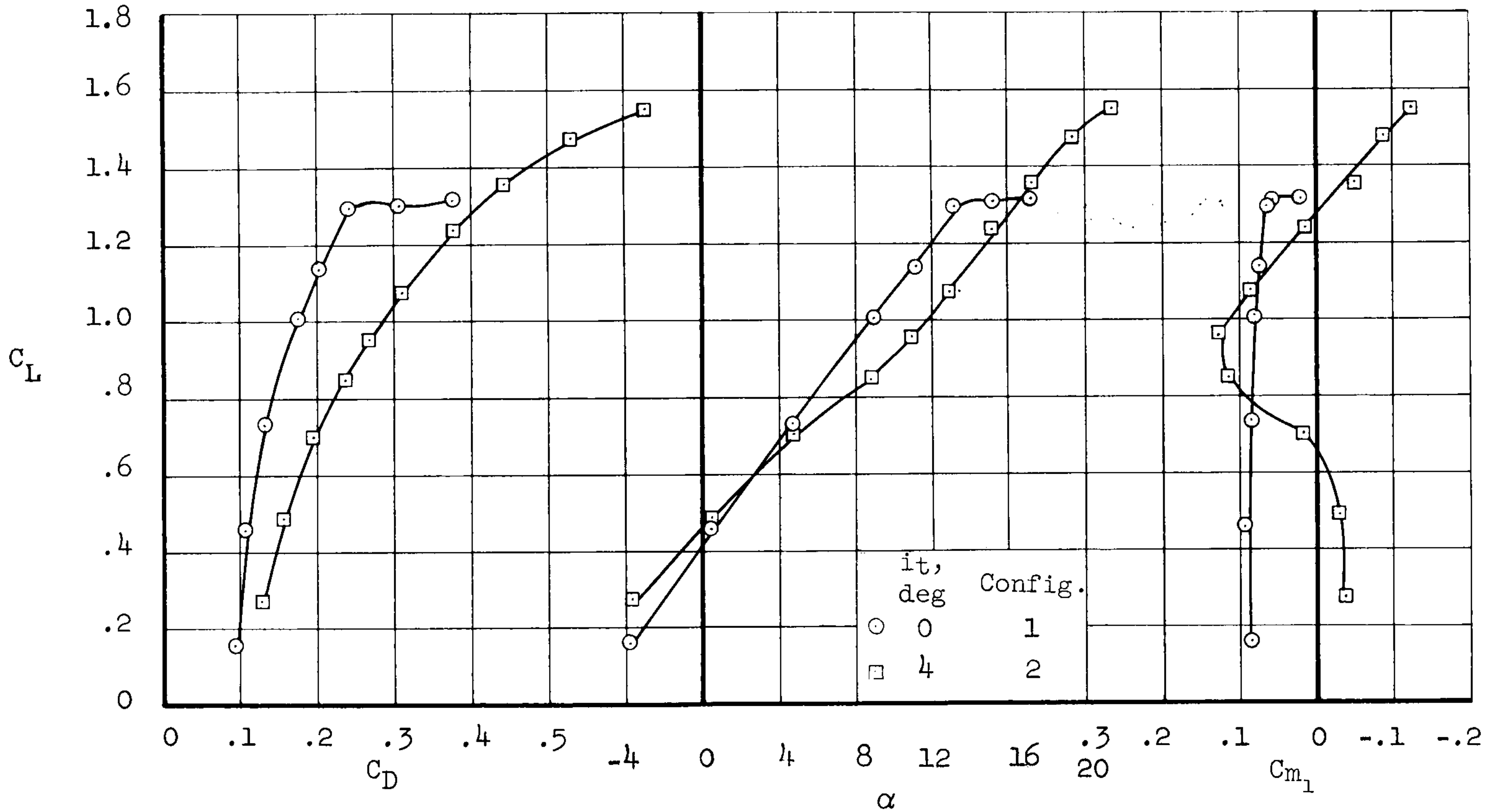

Figure 25.- Effect of configuration on power-off longitudinal characteristics; tail on, V = 60 knots, inlets sealed, $\beta = 90^{\circ}$, $\delta_f = 30^{\circ}$.

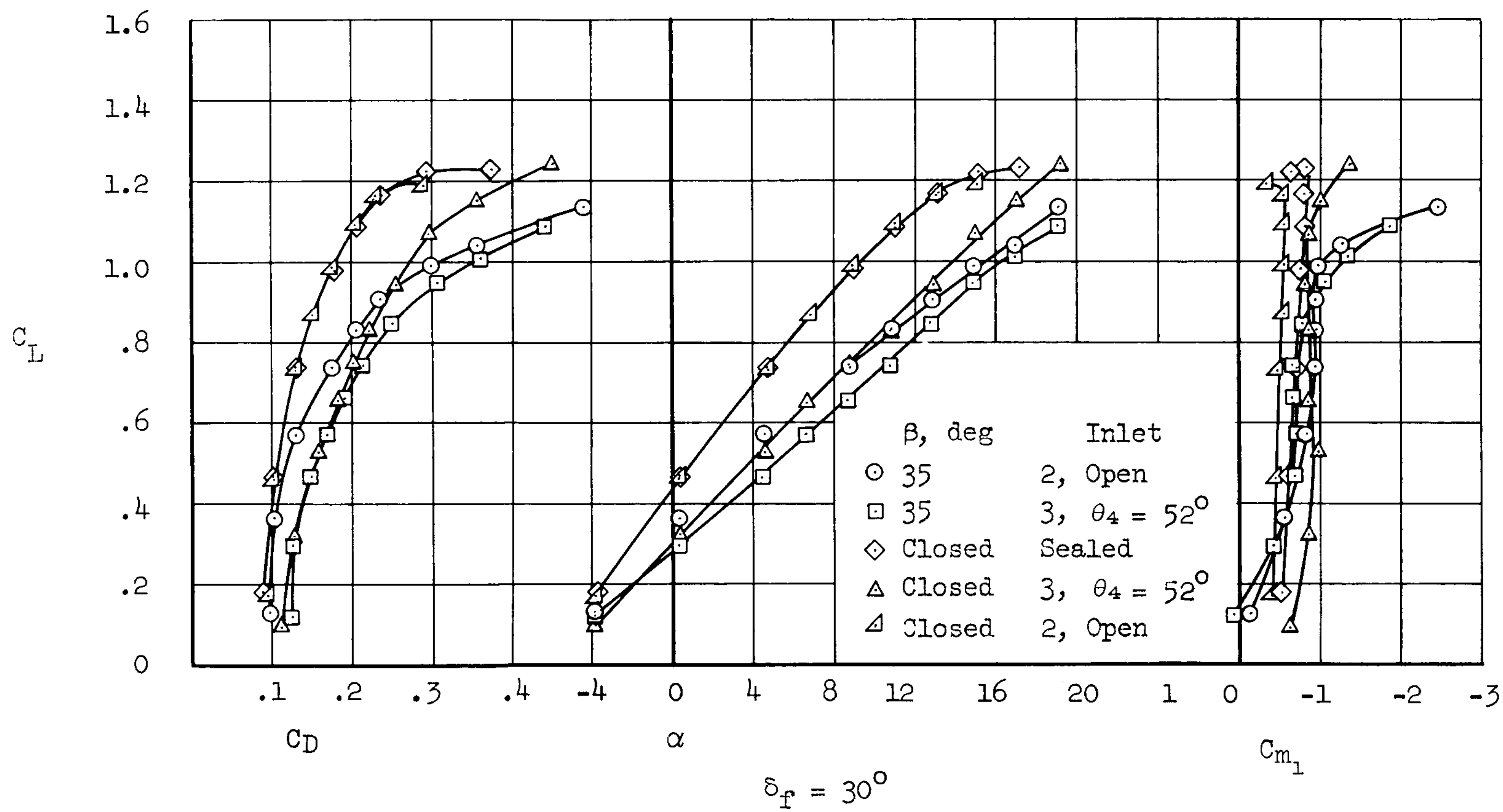

Figure 26.- Effect of various open or partly open fan inlets and exits on longitudinal characteristics with power off, tail on; $i_t = 4^o$, V = 80 knots, $\delta_f = 30^o$.

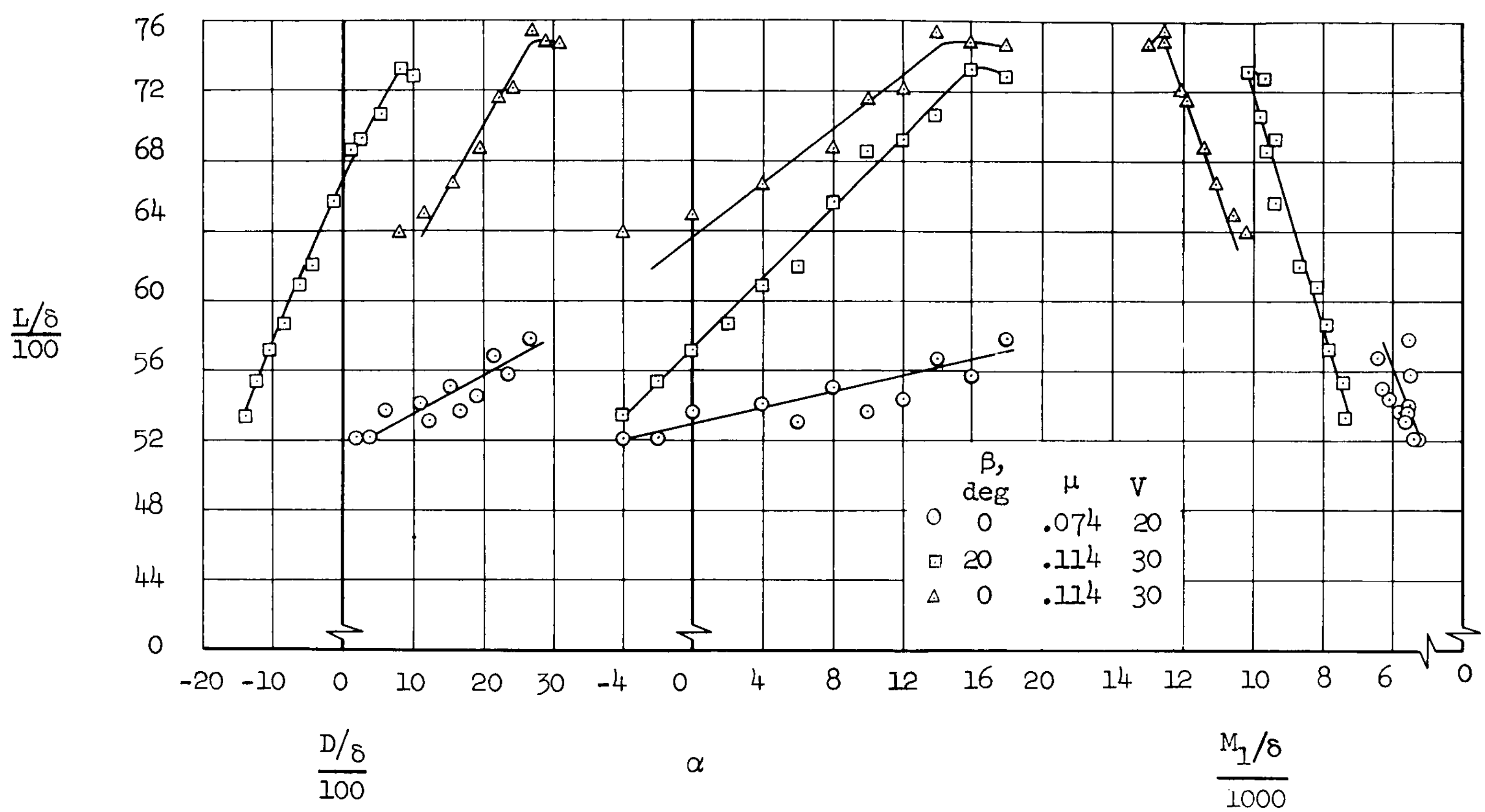

(a) Tail off.

Figure 27.- Longitudinal characteristics with fans operating at low tip-speed ratios; $\delta_f = 30^\circ$, 1700 RPM.

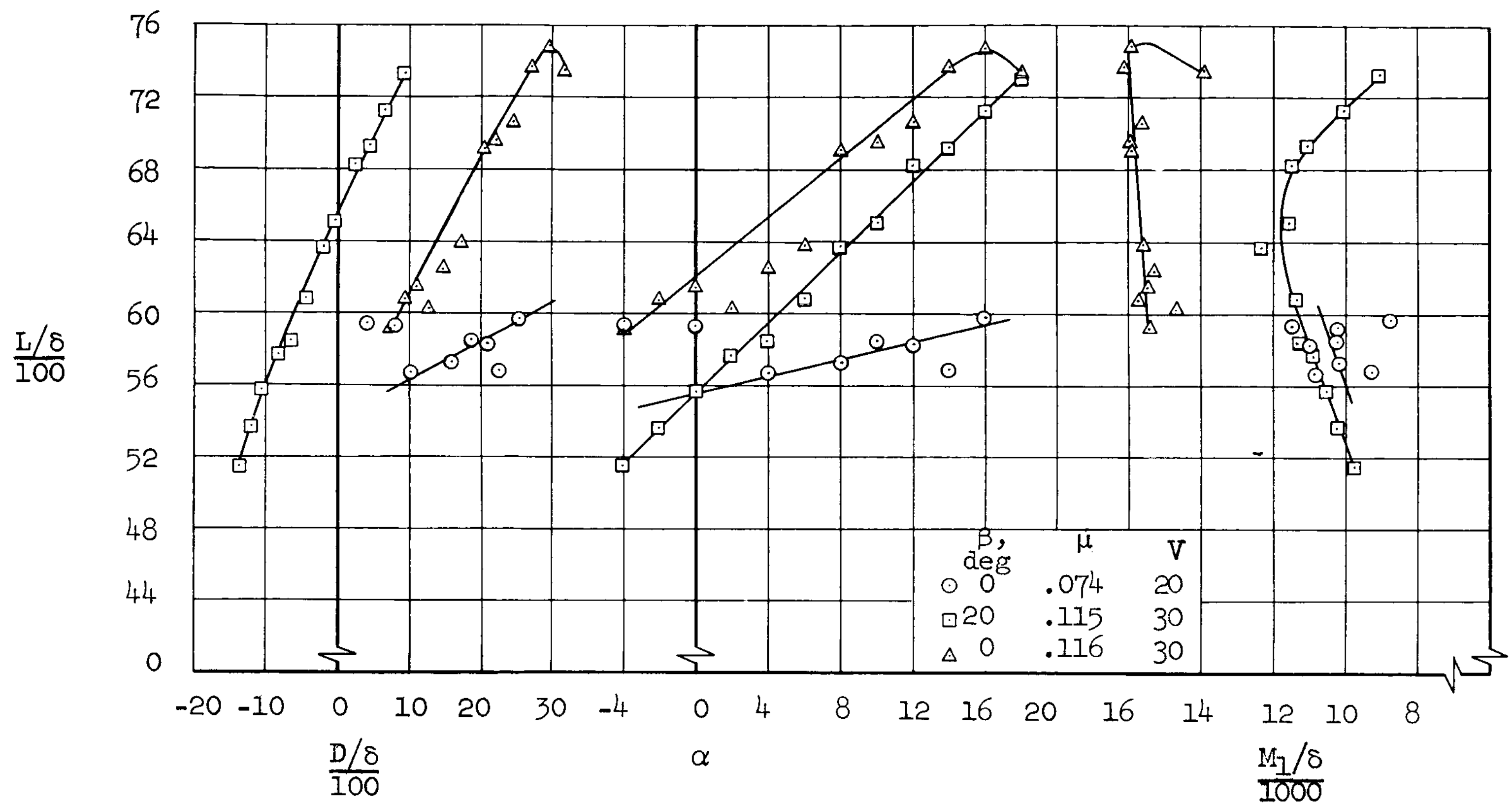

(b) Tail on, $i_t = 0^\circ$.

Figure 27.- Concluded.

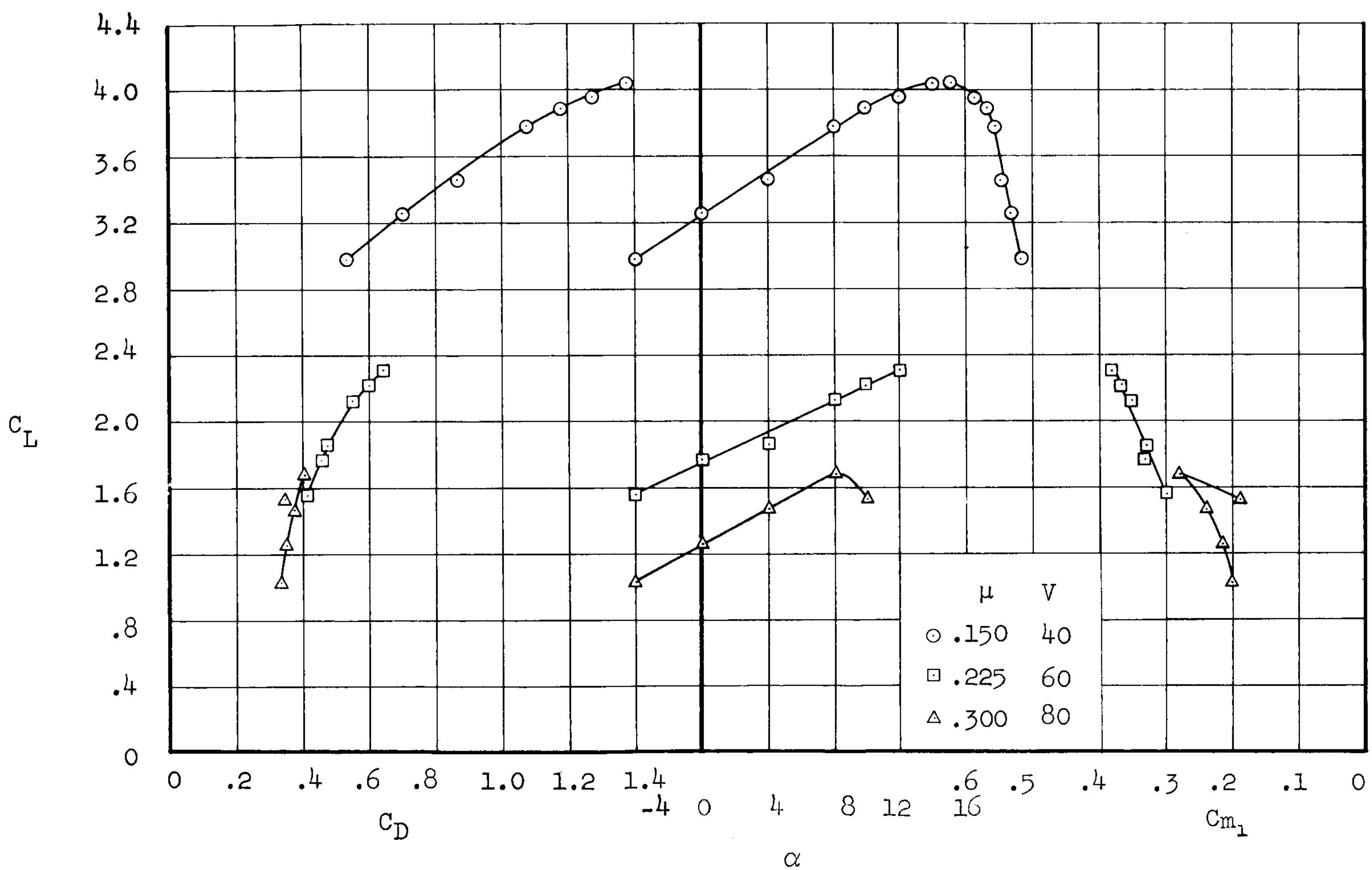

(a) $\beta = 0^{\circ}$

Figure 28.- Longitudinal characteristics with fans operating; tail off, $\delta_f = 30^{\circ}$, 1700 RPM.

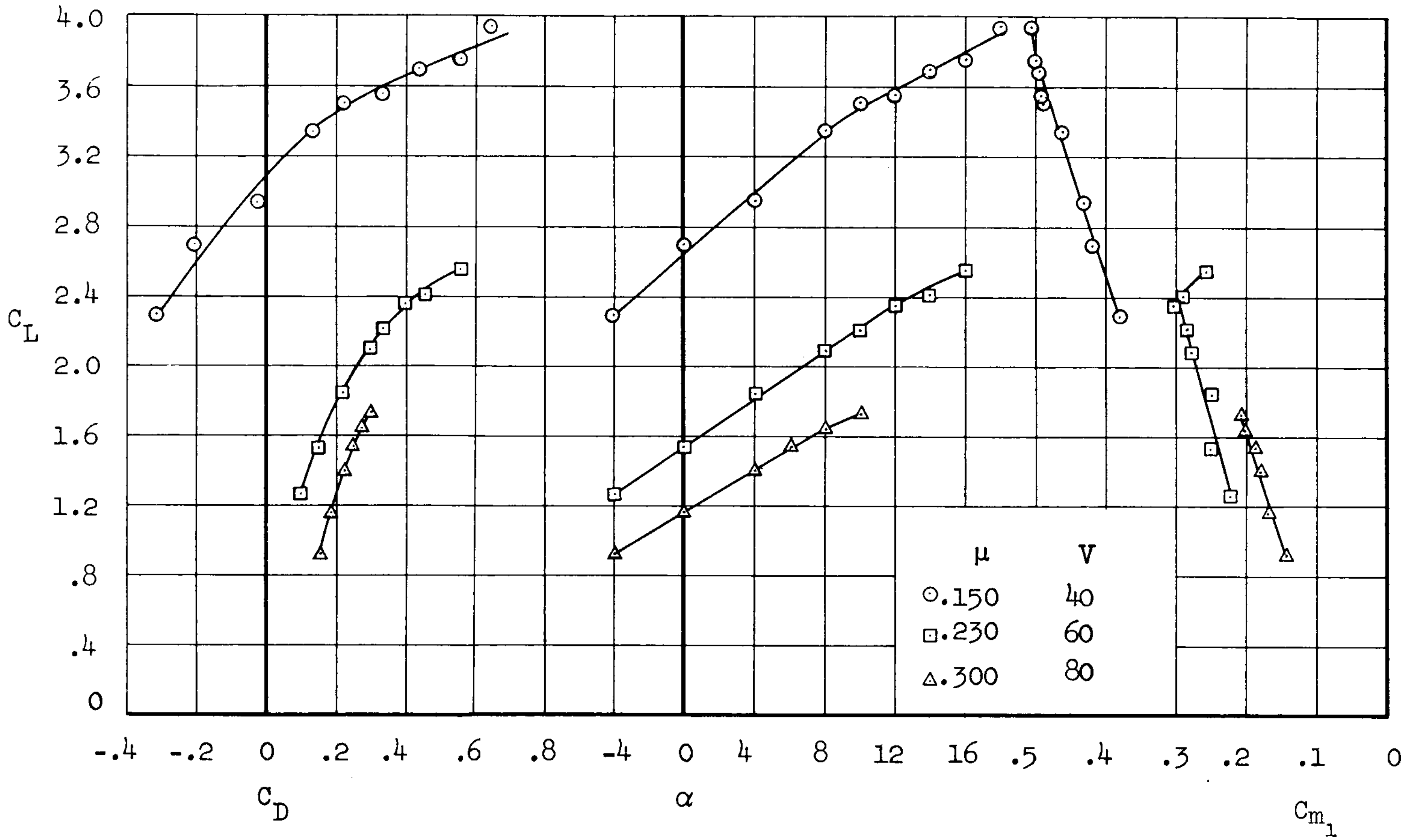

(b) $\beta = 20^{\circ}$

Figure 28.- Continued.

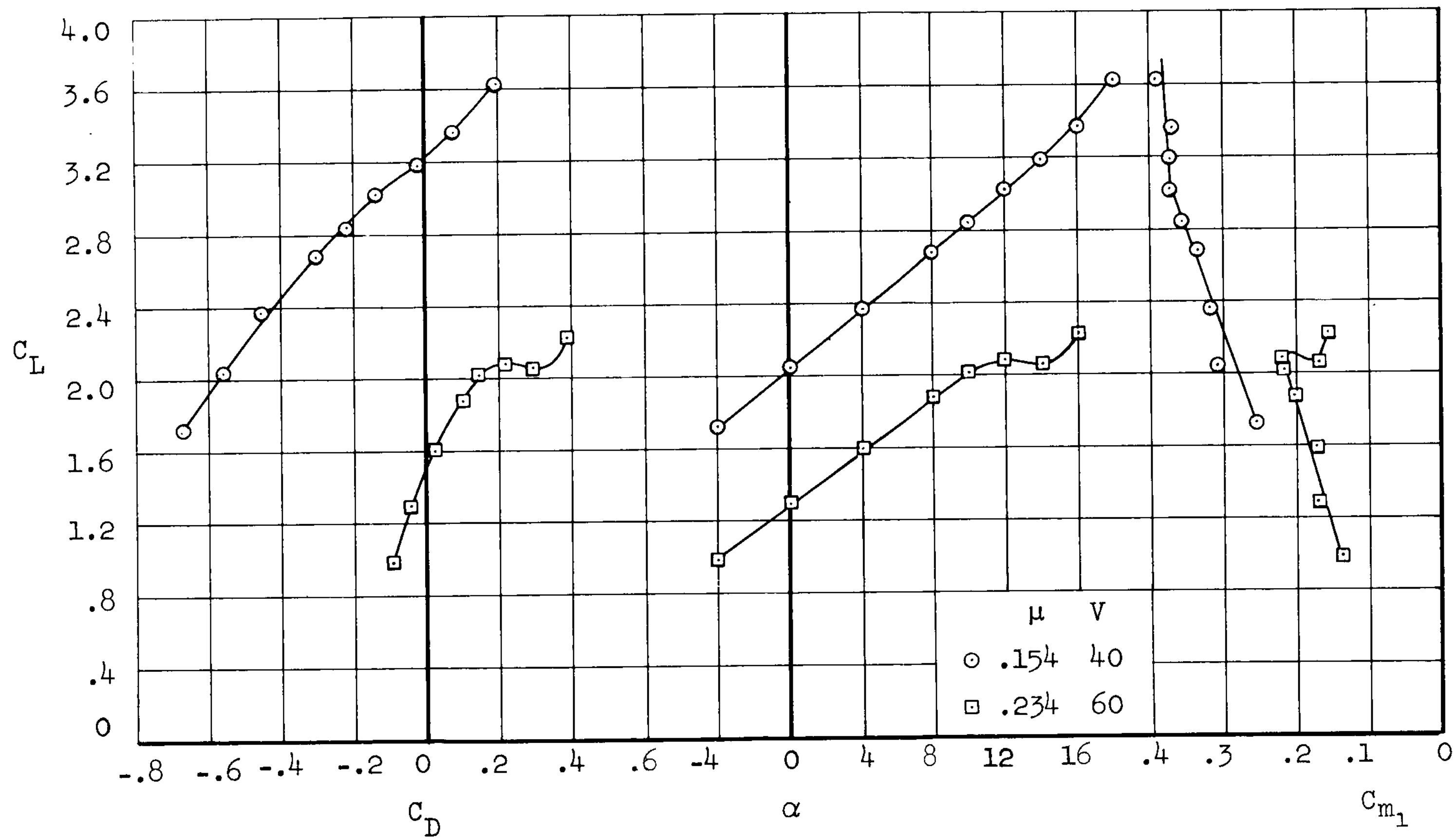

(c) $\beta = 35^{\circ}$

Figure 28.- Concluded.

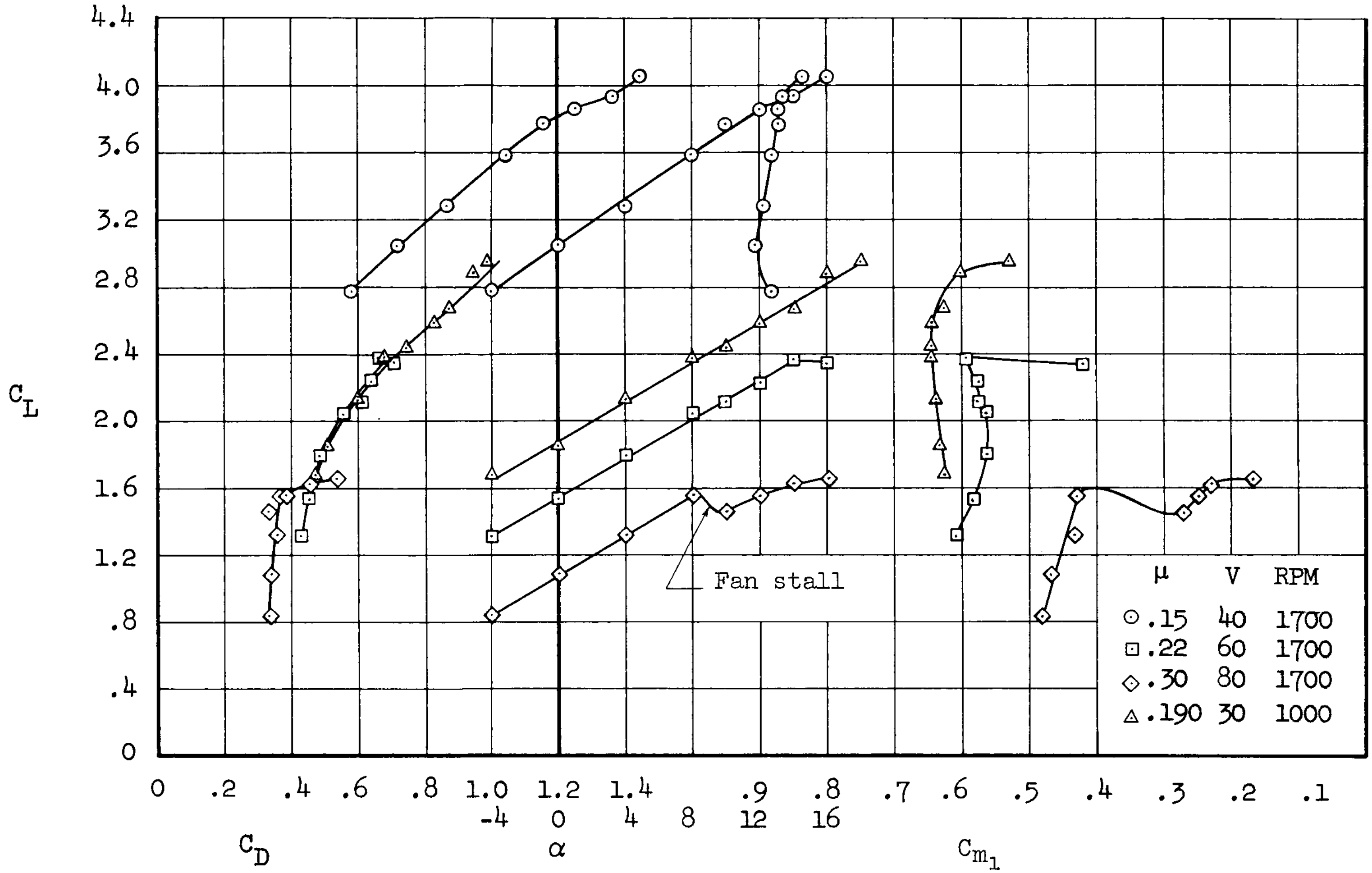

(a) $\beta = 0^\circ$

Figure 29.- Longitudinal characteristics with fans operating; tail on, $i_t = 0^\circ$, $\delta_f = 30^\circ$.

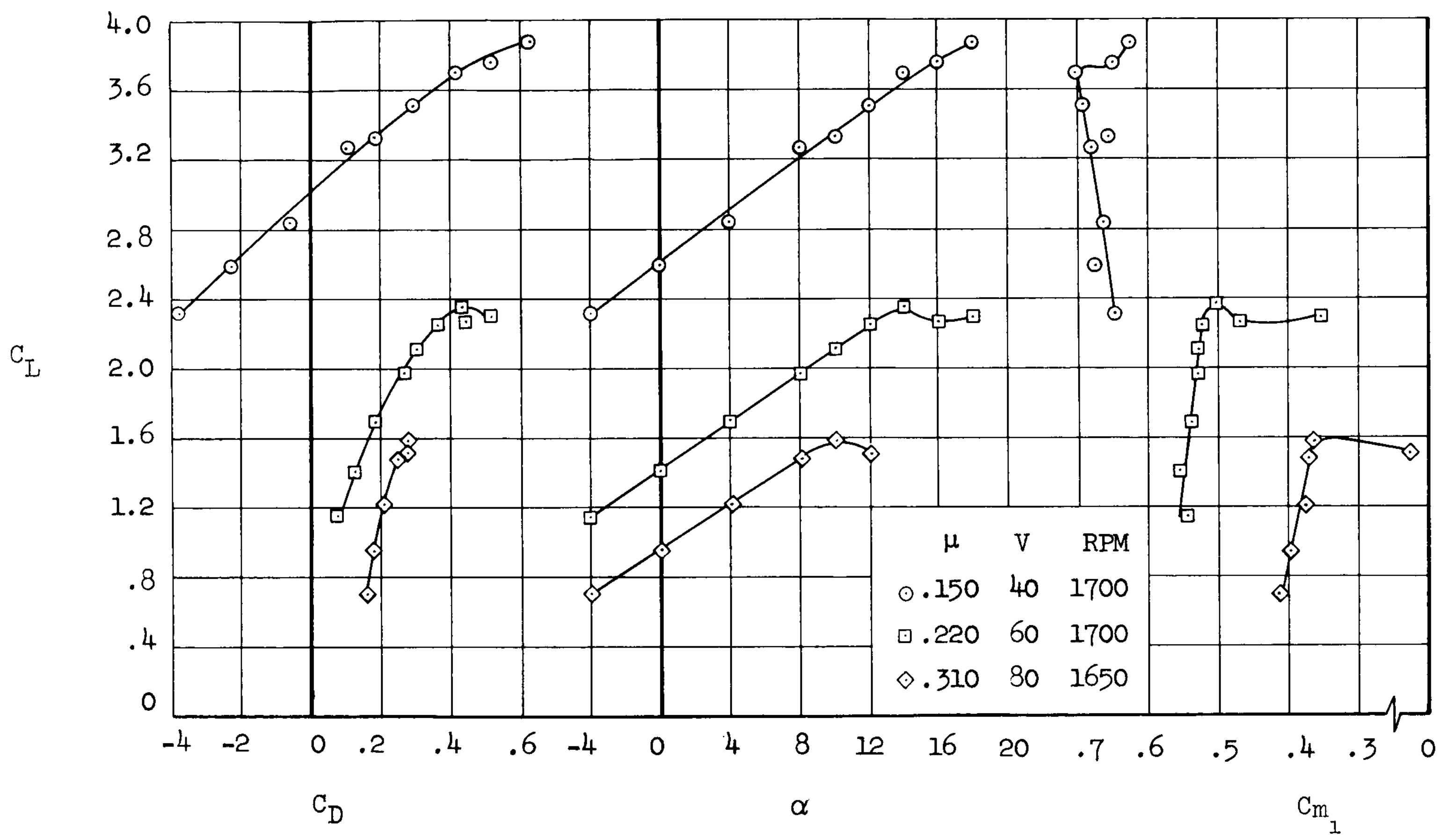

(b) $\beta = 20^{\circ}$

Figure 29.- Continued.

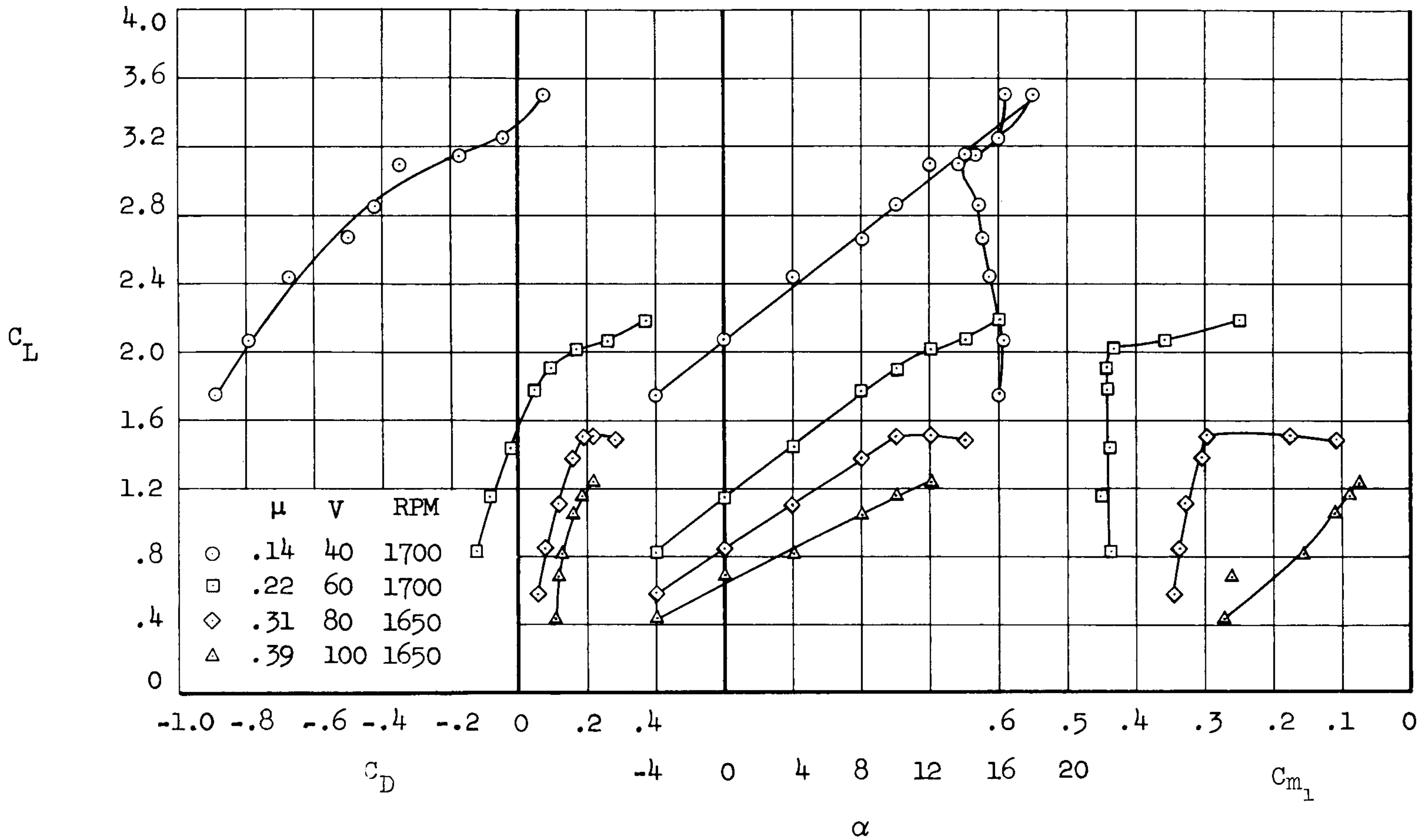

(c) $\beta = 35^{\circ}$

Figure 29.- Concluded.

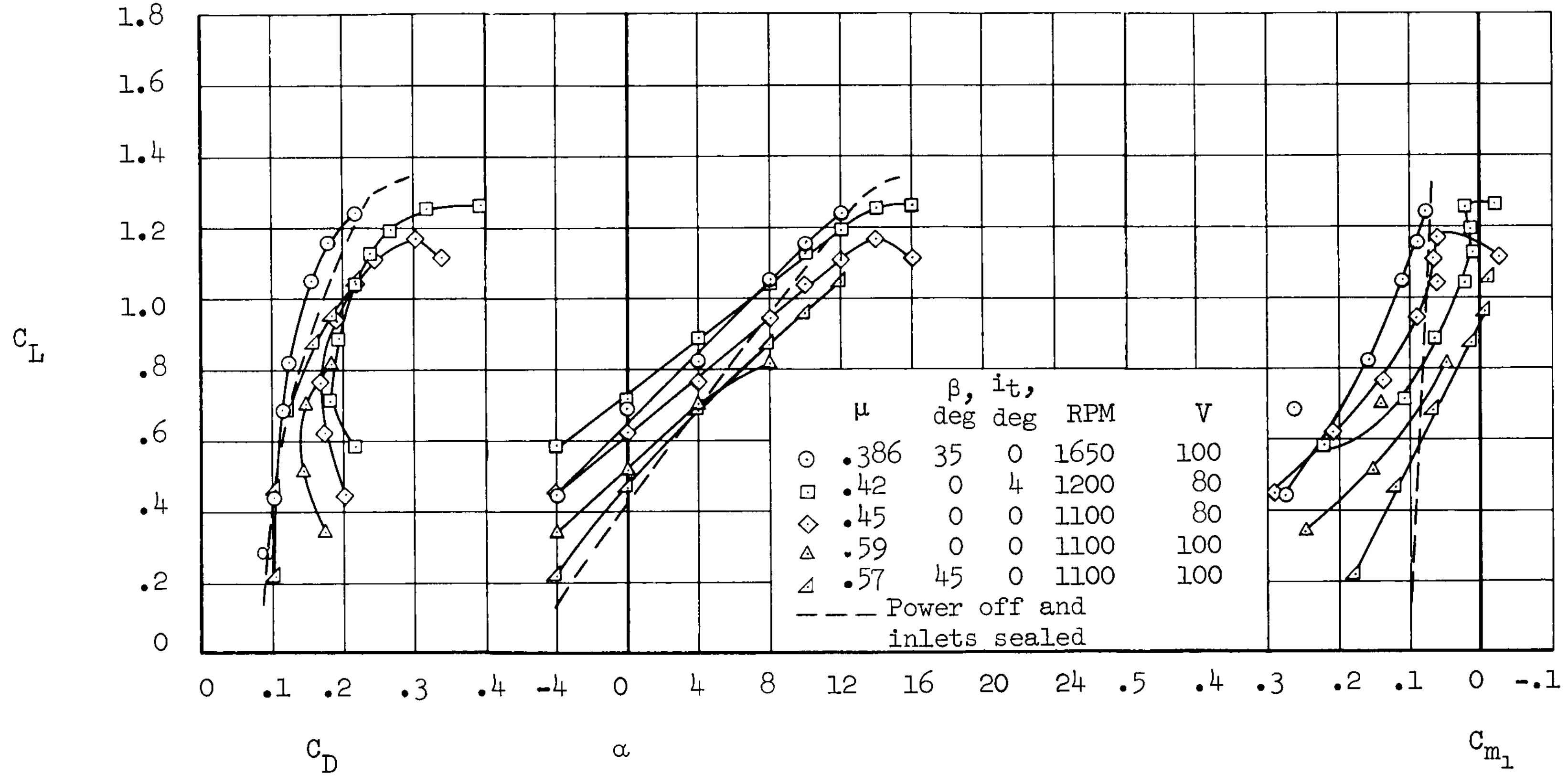

Figure 30.- Longitudinal characteristics with fans operating at high tip-speed ratios; tail on, $\delta_f = 30^{\circ}$.

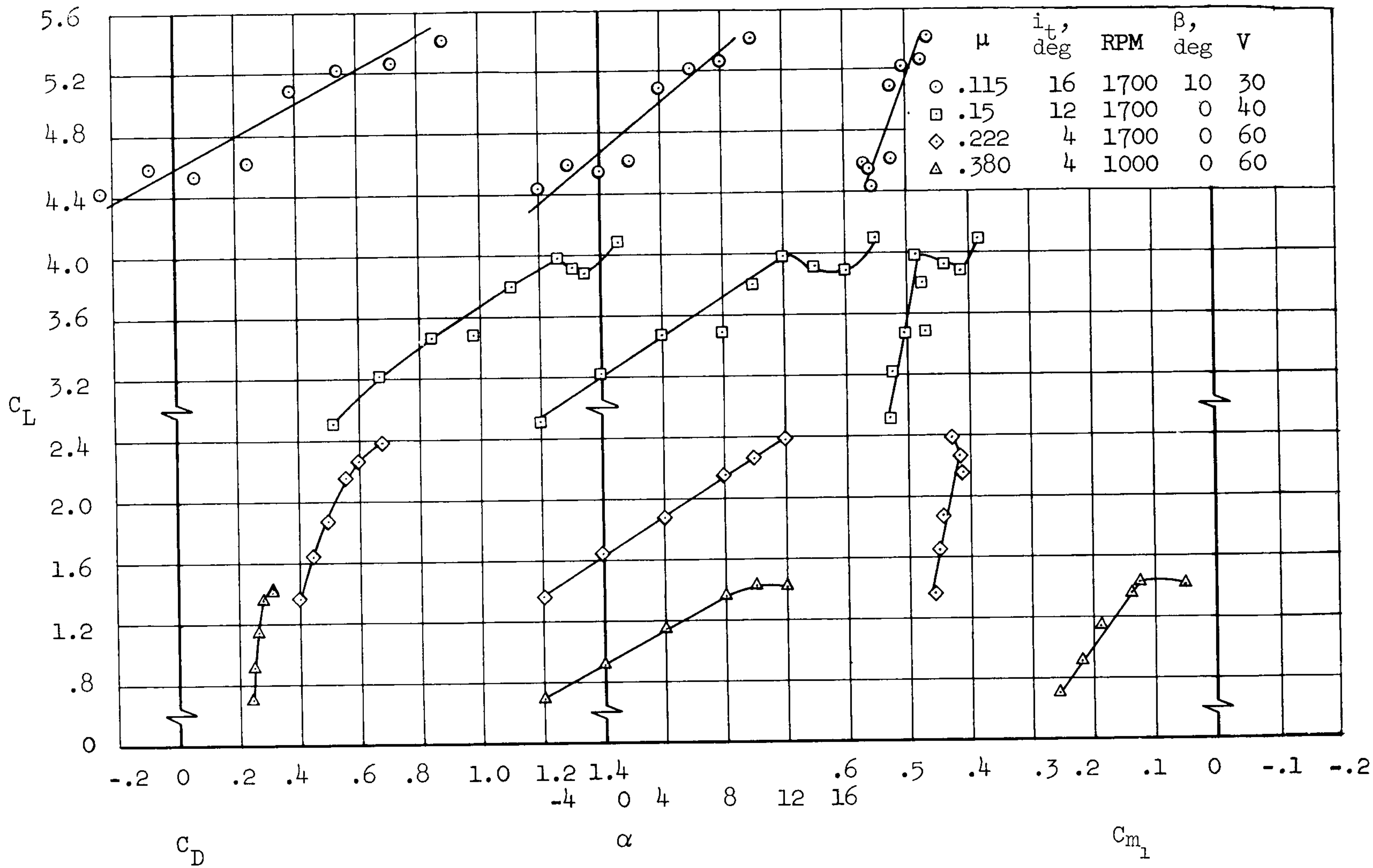

Figure 31.- Longitudinal characteristics with circular inlet vane (inlet 1); tail on, $\delta_f = 30^{\circ}$.

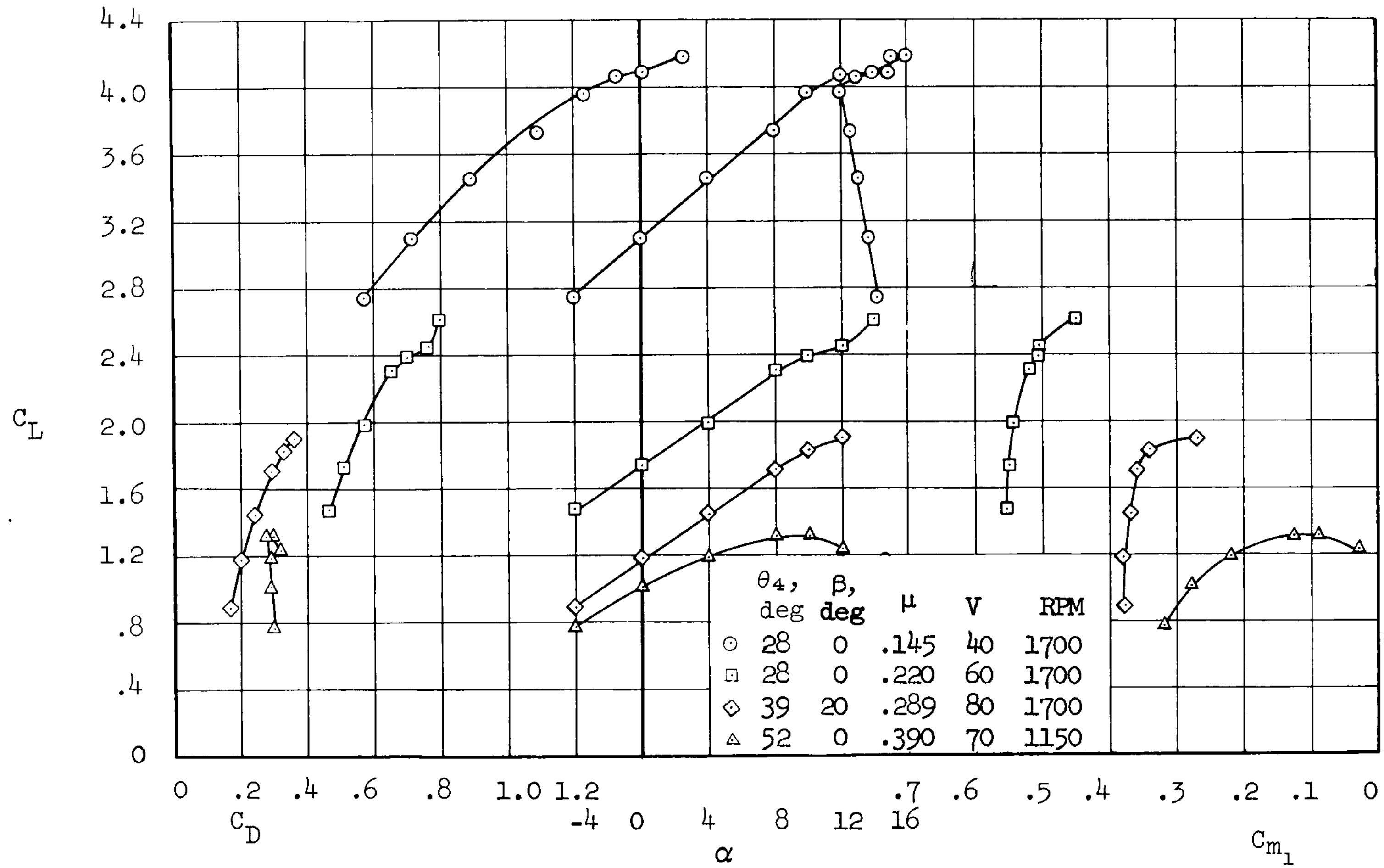

Figure 32.- Longitudinal characteristics with articulated inlet louvers (inlet 3); tail on, $i_t = 4^\circ$, $\delta_f = 30^\circ$.

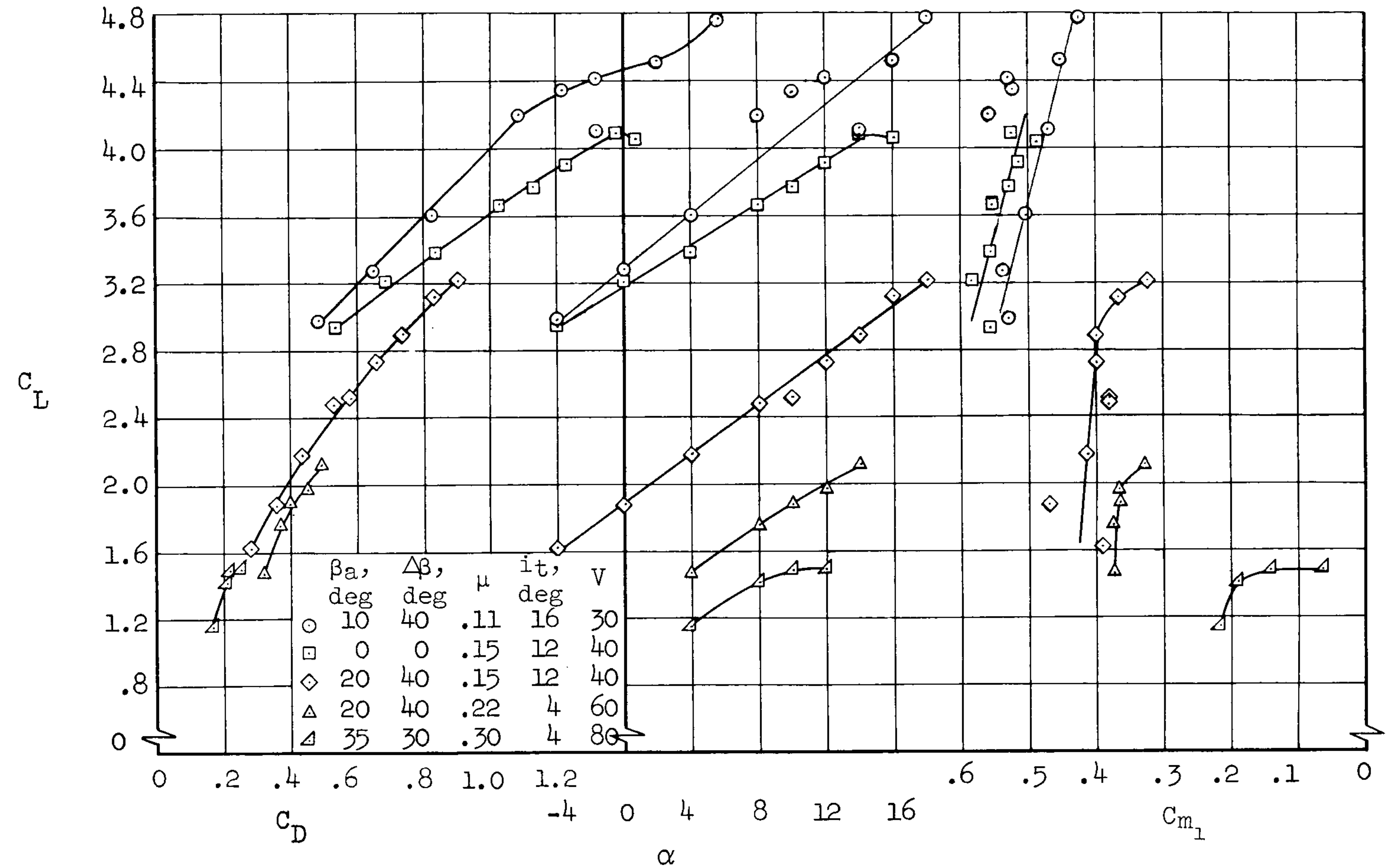

Figure 33.- Longitudinal characteristics with symmetrical differential exit-vane settings; tail on, $\delta_f = 30^\circ$, 1700 RPM.

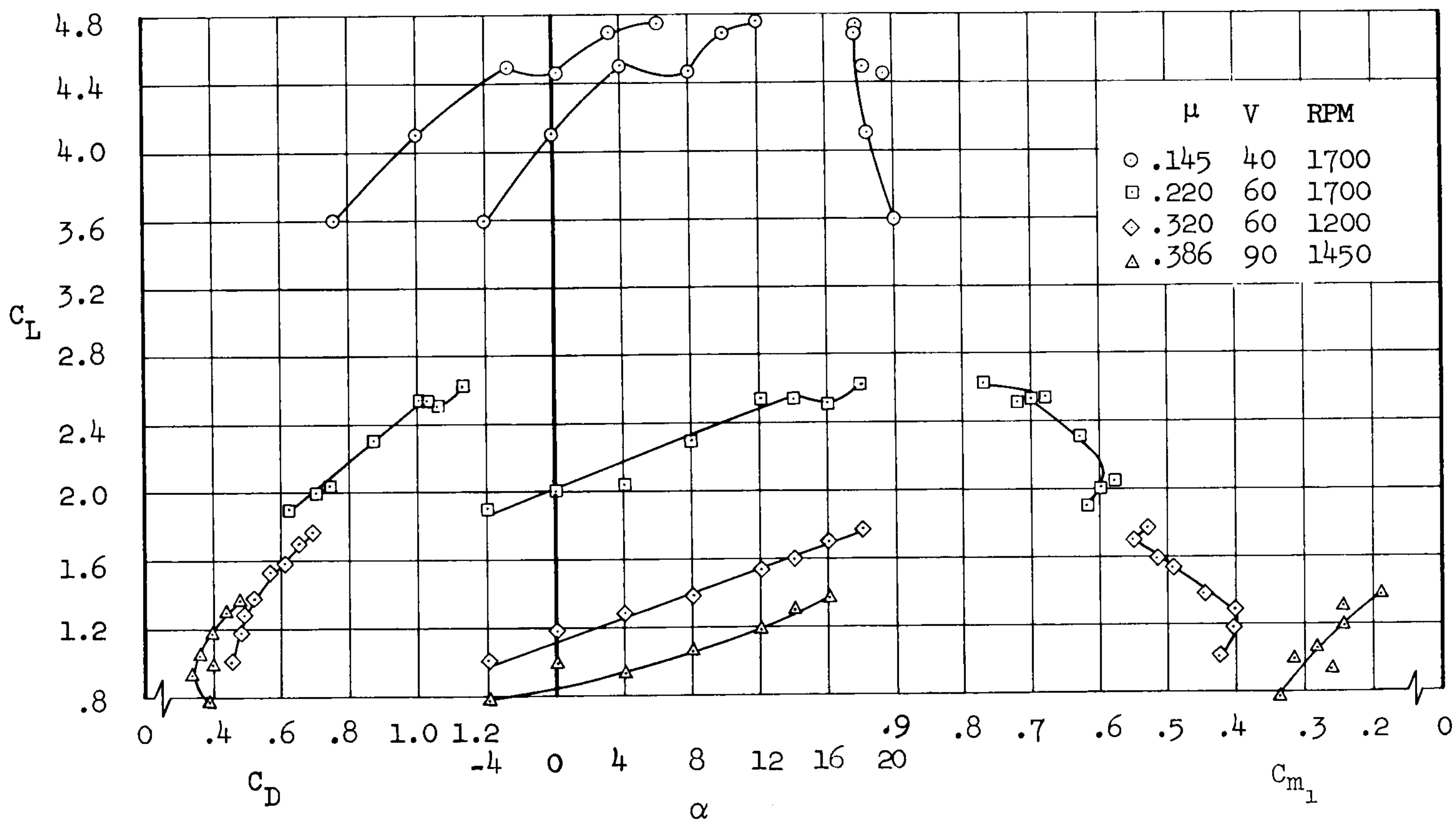

Figure 34.- Longitudinal characteristics with wing configuration 2; tail on, $i_t = 4^\circ$, $\delta_f = 30^\circ$, $\beta = 0^\circ$.

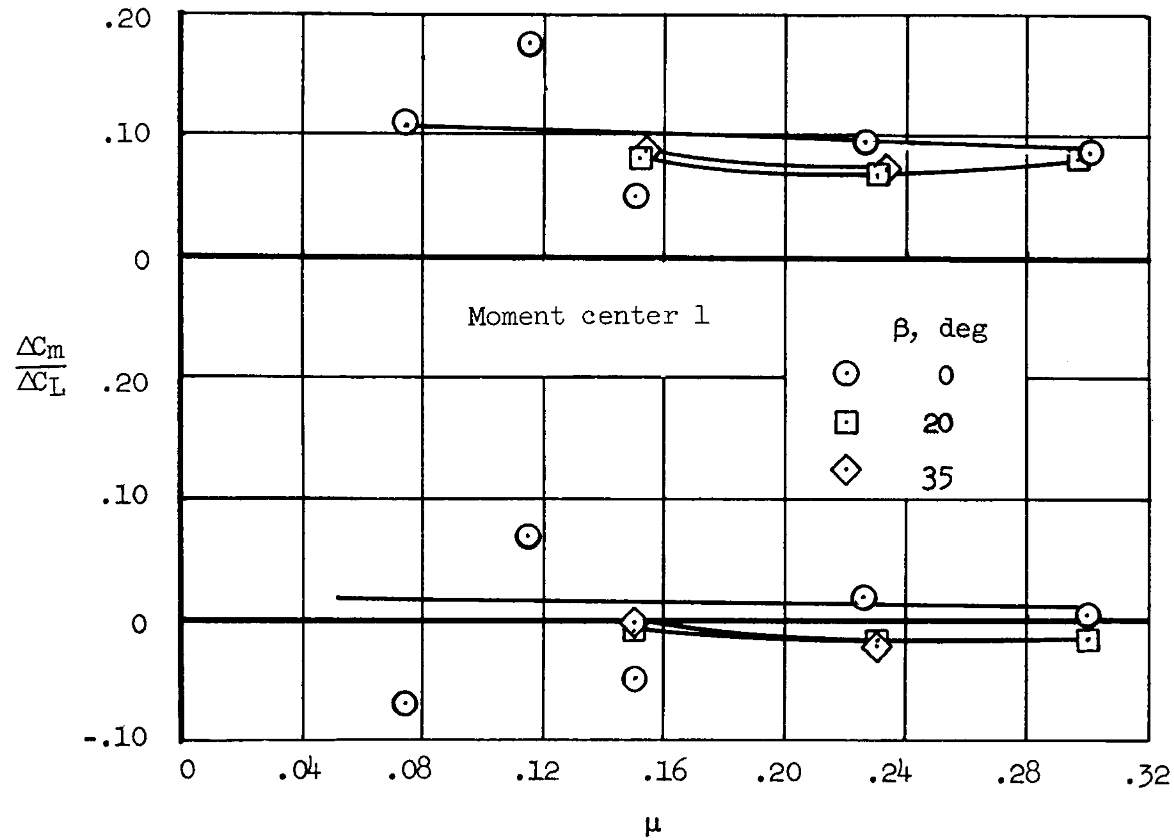

Moment center 2

Figure 35.- The variation of angle-of-attack stability with tip-speed ratio; tail off, $\delta_f = 30^{\circ}$, 1700 RPM.

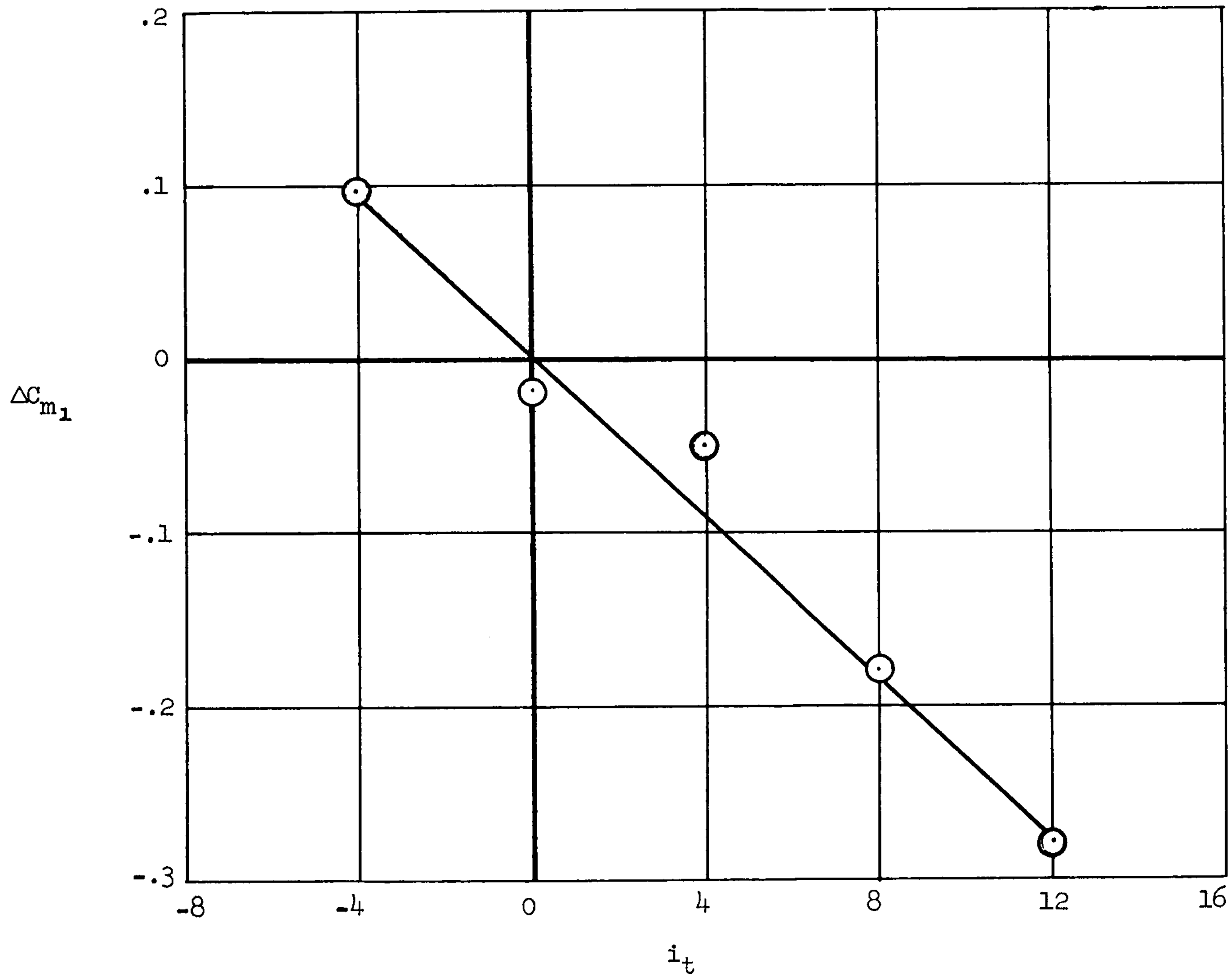

Figure 36.- Trim effectiveness of the horizontal tail; $\delta_f = 30^\circ$, $\alpha = 0^\circ$, 30 knots, $\mu = 0.115$, $\beta = 0^\circ$.

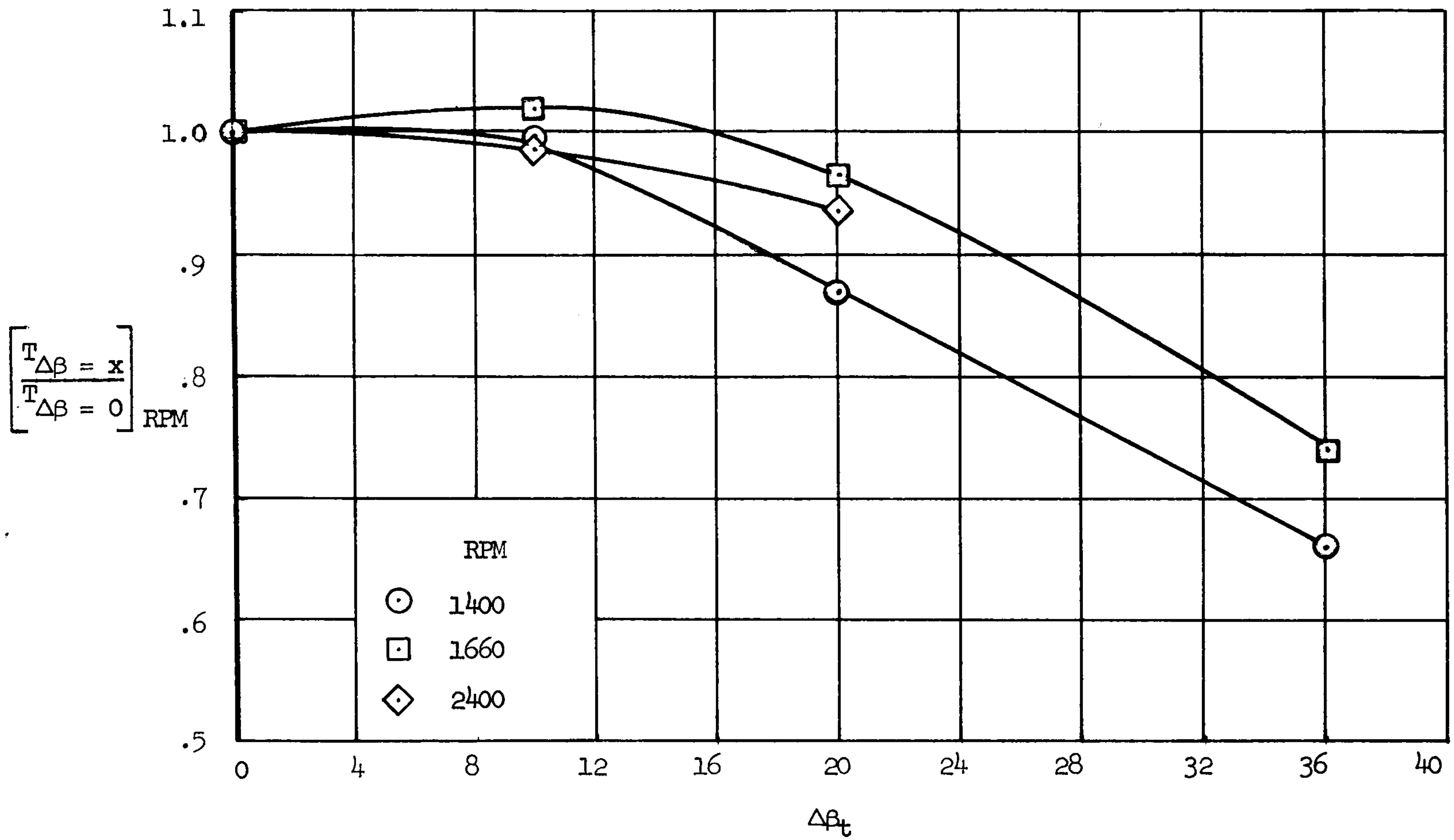

Figure 37.- Variation of static thrust with differential exit louver control; $\alpha = 0^{\circ}$, $\delta_f = 30^{\circ}$.

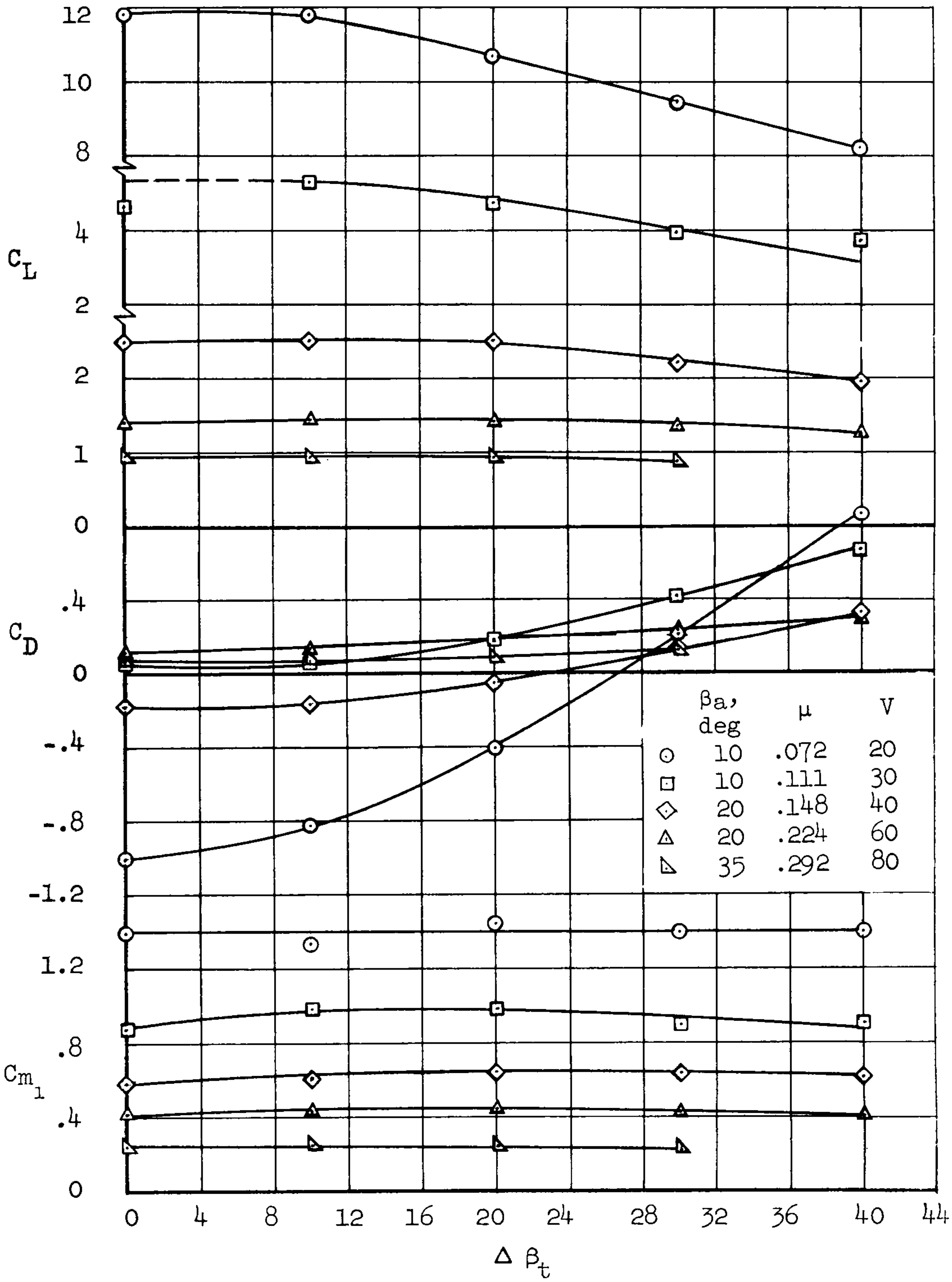

Figure 38.- The effect of thrust control on longitudinal characteristics; tail on, $i_t = 4^o$, $\delta_f = 30^o$, 1700 RPM.

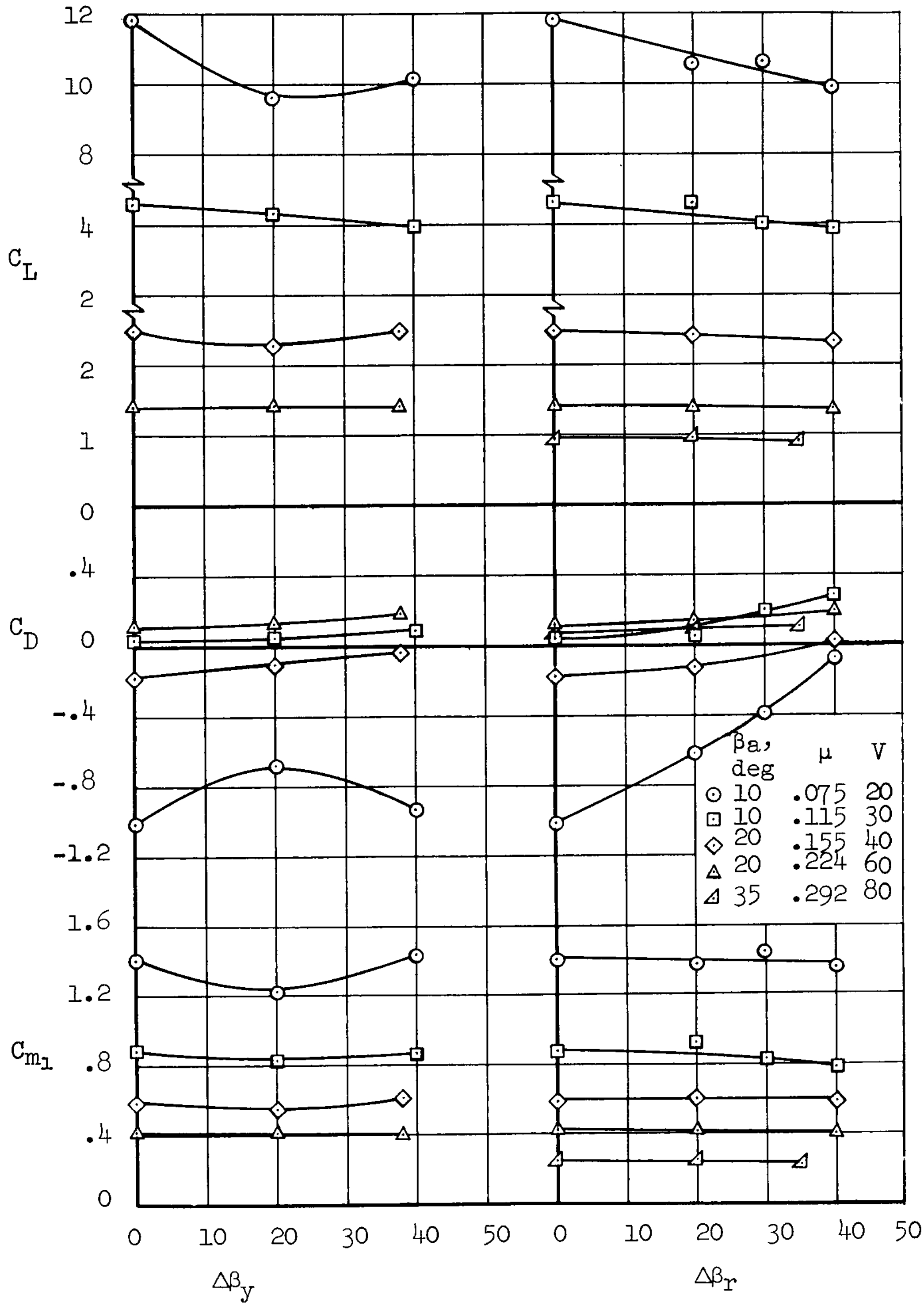

(a) Longitudinal characteristics.

Figure 39.- The effect of differential louver operation to produce yaw and roll; tail on, $i_t = 4^{\circ}$, 1700 RPM.

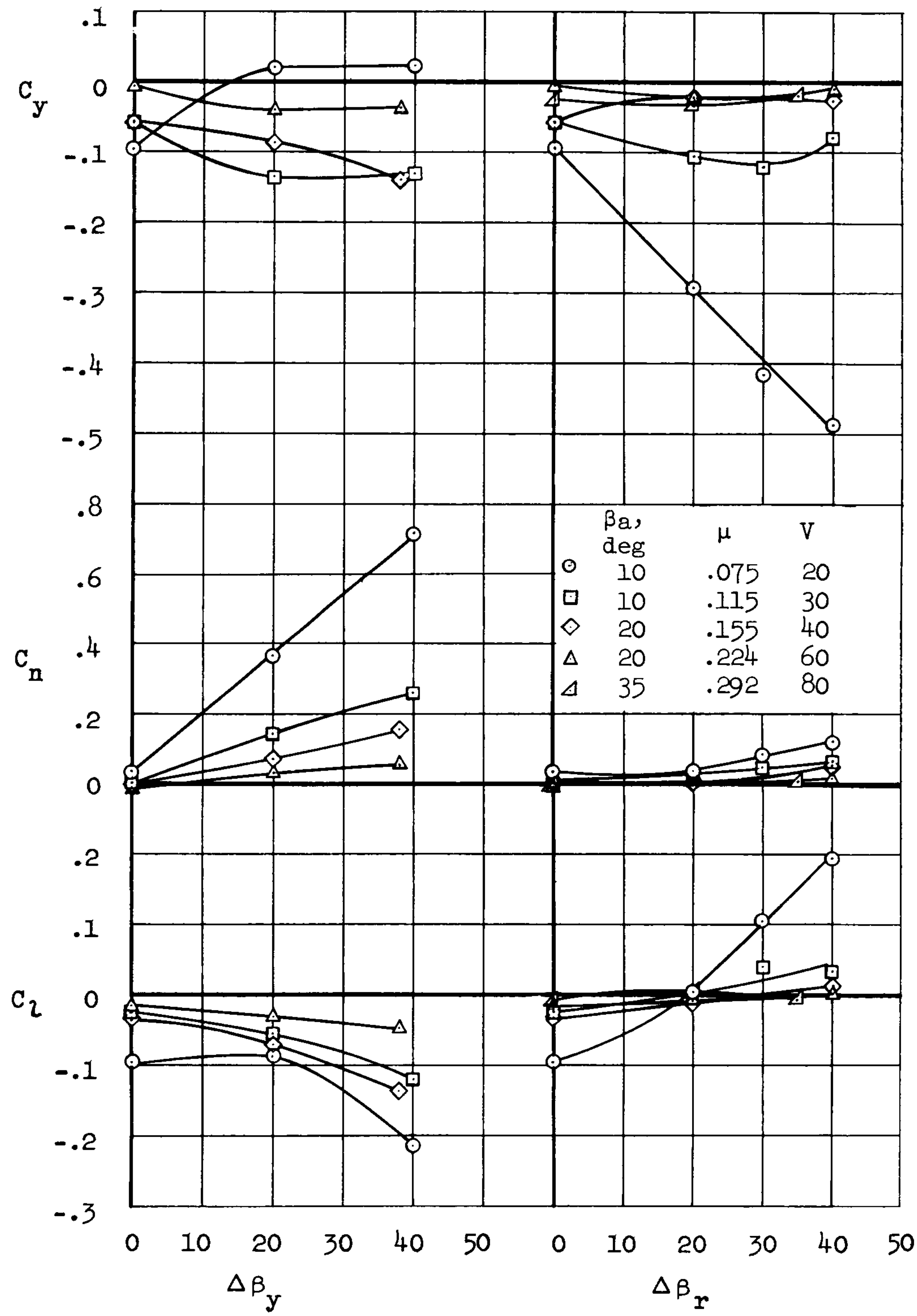

(b) Lateral-directional characteristics.

Figure 39.- Concluded.

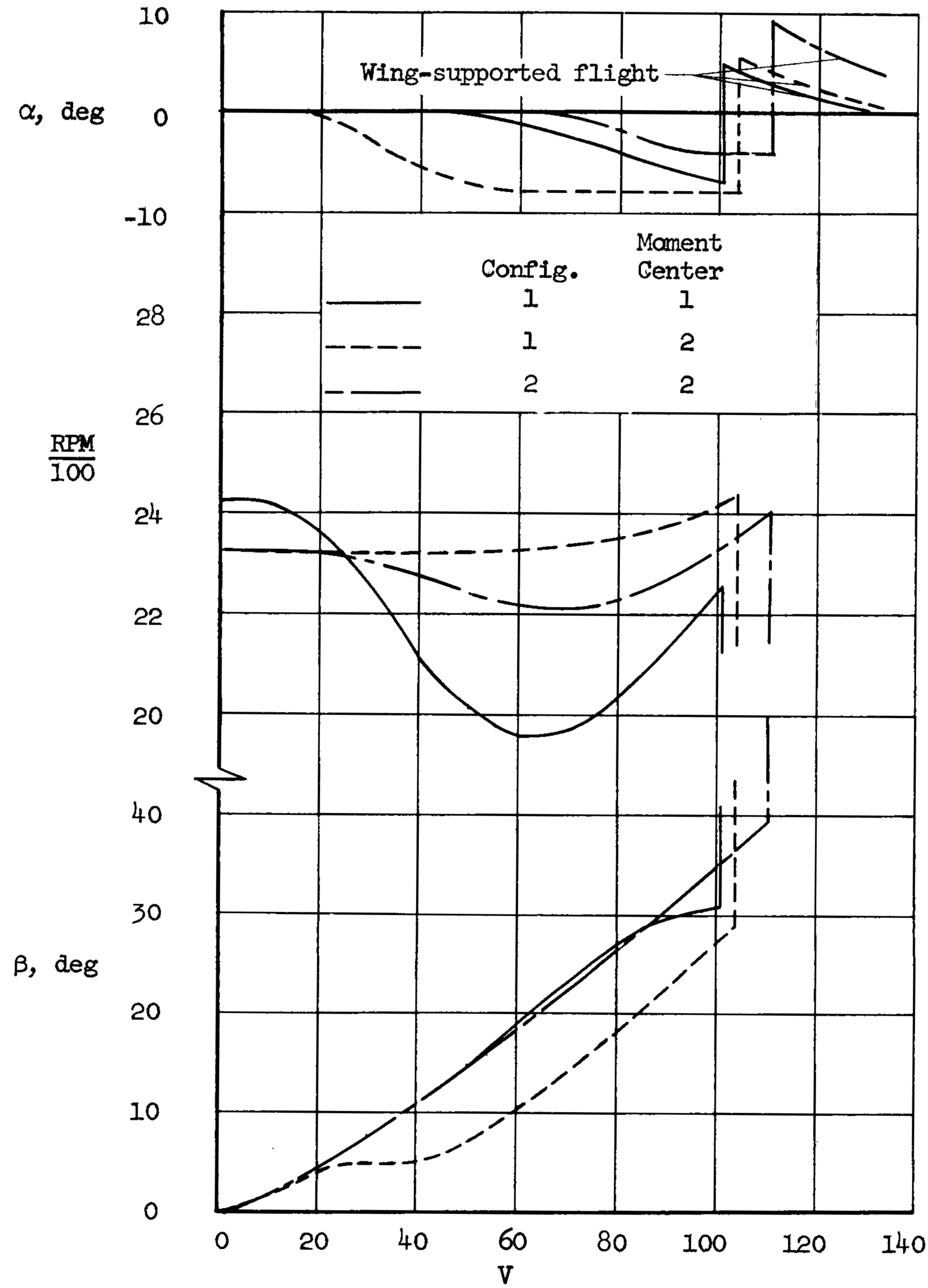

(a) Requirements for L = W, D = 0.

Figure 40.- Longitudinal requirements for balanced flight; $\delta_f = 30^\circ$, W = 11,660 lb.

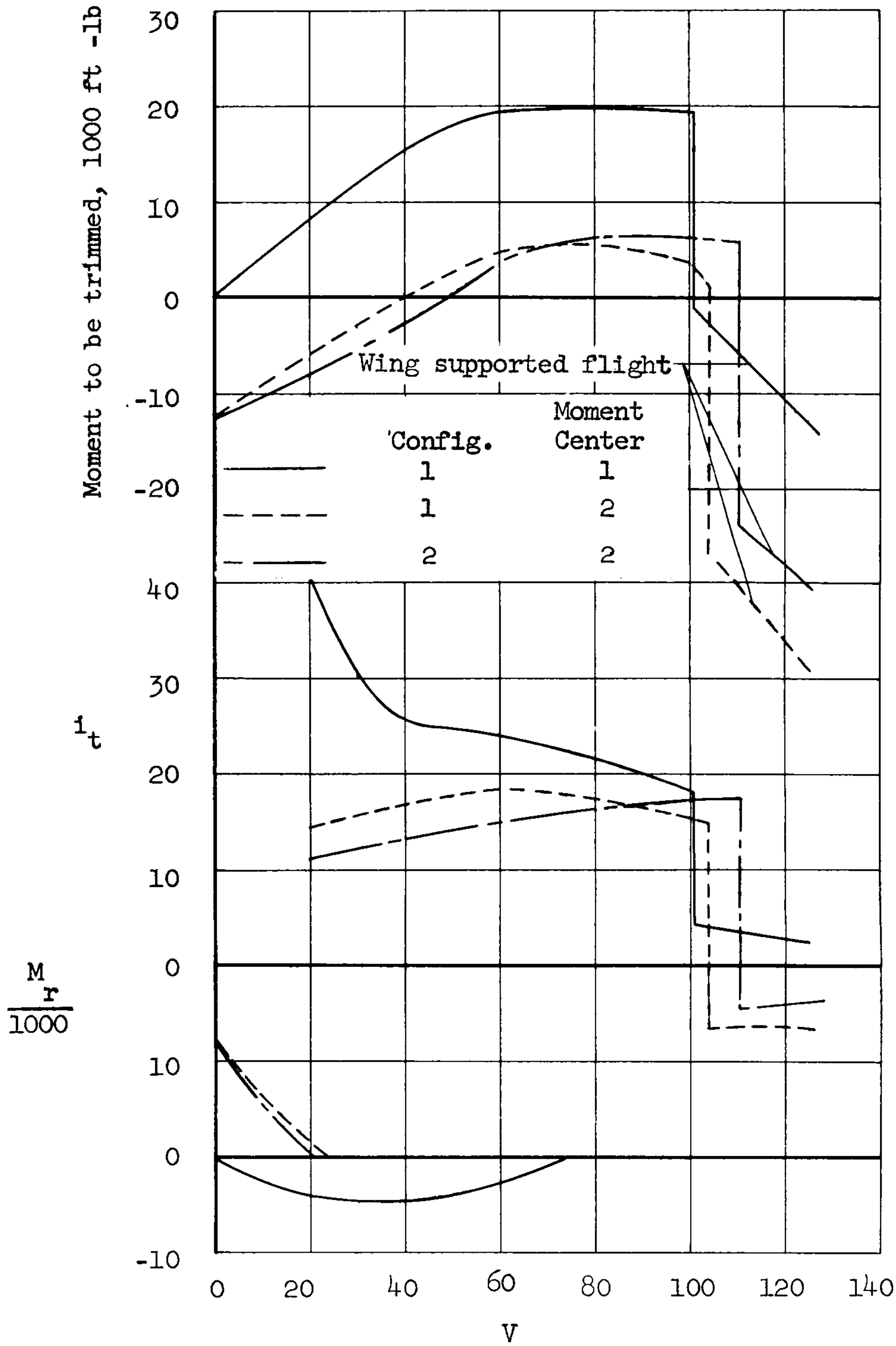

(b) Requirements for M = 0.

Figure 40.- Concluded.

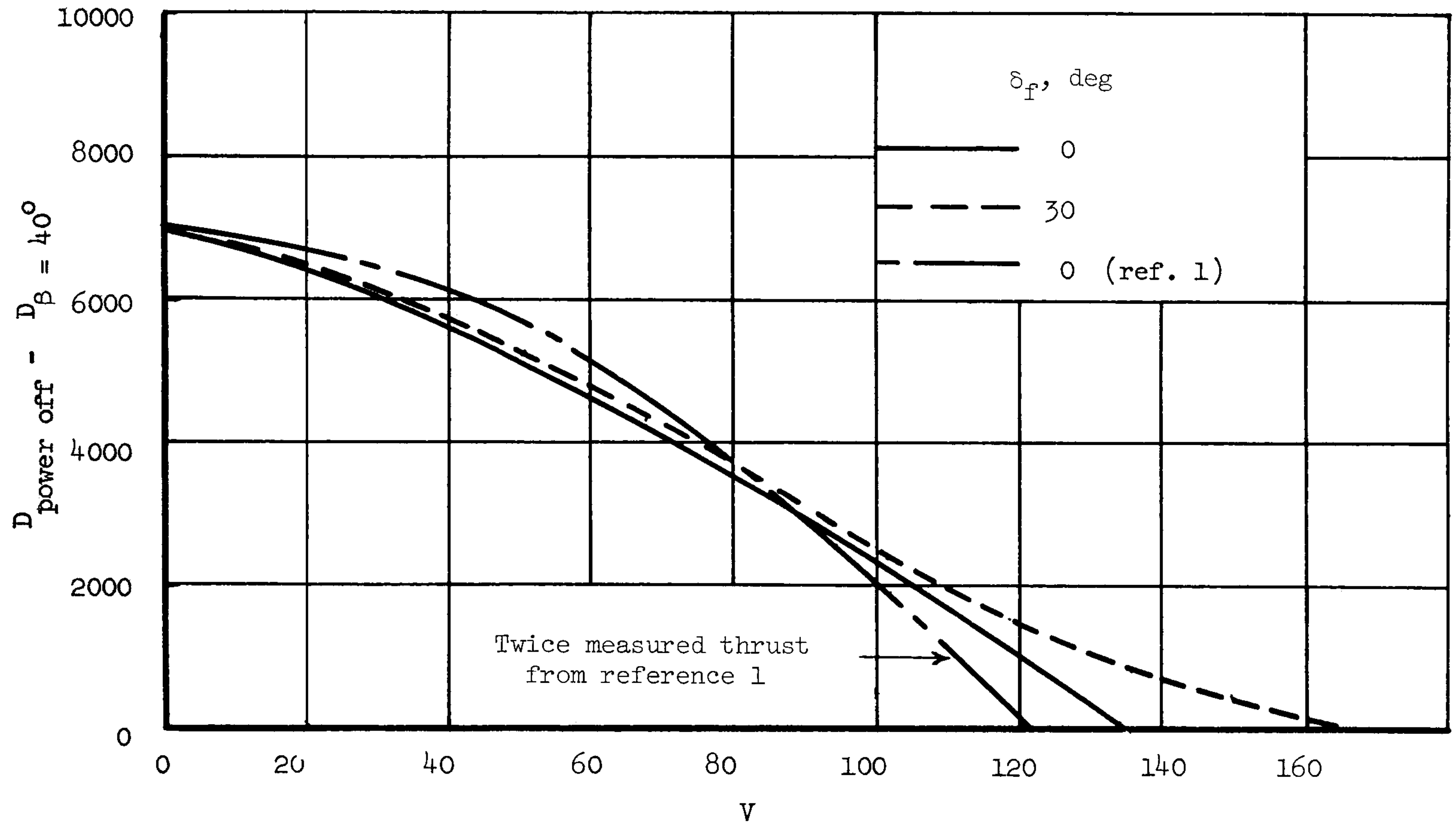

Figure 41.- The variation of thrust available with airspeed; 2600 RPM, $\alpha = 0^o$, $\beta = 40^o$.

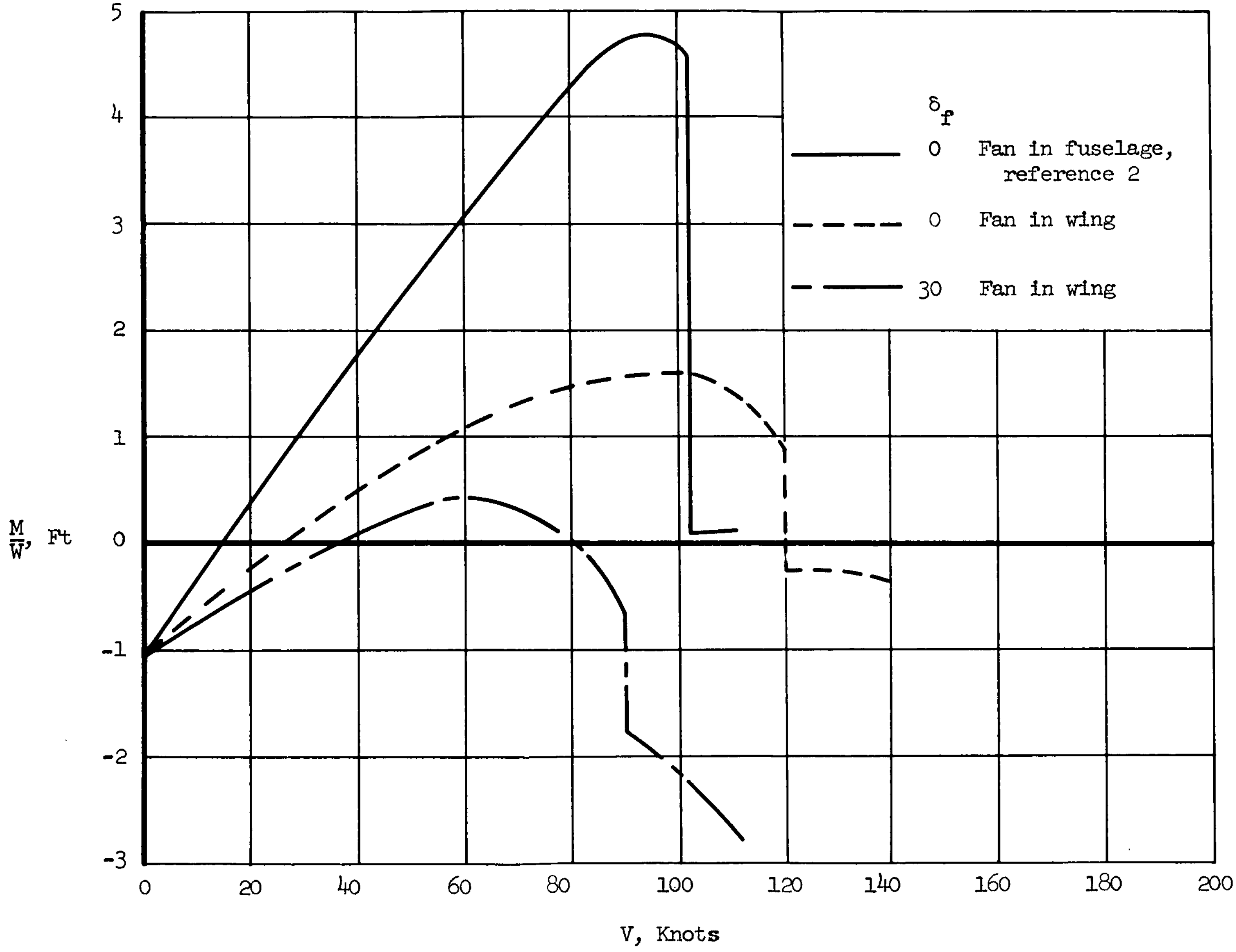

Figure 42.- Pitching moment required for trim; $\alpha = 0^{\circ}$.

NASA-Langley, 1963 A-710